縦磁界印加同軸線路形マイクロ波プラズマＣＶＤ装置の開発と成膜機構の研究

（研究課題番号　０７６５０３８３）

平成８年度科学研究費補助金　（基板研究（Ｃ）（２））
研究成果報告書

平成９年３月

研究代表者　　加藤　勇
（早稲田大学理工学部・教授）

目　次

１．はしがき

本研究は同軸線路形マイクロ波放電管に放電管軸方向（マイクロ波電界方向）と平行に直流磁界を印加して、プラズマの横方向への拡散を抑えることにより、電離電圧が高く放電しにくいガス、あるいは放電しにくいような低ガス圧において、プラズマＣＶＤ用の安定な高密度プラズマを作ることにある。ここで、膜堆積を行う堆積室内には直流磁界が漏れないようにして、等方的プラズマを作ること、またマイクロ波電力も漏れないようにして、静かな空間的アフターブロープラズマを作る必要がある。

本報告書は以上を目的として、平成７年－８年度の２年間にわたり行われた、装置の開発研究において得られた成果をまとめたものである。

＜研究組織＞

研究代表者　　加藤　勇　　（早稲田大学理工学部・教授）

＜研究経費＞

平成７年度	１，０００　千円
平成８年度	１，０００　千円
合計	２，０００　千円

Ⅱ　研究発表

1　学会誌、国際会議等

1) Naganori Takezawa, Isamu Kato, "In situ Measurement of Optical Constant of Ultra Thin Films Using Optical Fiber Sensor", SPIE Proceedings, Vol.2997, 1997

2) Naganori Takezawa, Isamu Kato, "Refractive Index Measurement of Silicon Thin Films Using Optical Waveguides", JJAP, Vol.36 No.2, 1997, pp.920-925

3) Xuantong Ying, Yoshinori Morita, Taro Kamiko, Isamu Kato, "Fabrication of SiN Film by Using Coaxial Line Type MPCVD System with Longitudinal Magnetic Field", Proceedings of ICRP-3/SPP-14, P1-31, 1997, pp.144-145

4) Taro Kamiko, Yoshinori Morita, Tadahiko Ando, Isamu Kato, "Influence of Longitudinal Magnetic Field Applied to Coaxial Line Type of Micro Wave Plasma(Ⅳ)", Proceedings of ICRP-3/SPP-14, P3-12, 1997, pp.403-404

5) Hirotaka Ogihara, Hidetaka Iizuka, Nobuyuki Koshiji, Isamu Kato, "Separation of Film Surface Heating Effect and Ion Implanting Effect", Proceedings of ICRP-3/SPP-14, Ⅳ a-6, 1997, pp.57-58

6) Naganori Takezawa, Nobuyuki Koshiji, "In situ Measurement of Change of Ultra Thin Films In Elapsed Time Using Optical Fiber Sensors", Proceedings of ICRP-3/SPP-14, P1-33, 1997, pp.148-149

7) 加藤勇、下田毅、山岸俊浩、”二重管式同軸線路形マイクロ波プラズマＣＶＤにおけるN_2／SiH_4プラズマのパラメーターの空間分布”、電気学会論文誌、Vol.116-A No.2, 1996, pp. 617-622

8) 森田義則、加藤勇、”ＲＦバイアス印加同軸線路形マイクロ波プラズマＣＶＤによるＳｉＮ膜の低温作製”、電子情報通信学会論文誌、Vol.J79-C-Ⅱ, 1996, pp.303-310

9) Isamu Kato, Toru Matsushita, Makoto Yamashita, "Dependence of Plasma Parameters on Electric Potential of Electrode in Microwave Plasma", Electronics and Communications in Japan, Vol.79 No.5, 1996, pp.58-65

10) Naganori Takezawa, Isamu Kato, "Optical Energy Gap Measurement of Semiconductor Ultrathin Films Using Optical Waveguides" JJAP, Vol.35 No.5A, 1996, pp.2826-2832

11) 神子太郎、山岸俊浩、森田義則、加藤勇、”同軸線路形マイクロ波プラズマにおける印加磁界の影響（Ⅱ）”、第１３回「プラズマプロセシング研究会」プロシーディングス、1A-4, 1996, pp.13-16

12) 山岸俊浩、神子太郎、森田義則、加藤勇、”同軸線路形マイクロ波プラズマにおける印加磁界の影響（Ⅲ）”、第１３回「プラズマプロセシング研究会」プロシーディングス、2C-2、1996, pp.175-178

13) 山下真、荻原博隆、加藤勇、”ＭＰＣＶＤにおける膜前面のシース電圧の制御と膜質”、第１３回「プラズマプロセシング研究会」プロシーディングス、1B3-3、1996, pp.109-112

14) 加藤勇、松下亨、山下真、”マイクロ波プラズマ中に設置した電極の電位がプラズマパラメータに与える影響”、電子情報通信学会論文誌、J79-C-Ⅱ No.1, 1996, pp.1-7

15) Isamu Kato, Toshiyuki Yoneda, Toru Matsushita, Makoto Yamashita, "Control of Radical Species in Microwave Plasma Chemical Vapor Deposition", Electronics and Communications in Japan, Vol.78 No.10, 1995, pp.97-104

16) 加藤勇、米田俊之、松下亨、山下真、”マイクロ波プラズマＣＶＤにおけるラジカル種の制御”、電子情報通信学会論文誌、J78-C-Ⅱ No.1、1995, pp.142-148

17) Isamu Kato, Toshiyuki Yoneda, Toru Matsushita, "Influence of Ion Bombardment on a-Si:H Films Fabricated by Plasma Chemical Vapor Deposition", Electronics and Communications in Japan, Vol.78 No.2, 1995, pp70-78

2　口頭発表

1）竹沢永訓、越路信行、石田知則、佐藤甲癸　加藤勇、”エバネッセント波を用いた放電停止後の半導体極薄膜表面変化のその場観測”、第４４回応用物理学関係連合講演会、１９９７年３月

2）飯塚英孝、臼田雅之、小柴博貫、神子太郎、加藤勇、”二重管式同軸線路形ＭＰＣＶＤ装置における水素プラズマへの磁界印加の効果”、第４４回応用物理学関係連合講演会、１９９７年３月

3）神子太郎、榎本貴幸、加藤勇、”同軸線路形ＭＰＣＶＤ装置において印加磁界がN_2プラズマに及ぼす効果（Ⅳ）”、第４４回応用物理学関係連合講演会、１９９７年３月

4）越路信行、加藤勇、”２重管式同軸線路型ＭＰＣＶＤを用いて作製したＳｉ系発光材料の研究”、第４４回応用物理学関係連合講演会、１９９７年３月

5）荻原博隆、岩田直之、加藤勇、”ａ－Ｓｉ：Ｈ膜成長中のイオン衝撃効果について”、第４４回応用物理学関係連合講演会、１９９７年３月

6）神子太郎、森田義則、安藤維彦、竹沢永訓、加藤勇、”同軸線路形ＭＰＣＶＤ装置において印加磁界がN_2プラズマに及ぼす効果”、第５７回応用物理学会学術講演会、１９９６年９月

7）飯塚英孝、神子太郎、森田義則、加藤勇、”同軸線路形マイクロ波プラズマ発生装置の基礎特性”、第５７回応用物理学会学術講演会、１９９６年９月

8）安藤維彦、神子太郎、森田義則、加藤勇、”同軸線路形マイクロ波プラズマのシミュレーション（Ⅲ）”、第５７回応用物理学会学術講演会、１９９６年９月

9）荻原博隆、越路信行、加藤勇、”ＭＰＣＶＤにおけるａ－Ｓｉ：Ｈ膜質に与えるイオン衝撃の効果”、第５７回応用物理学会学術講演会、１９９６年９月

10）森田義則、神子太郎、加藤勇、”縦磁界印加同軸線路形マイクロ波プラズマＣＶＤによるＳｉＮ膜の作製”、第５７回応用物理学会学術講演会、１９９６年９月

11）越路信行、荻原博隆、佐藤甲癸、宇高勝之、加藤勇、”ＭＰＣＶＤにおけるａ－Ｓｉ：Ｈ膜のフォトルミネッセンス（Ⅱ）”、第５７回応用物理学会学術講演会、１９９６年９月

12）竹沢永訓、越路信行、佐藤甲癸、加藤勇、”エバネッセント波を用いたリーク後の半導体極薄膜表面変化のその場観測”、第５７回応用物理学会学術講演会、１９９６年９月

13）神子太郎、山岸俊浩、森田義則、加藤勇、”同軸線路形ＭＰＣＶＤ装置において印加磁界がN_2プラズマに及ぼす効果（Ⅱ）”、第４３回応用物理学関係連合講演会、１９９６年３月

14）山岸俊浩、神子太郎、森田義則、加藤勇、”同軸線路形ＭＰＣＶＤ装置において印加磁界がＡｒプラズマに及ぼす影響（Ⅳ）、第４３回応用物理学関係連合講演会、１９９６年３月

15）安藤維彦、山岸俊浩、神子太郎、森田義則、加藤勇、”同軸線路形マイクロ波プラズマのシミュレーション（Ⅱ）”、第４３回応用物理学関係連合講演会、１９９６年３月

16）荻原博隆、山下真、飯塚英孝、越路信行、加藤勇、”無イオン衝撃作製のａ－Ｓｉ：Ｈ膜質の基板温度依存性”、第４３回応用物理学関係連合講演会、１９９６年３月

17）森田義則、加藤勇、”窒素ガス流量がＳｉＮ膜の膜特性に与える影響（Ⅱ）”、第４３回応用物理学関係連合講演会、１９９６年３月

18）野島信二、山下真、林錫　、加藤勇、”ＭＰＣＶＤ法によって作製されたフォトルミネッセンス”、第４３回応用物理学関係連合講演会、１９９６年３月

19）竹沢永訓、佐藤甲癸、加藤勇、”光ファイバーを用いた半導体極薄膜の光学的エネルギーギャップの測定”、第４３回応用物理学関係連合講演会、１９９６年３月

20）野島信二、山下真、堀田和重、宇高勝之、加藤勇、”２重管式同軸線路型ＭＰＣＶＤによるａ－Ｓｉ：Ｈ膜の長波長帯における屈折率測定”、第５６回応用物理学会学術講演会、１９９５年８月

21）堀田和重、竹沢永訓、野島信二、佐藤甲癸、加藤勇、”光導波路を用いたａ－Ｓｉ：Ｈ薄膜の赤外吸収スペクトル測定”、第５６回応用物理学会学術講演会、１９９５年８月

22）和井田裕一、山岸俊浩、森田義則、神子太郎、加藤勇、”同軸線路形マイクロ波プラズマのシミュレーション”、第５６回応用物理学会学術講演会、１９９５年８月

23）山岸俊浩、森田義則、神子太郎、加藤勇、”同軸線路形ＭＰＣＶＤ装置において印加磁界がＡｒプラズマに及ぼす影響（Ⅲ）”、第５６回応用物理学会学術講演会、１９９５年８月

24) 神子太郎、山岸俊浩、森田義則、加藤勇、”同軸線路形ＭＰＣＶＤ装置において印加磁界がN_2プラズマに及ぼす効果”、第５６回応用物理学会学術講演会、１９９５年８月

25) 山下真、荻原博隆、加藤勇、”ＭＰＣＶＤにおけるイオン衝撃エネルギーの制御”、第５６回応用物理学会学術講演会、１９９５年８月

26) 森田義則、中島達治、山岸俊浩、加藤勇、”マイクロ波プラズマにおけるＲＦバイアス印加効果”第５６回応用物理学会学術講演会、１９９５年８月

Ⅲ　研究成果

1　研究の背景

太陽電池はクリーンなエネルギー源として話題に上ってから久しいが、未だに十分な実用化段階に至っていない。その最大のネックは、低価格で大面積の良質な水素化アモルファスシリコン（ａ－Ｓｉ：Ｈ）膜の作製技術が確立していないことにある。その作製法の主流は高周波（ＲＦ）放電を用いた化学気相堆積であるが、近年ではマイクロ波放電を用いる方法が多くなり、マイクロ波プラズマＣＶＤ法の研究が盛んに行われている。私は以前より二重管式同軸線路形マイクロ波プラズマＣＶＤ装置を開発し[１]、マイクロ波プラズマを用いたａ－Ｓｉ：Ｈ膜や窒化シリコン（ＳｉＮ）膜の作製研究を行ってきている。これは、電子レンジの普及に伴いマイクロ波発振器が低価格となることを見越すと共に、空間的均一性のよい、高電子温度、高電子密度のプラズマを容易に得られること、そして無電極放電であるため純粋なプラズマが得られることを着目したことによる[２][３]。

また、本マイクロ波プラズマＣＶＤ方式の特徴は、マイクロ波の波長が短いことを生かして、キャビティー構造を用いて、マイクロ波電力を所定の空間に閉じ込めることによりマイクロ波電力の注入されている放電プラズマを所定の空間内にのみ発生できることにある。この装置により初めて、ａ－　Ｓｉ：Ｈ膜を放電プラズマの外で作製できるようになった[１][４]。すなわち、放電プラズマに接続された膜堆積室にはプラズマの拡散と流れによって空間的な分離によって作られた、エネルギー注入のないプラズマ（空間的アフターグロープラズマ）が作られている。この空間的アフターグロープラズマ内で成膜することにより、プラズマ照射による基板あるいは膜表面加熱、そして膜への損傷を防ぐことが可能となった。ここではプラズマによる基板加熱がないので、高分子材料（いわゆるプラスチック）のような低融

点物質上にもａ－Ｓｉ：Ｈ膜が作製可能であることを示した[５]。

また、以前に行われた重点領域研究「反応性プラズマの制御」の研究計画「マイクロ波プラズマの発生法とその構造の制御」において、マイクロ波プラズマパラメータの空間分布を克明に測定し、これに基づき、プラズマの発生機構、およびプラズマの閉じ込め機構について明らかにしてきた[６][７]。さらに薄膜を作製する際に用いられる、膜堆積を行う所の反応性プラズマ（Ａｒ／SiH_4プラズマおよびN_2／SiH_4プラズマ）中でのプローブ測定法を世界に先駆け、新たに考案し、この測定を可能とならしめ、膜を堆積している時の反応性プラズマパラメータ（電子温度、電子密度、プラズマ空間電位 等）の空間分布を始めて測定した[７][８][９]。さらに、基板に印加したＤＣバイアス電圧によるイオン衝撃エネルギーの制御性を明らかにした。すなわち、基板に流入するイオン流の単位面積、単位時間当たりの密度（イオンフラックス密度）を一定としたとき、イオン衝撃エネルギーはイオンの加速電圧となり、基板上のプラズマのシース電圧となるわけであるが、これを始めて測定し、基板面積をパラメータとして、印加したＤＣバイアス電圧とシース電圧との関係を明らかにしたものである[１０][１１]。このような制御されたプラズマを用いて薄膜の作製研究を行い、ラジカルを低速で基板に軟着陸させることにより、低温で高品質な薄膜を作製できることを示してきた[１２][１３]。以上のような研究成果が本研究の背景となるものである。

これまでの私の研究は無磁界であることを特徴の一つとしてきた。他方、有磁界型のプラズマＣＶＤにおいてはマイクロ波電界と直流磁界を直交させることにより、電子サイクロトロン共鳴（ＥＣＲ）効果を用い、高エネルギー電子を作り、SiH_4を解離させることを目的としてきた。しかしながら、ＥＣＲ法ではプラズマが空間的に不均一であること、共鳴を用いるのでプラズマの安定性が悪いこと、かつ低ガス圧のみでしかＥＣＲ効果が得られないこと、そして磁力線が基板位置までのびるので基板前で異方性プラズマとなるので、成膜に適さないこと、等の欠点を持つことが分かってきた。これら

の点をふまえて、新たなプラズマ作製法として本研究を立案した。

研究の背景における参考文献

[1] Isamu Kato, Shin-ichi Wakana and Shinnji Hara, "Microwave Plasma CVD System to Fabricate α-Si Thin Films out of Plasma", JJAP, Vol.22 No.1, January 1983, pp.L40-L42

[2] 加藤勇、若菜伸一、"新しいマイクロ波プラズマ化学気相堆積装置"、真空、Vol.26-7,1983, pp.30-38

[3] Isamu Kato, Shinji Hara annd Shin-ichi Wakana, "Analysis of Radial Distribution of Plasma Parameters in a Coaxial-Line Microwave Discharge Tube", J.Appl.Phys.,Vol.54 No.9, September 1983, pp.4883-4888

[4] 加藤勇、矢野元康、"同軸線路形マイクロ波プラズマＣＶＤ法によるプラズマ内外でのａ-Ｓｉ：Ｈ薄膜の作成、電子通信学会論文誌、Vol.69-C No.5, 1986, pp.662-668

[5] 加藤勇、上田哲也、畑中和久、"二重管式同軸線路形マイクロ波水素プラズマＣＶＤによるａ-Ｓｉ：Ｈ膜の作成"、電子情報通信学会論文誌、Vol.J70-C No.1, 1987, pp.78-88

[6] 伊藤尚己、加藤聖隆、加藤勇、"ＲＦバイアス印加マイクロ波プラズマＣＶＤによる薄膜の作成"、電子情報通信学会論文誌、Vol.74-C-II No.1, 1991, pp.21-25

[7] 加藤勇、臼居隆志、阪本匡、"マイクロ波プラズマＣＶＤにおけるプラズマパラメータの空間分布"、Trans.IEEE of Japan, Vol.112-A No.5, May 1992, pp.355-362

[8] Isamu Kato, Tadashi Sakamoto and Tsuyoshi Shimoda, "Method of Probe Measurement in N2/SiH4 Microwave Plasma, JJAP, Vol.33 Part1 No.1, January 1994, pp.307-310

[9] Isamu Kato, Tsuyoshi Shimoda and Toshihiro Yamagishi, "Removal Conditions of Films Deposited on Probe Surface", JJAP, Vol.33 Part1 No.6A, June 1994, pp.3586-3589

[10] 加藤勇、米田俊之、"マイクロ波プラズマにおけるＤＣバイアスと基板テーブル面積のプラズマパラメータへの影響、Trans. IEEE of Japan, Vol.114-A No.5, May 1994, pp.375-380

[11] 加藤勇、米田俊之、松下亨、"プラズマＣＶＤによって作製されたａ-Ｓｉ：Ｈ膜に与えるイオン衝撃の影響"、電子情報通信学会論文誌 、Vol.J77-C-II No.9, 1994, pp.384-391

[12] 加藤勇、米田俊之、松下亨、"プラズマＣＶＤ法におけるＤＣバイアスと基板テーブル面積のＳｉＨ結合量への影響、Trans.IEEE of Japan, Vol.114-A No.10, October 1994 pp.718-722

[13] 加藤勇、米田俊之、松下亨、山下真、"マイクロ波プラズマＣＶＤにおけるラジカル種の制御"、電子情報通信学会論文誌、Vol.J78-C-II No.4, 1995, pp.142-148

2　研究目的

本研究目的は、直流磁界を用いて空間的に均一なプラズマを、種々のガス（放電し易いガスから放電しにくいガス）において、高いガス圧から低いガス圧にわたって安定に発生できる、プラズマＣＶＤ用の新しいプラズマ発生装置を開発することにある。その設計方針は、マイクロ波電力と直流磁界を所定の空間に閉じ込めて、その空間からプラズマと活性種を膜堆積室内に流入させマイクロ波電力のない、低温で静かな空間的アフターグロープラズマ内で、かつ磁力線の影響のない等方的プラズマ内で、成膜を可能とすることにある。これにより、より高品質なシリコン系薄膜（ａ－Ｓｉ：ＨおよびＳｉＮ膜等）を作製することを目的とする。

3　研究成果概要

平成７年度には比較的放電しやすいＡｒガスとN_2ガスを用い、主として放電実験を行い、従来無磁界では放電が不安定となり、電子密度が低下してしまうような、低ガス圧でも安定で、かつ高電子密度のプラズマが得られることを明らかにした。さらに、比較的放電しにくいH_2ガスにおいても同様の実験を行い、H_2ガスにおいても安定で、かつ高電子密度のプラズマが得られるという見込みを得て、目的の前半を達成した。

平成８年度には、主として膜堆積に注目して実験を行い、Ａrガス、N_2ガスを用いた場合には無磁界の場合と比較して、膜質を劣化させることなく、より高速な膜堆積の行えることを明らかにした。さらに、H_2ガスの場合には、無磁界では電子密度が低いため、a-Ｓｉ：Ｈ膜の堆積速度はかなり遅いものであったが、約１４００ガウスの磁界印加により、安定でかつ高電子密度のプラズマが得られることを示し、７Å／ｓという高速の膜堆積が行える

ことを明らかにし、目的の後半を達成した。

その詳細はその添付論文に記載されているが、無磁界時と有磁界時とを比較して、添付論文に従って、以下にその概要をまとめる。

［１］無磁界時における放電の安定性をＡｒガスとN_2ガスにおいて調べた。ここで、ＡｒガスとN_2ガスは本研究でいうところの放電し易いガスに相当する。さらに、安定な放電時における電子温度電子密度及びプラズマの空間電位等のプラズマパラメータを測定し、プラズマの均一性について検討し、ＣＶＤ用のプラズマとして十分に均一なプラズマが得られることを明らかにした。またイオン衝撃効果について検討を加え、イオン衝撃効果の内、堆積中の膜表面加熱効果が、基板加熱効果と同様の膜質改善効果を持つことを明らかにした。しかしながら、イオン衝撃効果の内のイオン打ち込み効果により、膜質は総合的に悪くなることを明らかにした。添付論文［１５］［１６］［１７］参照。

［２］イオン衝撃エネルギーは膜表面に流入するイオンフラックス密度を一定にしたとき、膜表面のシース電圧に比例する。そこで、基板に印加するＤＣバイアスを変えシース電圧を測定し、イオン衝撃エネルギーが膜質に与える効果を明らかにすると共に、基板をアースして、二重管の内管にＤＣバイアスを印加しても、ほぼ同時の効果の得られることを明らかにした。添付論文［９］［１３］［１４］参照。

［３］Ａｒガス放電における直流磁界印加効果をプラズマパラメータの測定に基づき詳細に検討した。その結果、径方向、周方向に関するプラズマの均一性の良いこと、印加磁界強度によってはＥＣＲ効果も表れるが、その効果は弱く、軸方向磁界は径方向へのプラズマの拡散を抑えプラズマを安定させる効果が強いことを明らかにした。添付論文［１１］［１２］参照。

［４］光ファイバーをセンサーとする極薄膜の高感度測定を開発して、極薄膜のエネルギーギャップＥ０を測定した。さらに、このセンサーにより成膜後の空気リーク時における膜質の変化を測定できることを明らかにした。また、膜成長時の膜質を測定し、成膜機構を検討しうる可能性を明らかにした。添付論文［１］［２］［６］［１０］参照。

［５］ＲＦバイアスを印加して，ＳｉＮ膜を作製し、ａ－Ｓｉ：Ｈ膜作製時におけるＤＣバイアス印加効果と同時の効果が得られることを明らかにした。添付論文［７］［８］参照。

［６］イオン衝撃効果には、成長中の膜表面加熱効果と、成長中に膜中にイオンを打ち込み膜組成を変えるようなイオン打ち込み効果があることを明らかにすると共にその分離に成功した。添付論文［５］参照。

［７］直流磁界を印加した場合のN_2プラズマについて詳細に測定した。また直流磁界印加により、ＳｉＮ膜の膜質を劣化させることなく、無磁界時より、より高速な膜堆積を行うことができることを明らかにした。添付論文［３］［４］参照。

［８］H_2ガス放電においては無磁界時に十分密度の高いプラズマが作製できず、ａ－Ｓｉ：Ｈの堆積速度は遅いものであったが、軸方向磁界印加により、プラズマの径方向への拡散が抑えられ、ＣＶＤに必要な十分高密度なプラズマが得られることを明らかにした。その結果、H_2プラズマを用いて、７Å／ｓという高速堆積ができることを明らかにした。

Ⅳ　添付論文

[13] 山下真、荻原博隆、加藤勇、”ＭＰＣＶＤにおける膜前面のシース電圧の制御と膜質”、第１３回「プラズマプロセシング研究会」プロシーディングス、1B3-3, 1996, pp.109-112 ・・・７０

[14] 加藤勇、松下亨、山下真、”マイクロ波プラズマ中に設置した電極の電位がプラズマパラメータに与える影響”、電子情報通信学会論文誌、J79-C-Ⅱ No.1, 1996, pp.1-7 ・・・７４

[15] Isamu Kato, Toshiyuki Yoneda, Toru Matsushita, Makoto Yamashita, "Control of Radical Species in Microwave Plasma Chemical Vapor Deposition", Electronics and Communications in Japan, Vol.78 No.10, 1995, pp.97-104 ・・・８１

[16] 加藤勇、米田俊之、松下亨、山下真、”マイクロ波プラズマＣＶＤにおけるラジカル種の制御”、電子情報通信学会論文誌、J78-C-Ⅱ No.1、1995, pp.142-148 ・・・８９

[17] Isamu Kato, Toshiyuki Yoneda, Toru Matsushita, "Influence of Ion Bombardment on a-Si:H Films Fabricated by Plasma Chemical Vapor Deposition", Electronics and Communicationsin Japan, Vol.78 No.2, 1995, pp70-78 ・・・９６

In situ measurement of the optical constant of ultra thin films using optical fiber sensor.

Naganori Takezawa and Isamu Kato

Department of Electronics and Communication, School of Science and Engineering,
Waseda University, 3-4-1 Okubo, Shinjuku-ku, Tokyo 169, Japan

ABSTRACT

We use an optical fiber sensor whose part of clad is removed for the optical constant of ultra thin film measurement. The sensitivity of the sensor is increased by decreasing the diameter of the optical fiber and / or increasing the length of the film deposited part. The result of the *in situ* measurement method of change of a-Si:H ultra thin films by oxidation with passage of time by leaking from vacuum to atmospheric air is shown. We use an optical fiber sensor whose length of the film deposited part is 100 mm, diameter of the core is 110 μm and the core material is silica. a-Si:H film with approximately 10 nm in thickness is deposited on the core of the optical fiber sensor. The oxidation saturates in approximately 600 s. The larger attenuation of transmitted light at the long wavelengths from 685 to 800 nm is observed. This phenomenon is maybe due to the change of defects by relaxation

Keywords; Fiber Sensor, Waveguide Sensor, In Situ Measurement, Oxidation, Ultra Thin Film, a-Si:H

1. INTRODUCTION

We have studied a method to measure the dependence of the light transmittance on the plasma chemical vapor deposition (CVD) film thickness for the measurement of the optical constants of thin films[1,2,3]. The films are deposited on an optical fiber whose part of the clad is removed or on a slab optical waveguide as a sensor. During the deposition of films in the plasma CVD system, the transmitted light which goes through the sensor decreases exponentially with periodic oscillation corresponding to the increase of film thickness. The reason is that the electric field strength concentrates periodically in the film. By removing the oscillation mathematically, we determined the optical energy gap[1]. Then, we also determined the refractive index from the value of the first valley in the oscillation or the period of the oscillation[2,3]. In our new method, we have been able to measure the optical energy gap of the ultra thin a-Si:H film with approximately 20 nm in thickness which is about 1/40 comparing with what in the conventional method and the refractive index of the ultra thin film with approximately 10 nm in thickness[1,2]. A film thickness of approximately 1 μm was need to obtain sufficient interaction between a film and light in the conventional method[4]. As compared with this, the measurement of the ultra thin films mentioned above is possible in our method because the length of interaction takes long sufficiently toward the propagation direction of light. The same thing is able to correspond in the measurement using the optical fiber whose part of clad is removed as a sensor. By increasing the sensitivity of these optical waveguided type sensors, the change of many physical quantities which have not been measured before could be measured *in situ*.

On the other hand in thin film fabrication, the change of the films just after a leak by atmospheric air was not measured when fabrications were finished. The measurement of the surface oxidation layer of thin films was usually obtained by executing the etching of the surface and measurement of the X-ray photoelectron spectroscopy alternatively after leaking by atmospheric air and putting the films out of a fabrication chamber. Therefore, the film surface oxidation progress measurement of change in elapsed time after the leak from vacuum to atmospheric air is not completed.

In this report, using the high sensitivity optical fiber sensor obtained from results of investigation by increasing the sensitivity of the optical fiber sensor, we show an *in situ* measurement method of change of a film quality with passage of time just after leaking a-Si:H ultra thin films to atmospheric air.

2. INVESTIGATION OF HIGH SENSITIVITY OF THE OPTICAL WAVEGUIDE SENSOR IN SIMULATION

Conditions of increasing the sensitivity of the optical waveguide sensor are clarified in the four-layer slab waveguide simulation. The four-layer slab waveguide consists of air, film, waveguide and air. The length of the part on which the film is deposited is l [mm], and the thickness of the optical waveguide is t [μm]. Transmittance dependence on deposited film thickness of the four-layer slab waveguide is obtained from solutions of an eigenvalue equation[4]. A wavelength λ is 632.8 nm, the refractive index of air n_0 is 1 - j0, the refractive index of deposited a film n_f is 2.88 - j0.029 and the refractive index of an optical waveguide n_w is 1.457 - j0. The value of n_f is a typical value of a-Si:H, and the value of n_w is that of fused silica. The waveguided mode is the TE mode, and the mode number is 100.

Figure 1 and 2 show the calculation results using the values mentioned above.

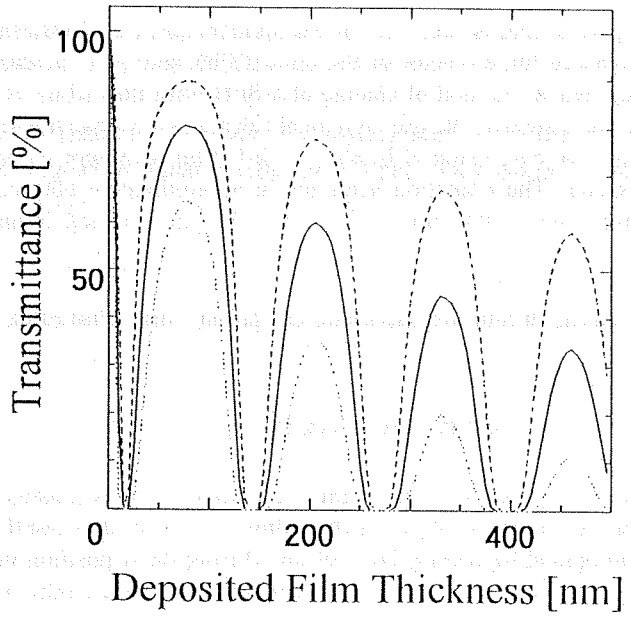

Fig. 1. Transmittance dependence on deposited film thickness at l = 50, 100 and 200 mm when t = 100 μm.

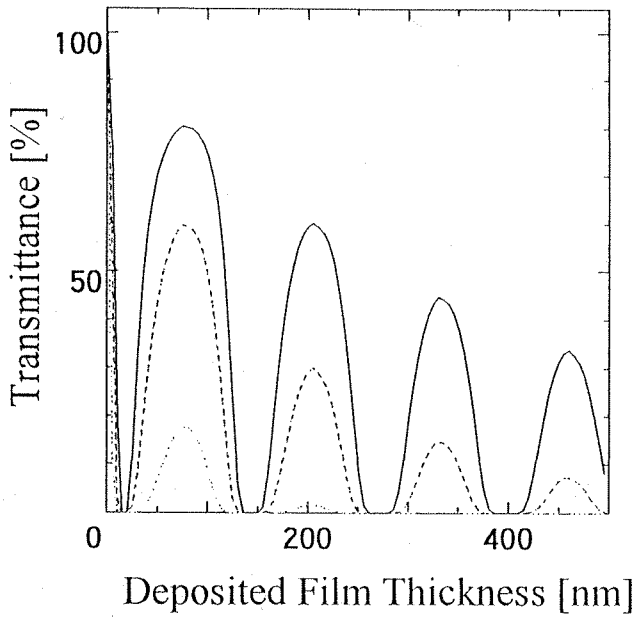

Fig. 2. Transmittance dependence on deposited film thickness at t = 100, 150 and 200 μm when l = 100 mm .

Figure 1 shows the results at l = 50, 100 and 200 mm when t = 100 μm, and Fig. 2. shows the results at t = 100, 150 and 200 μm when l = 100 mm . It is clarified that transmittance has periodic oscillation. The reason of the oscillation is that the electric field concentrates periodically in the film layer which has large absorption coefficient[1]. It is clarified that transmittance decreases when the value of l increases from Fig. 1. Also, it is clarified that transmittance decreases when the value of t decreases from Fig. 2. Absorption increases when l increases. Ratio of light without interaction with a deposited film and the whole waveguided light decreases when t decreases. From these phenomena, the equivalent absorption coefficient of the entire four-layer slab waveguide increases. Consequently, even if the absorption coefficient of the deposited film is small the sufficient absorption for measuring can be obtained and the sensitivity of the sensor increases. The same conclusion is derived for the another mode numbers, another wavelengths and the TM mode. The same tendency was confirmed in experiments[1]. Therefore, to increase the sensitivity of the slab waveguide sensor, we need increase l and / or decrease t. However, the waveguided light is absorbed too much when l increases or t decreases too much. Therefore, the upper limit of l and the lower limit of t exist depending on the absorption coefficient of deposited films, the sensitivity of a detector and the proceedings of the noise reduction.

3. INVESTIGATION OF HIGH SENSITIVITY OF OPTICAL FIBER SENSOR IN EXPERIMENT

Conditions of increasing the sensitivity of the optical waveguide sensor are clarified in experiment. The optical fiber sensor and its setup in fabrication chamber are shown.

Fig. 3. Details of the optical fiber sensor.

Figure 3 shows the optical fiber sensor structure. This is a step index type optical fiber with silica core and polymer clad. The clad is removed for deposition of a-Si:H films. The length of the clad removed part is l [mm] and its diameter of the core is ϕ [μm].

Our experimental setup - the double-tubed coaxial-line-type microwave plasma CVD system is shown in Fig. 4[5]. As shown in Fig. 4, a-Si:H is fabricated from SiH_4 by using Ar plasma flowing from the bottom side of the system.

Fig. 4. Experimental setup, with our optical fiber sensor.

The optical fiber sensor is set on the substrate table in this chamber. The input port of the optical fiber is connected with a halogen lamp

light source and the output port is connected with a spectrum analyzer.

Fig. 5. Transmittance dependence on deposited a-Si:H film thickness at λ = 650 nm using the optical fiber sensors.

Figure 5 shows transmittance dependence on deposited a-Si:H film thickness at λ = 650 nm using the optical fiber sensors. By comparing the data of the l = 50 mm and ϕ = 110 μm sensor with the data of the l = 100 mm and ϕ = 110 μm sensor, it is clarified that transmittance decreases when l is large in Fig. 5. Also, by comparing the data of the l = 100 mm and ϕ = 200 μm sensor with the data of the l = 100 mm and ϕ = 110 μm sensor, it is clarified that transmittance decreases when ϕ is small. The values of the film thickness where the peaks of the periodic oscillations of transmittance appear are different among the sensors because we consider that the refractive indexes of the deposited film are different as depositions are not at same time. Especially, the different film thickness of the peaks between the sensors of ϕ = 110 μm and 200 μm course that the refractive indexes of core are different as the makers of the fibers are different, we consider. The same conclusion was derived for 400 through 800 nm in wavelength in our measurement.

Increasing l corresponds to increasing l of the optical waveguide sensor. It is considered that decreasing ϕ corresponds to decreasing t of the optical waveguide sensor. Therefore, it is clarified that to increase the sensitivity of the optical fiber sensor, we need increase l and l or decrease ϕ.

4. CHANGE OF LIGHT TRANSMITTANCE AFTER LEAK

Transmitted light is measured in about 10 minutes after the fabrication. Using the optical fiber sensor, whose length of the film deposited part l is 100 mm and diameter of the core ϕ is 110 μm, a-Si:H film with approximately 10 nm in thickness is fabricated on the optical fiber sensor. The film change by oxidation is measured *in situ*. The period to take the leak of the CVD chamber from vacuum to atmospheric air is approximately 20 s.

Fig. 6. Transmittance spectra in experiment using the optical fiber sensor.

Figure 6 shows transmitted light spectra. In Fig. 6, the upper data is the spectrum of the sensor without the film. The middle data is the spectrum after depositing a-Si:H of approximately 10 nm in thickness and letting it stand in approximately 30 minutes in vacuum, namely, the spectrum before the leak. The lower data is the spectrum at 680 s after leaking the chamber. The attenuation between the upper spectrum and the middle spectrum means the absorption by a-Si:H, the interference and the scattering of transmitted light . The attenuation between the middle spectrum and the lower spectrum means the change of transmittance by the leak.

Fig. 7. Transmittance change with passage of time.

Figure 7 shows the change of light transmittance through the optical fiber sensor with passage of time at wavelengths of 800, 750, 700 and 685 nm. From Fig. 7, it is clarified that the transmittance at every wavelength decreases after leaking the CVD system and it saturates in approximately 600 s.

It is considered that the film is changed by oxidation and the oxidation saturates around 600 s from Fig. 7. By comparing the rate of the change of transmittance among the wavelengths, it is clarified that the large rate of the change occurs at long wavelengths. It was reported that defects are changed by relaxation by the bias light in the region of 0.8 eV < h ν < 1.8 eV (λ = 690 nm ~ 1.55 μm) for a-Si:H because of the shift of the quasi-Fermi-level to the conduction band or an increase in the concentration of dangling-bond centers D^- [6,7]. The result in this experiment in Fig. 6 shows the similar tendency to the dependence of the absorption coefficient on energy owing to the change of defects described in above references. We consider that the similar phenomena occur by oxidation in the high energy side of the Urback tail region (1.5 eV < h ν < 1.8 eV corresponding to 690 nm < λ < 800 nm).

5. CONCLUSIONS

Using the optical waveguide as a sensor, it was shown that the sensitivity increases by increasing l and l or decreasing t in

the four-layer slab optical waveguide simulation. Using the optical fiber as a sensor, we found the experimental results consisted with the above theoretical analysis of the slab optical waveguide. The *in situ* measurement of the physics quantity which has not measured before was shown with the high sensitive sensor. Concretely, the *in situ* measurement of the change of the film quality due to the oxidation can be completed with the high sensitive optical fiber sensor.

6. ACKNOWLEDGMENT

This work was supported by a Waseda University Grant for Special Research Project in 1996.

7. REFERENCES

1 N. Takezawa and I. Kato, "Optical energy gap measurement of semiconductor ultrathin films using optical waveguide," Jpn. J. Appl. Phys., Vol. 35, pp. 2826 - 2832, May 1996.
2 N. Takezawa, I. Kato and S. Nojima, "Refractive index measurement of silicon thin films using slab optical waveguide." Jpn. J. Appl. Phys., accepted for publication ,February 1997.
3 S. Nojima, N. Takezawa, K. Hotta and I. Kato, "Refractive index measurement of MPCVD thin films using slab waveguide," Proc. 12th Sympo. Plasma Processing, ed. T. Makabe Div. Plasma Electronics, Jpn. Soc. Appl. Phys., pp. 325 - 328, 1995.
4 . R. Swanepoel, " " J. Phys. Vol. E 16, pp. 214 - ,1983.
5 I. Kato and M. Yano: Trans. IEE Jpn. **J69-C** (1986) 662.
6 A. G. Kazanskii and E. P. Milichevich: Sov. Phys. Semicond., **19** (1984) 323.
7 S. Lee, S. Kumar, C. R. Wronski and N. Maley: J. Non-Cryst. Solids, **114** (1989) 316.

Jpn. J. Appl. Phys. Vol. 36 (1997) pp. 920-925
Part 1, No. 2, February 1997

Refractive Index Measurement of Silicon Thin Films Using Slab Optical Waveguides

Naganori TAKEZAWA, Isamu KATO and Shinji NOJIMA

Department of Electronics and Communication, School of Science and Engineering, Waseda University, Tokyo 169, Japan

(Received June 24, 1996; accepted for publication November 8, 1996)

Measurement of the real part of the refractive index (n_f') of silicon thin films using a slab optical waveguide (SOW) is discussed. Upon deposition of thin films on a SOW, the transmittance decreases with periodic oscillation owing to the multiple reflection. It is clarified from a simulation of a four-layer SOW that the period of oscillation is reduced when n_f' increases. In this paper, we discuss a method of determining the n_f' from correspondence of the minimum film thickness (d_0) in which the oscillation valley appears as a calculation result of transmittance for the TE_0 mode to d_0 in an experiment in which the refractive index and sizes of SOW are known without considering higher modes or the TM mode. Good agreement is observed in comparison of the result of the measurement with that of the ellipsometer at a wavelength of 632.8 nm. Therefore, it can be shown that the distributions of n_f' of *a*-Si:H and SiN thin films at wavelengths from 400 to 800 nm are obtained in the same manner. In order to achieve higher accuracy of the measurement, a SOW with a larger refractive index is used.

KEYWORDS: optical fiber sensor, refractive index, slab optical waveguide, a-Si:H, SiN, thin film, MPCVD

1. Introduction

Sensors which use optical fibers such as temperature sensors,[1] pressure sensors[2] and gas sensors,[3] have been actively developed, and optical functional devices by which a metal or semiconductor film is fabricated on an optical waveguide have been studied.[4-7] The phenomenon in which the combinations of light with a film on a waveguide differ between the TE and TM modes according to the fabricated film thickness is applied to the realized waveguide type TE/TM mode filters. The extinction ratio of the transmitted light of the TE and TM modes is 34 dB for metal film fabrication.[5] The extinction ratio with hydrogenated amorphous silicon (a-Si:H) is 30 dB.[6] The extinction ratio with silicon nitride (SiN) is 27 dB.[7] An optical energy gap (E_0) measurement of *a*-Si:H with approximately 20 nm has been performed with the dependence of transmittance on the deposited film thickness by depositing semiconductor films on a slab optical waveguide (SOW) used as a sensor.[8] In this study, it was clarified that the transmittance decreases with periodic oscillation. We propose a new measurement method for the real part of the refractive index (n_f') of silicon thin films such as *a*-Si:H and SiN on SOW from the minimum film thickness (d_0) at which the valley of the oscillation appears. The refractive index of thin films can be measured using interference fringes by perpendicularly irradiating light onto a film or by using ellipsometry. In the method using interference fringes, the refractive index is obtained from the interval of the fringes appearing in the dependence of transmittance on the wavelength.[9] In the ellipsometry method, the refractive index is obtained from the reflection coefficients and the relative phases of the *p* and *s* waves.[10] A film thickness of approximately 1 μm is needed to obtain sufficiently narrow interval fringes for the method using the interference fringes. On the other hand, in our method, the refractive index can be determined below 20 nm in thickness. Furthermore, this method is not influenced by the atmosphere because films are deposited on a SOW sensor which is in a fabrication chamber. While light is absorbed and scattered in plasma for the ellipsometry method because light goes through plasma, there is an advantage in this method in that absorption by plasma does not exist using light which goes through the SOW.

In this report, it is shown by a simulation of a four-layer SOW that the value of the film thickness at a peak in the dependence of the effective absorption coefficient (α_m) for the mode number m on the film thickness (d) is changed by n_f'. The peaks match the valleys appearing in the dependence of transmittance on d. A method to obtain n_f' from the correspondence of d_0 of a calculated result to d_0 of an experimental result, by changing n_f' in the simulation for the TE_0 mode is shown. Distributions of n_f' from 400 to 800 nm in wavelength for three films with different n_f' are shown.

2. Dependence of α_m on d in the Four-layer SOW Simulation

Figure 1 shows the structure of the four-layer SOW. The SOW consists of air, film, optical waveguide and air. The thickness of the deposited film is defined as d nm, the length of the part on which the film is deposited is defined as l mm, and the thickness of the SOW is defined as t μm. The refractive index of air n_0 is $1 - j0$, the refractive index of film n_f is $n_f' - jn_f''$, and the refractive index of optical waveguide n_w is $n_w' - jn_w''$. The guided light is in the direction of z. The effective refractive index of the four-layer SOW N_m which is $N_m' - jN_m''$ and the profile of the electric field distribution for the guided mode of the mode number m are obtained from solutions of an

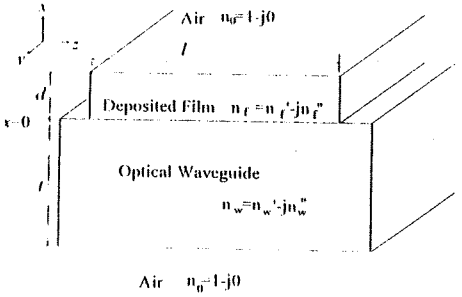

Fig. 1. Structure of the four-layer SOW.

eigenvalue equation for a transversely guided mode.[11]

We obtain the dependence of α_m on d in the four-layer SOW at a wavelength of 632.8 nm. N'_m and N''_m are obtained by the four-layer SOW simulation. α_m is obtained with N''_m using

$$\alpha_m = 4\pi/\lambda \cdot N''_m, \tag{1}$$

where λ is the wavelength.

The material of the SOW is fused silica and that of the films is *a*-Si:H in the simulation. The constant values used in the simulation are as follows. n_f is $4.0 - j0.1$ at 632.8 nm. The value of n'_f is almost the highest one measured by the conventional ellipsometer for *a*-Si:H films with a thickness of 1 μm which are fabricated by a double-tubed coaxial-line type microwave plasma chemical vapor deposition (MPCVD) system.[7] The value of n''_f is almost the highest one calculated with the absorption coefficient obtained from the ultraviolet-visible spectroscopy spectrum for the same *a*-Si:H films. The value of n'_w is 1.457 at 632.8 nm when the material is fused silica, and n''_w is null because l is short enough. t is 100 μm. The maximum mode number of the four-layer SOW is 335 for both the TE mode and the TM mode with the values set in this section.

2.1 *Dependence of α_m on d for the TE_0 mode and the TM_0 mode*

Figure 2 shows the dependences of α_m on d for the TE_0 and TM_0 modes. It is clarified that α_m has periodic peaks in both the TE_0 mode and the TM_0 mode. The field strength is enlarged when the number of antinodes of the field increases one by one at each constant film thickness from the calculation of the field distribution. At this moment, α_m exhibits a peak because the field distribution concentrates in the film.[8]

2.2 *Dependence of α_m on d with n'_f*

For the TE_0 mode, Fig. 3 shows the dependence of α_m on d with $n'_f = 2.0$, 3.0 and 4.0. It is clarified that the period of the α_m peaks increases when n'_f becomes small. Figure 4 shows the profile of the field distribution around the film at $d = 300$ nm with $n'_f = 2.0$, 3.0 and 4.0 for the TE_{300} mode. The wave vector k_i in a material with the real part of the refractive index n'_i is expressed as

$$|k_i| = 2\pi/\lambda \cdot n'_i. \tag{2}$$

Because $n'_f > n'_w$, the wave vector component (k_{fx}) in the direction of x in the film is smaller than that (k_{wx}) in the SOW. From Fig. 4, it is clarified that the period of the amplitude of the field distribution decreases at the same value of d. α_m reaches peaks with increasing d when the number of antinodes in the film increases. Therefore, when the period of the field amplitude decreases, namely, when n'_f enlarges, the period of α_m peaks becomes smaller. The same conclusion is derived for the TM mode qualitatively.

As mentioned above, by depositing a silicon film on a SOW whose refractive index and sizes are known, n'_f is measured from the thickness in which the peaks of α_m are obtained, or, in which the valleys of transmittance are obtained in the dependence on d.

2.3 *Dependence of α_m on d for the mode number m*

Figure 5 shows the dependence of α_m on d when the mode numbers m of the TE mode are 0, 10 and 100. It is clarified that the values of d with which α_m peaks are almost the same even if m changes. Furthermore,

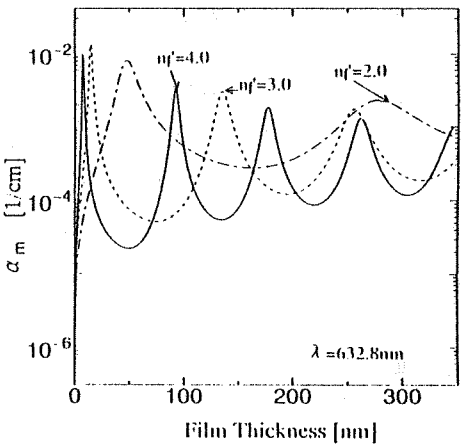

Fig. 3. Dependence of α_m on d for the TE_0 mode at $n'_f = 2.0$, 3.0 and 4.0.

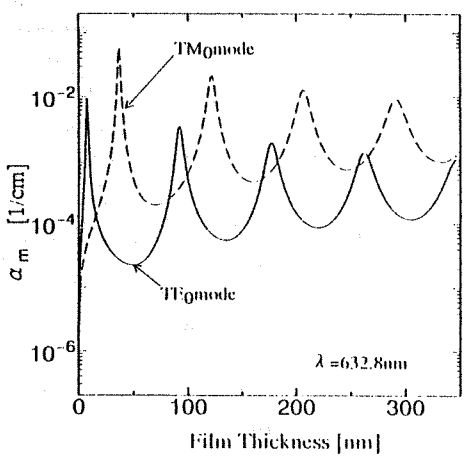

Fig. 2. Dependence of α_m on d for the TE_0 and TM_0 modes.

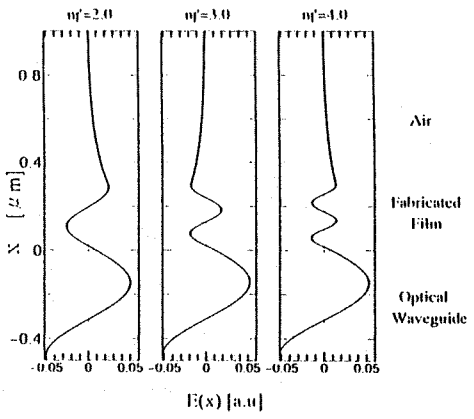

Fig. 4. Field strength distributions for the TE_{300} mode at $n'_f = 2.0$, 3.0 and 4.0 around a film of 300 nm in thickness and $\lambda = 632.8$ nm.

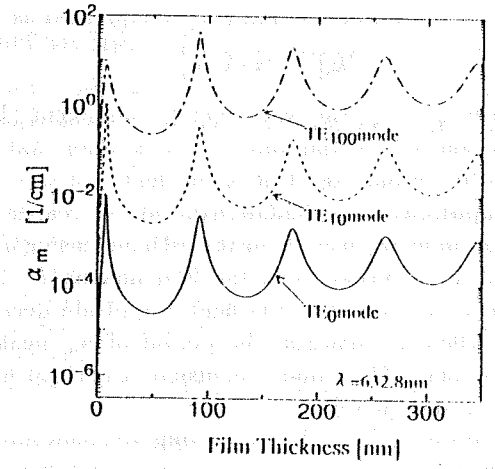

Fig. 5. Dependences of α_m on d for the TE_0, TE_{10} and TE_{100} modes.

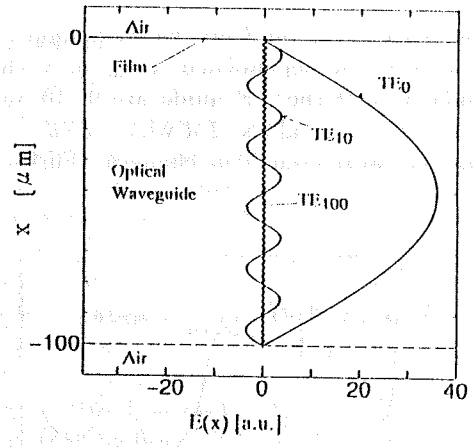

Fig. 6. Field strength distributions for the TE_0, TE_{10} and TE_{100} modes at $\lambda = 632.8$ nm.

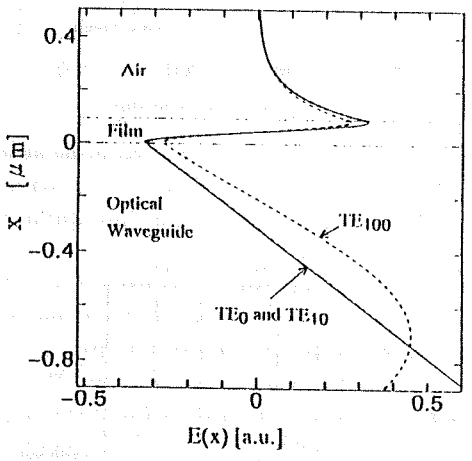

Fig. 7. Field strength distributions for the TE_0, TE_{10} and TE_{100} modes around a film of 92 nm in thickness and $\lambda = 632.8$ nm.

the value of α_m increases for higher m. α_m reaches a second peak at $d = 92$ nm. In this case, Fig. 6 shows the profiles of the field distribution at m of 0, 10 and 100 for the TE mode. The profiles of the field distribution around the film are shown in Fig. 7, since the film is very thin compared with the SOW. From Fig. 6, it is clarified that the maximum relative field strength in the SOW is smaller at the higher value of m. The maximum field strength is 35.85 in the TE_0 mode, 3.587 in the TE_{10} mode and 0.4584 in the TE_{100} mode. It is clarified that the energy distribution in the SOW becomes smaller at a higher value of m. On the other hand, it is clarified that the field distributions are almost the same in the film even if m is high in Fig. 7. Therefore, the ratio of absorption increases for higher m. α_m increases when the field distribution is smaller in the SOW and is almost the same in the film, because α_m means the equivalent absorption coefficient for the entire four-layer SOW. The same conclusion is derived for the TM mode qualitatively.

2.4 *d at which the first peak of α_m is obtained*

For the case when n_f' is 2.0, 3.0 and 4.0 and n_f'' is 0.01, 0.05 and 0.1, the film thicknesses (d_0) at which the first peak appearing in the dependence of α_m on d is obtained are shown in Table I for the TE mode of the mode number 0 and the maximum mode number of the potential guided light. The ranges of n_f' and n_f'' cover that of the silicon thin films fabricated using our MPCVD. d_0 becomes smaller when n_f' enlarges, from Table I. Furthermore, d_0 hardly changes even if n_f'' enlarges at $n_f' = 3.0$ and 4.0. However, when n_f'' is 0.1, compared with $n_f'' = 0.01$ and 0.05 at $n_f' = 2.0$, d_0 becomes smaller by approximately 0.5 nm. This means that the value of n_f'' must be considered for the film whose n_f' is small enough and n_f'' is approximately 0.1. Next, the difference of d_0 becomes appreciable as determined by comparison of the mode number of 335 with that of 0. Therefore, consideration for the higher mode number is also needed.

Table II shows the same calculation as Table I for the TM mode. The same conclusions are derived for the TM mode as for the TE mode. d_0 cannot be recognized at $n_f' = 2.0$ and $m = 335$ because the dependence of α_m on d becomes broad and the peaks disappear. The Brewster angle exists at the bound between the SOW and the film since the TM mode is the light of the p polarization. Reflection at the bound is less when the incident angle of light approaches the Brewster angle. In this case, the peaks of the dependence of α_m on d cannot be recognized. This result is agreed for the whole TM mode. In the same way, because the reflection at the bound between the SOW and the film is less when the value of the real part of the refractive index of SOW and that of the film become the same, such as $n_f' = 2.0$, many modes in which the peaks of the dependence of α_m on d

Table I. d_0 variation with n_f' and the TE_0 mode at $n_w'' = 1.457$, $t = 100\,\mu$m and $\lambda = 632.8$ nm.

n_f' / n_f''	2.0		3.0		4.0	
	TE_0	TE_{335}	TE_0	TE_{335}	TE_0	TE_{335}
0.01	48.5	42.0	14.8	14.2	7.5	7.4
0.05	48.3	41.9	14.8	14.2	7.5	7.4
0.1	48.0	41.7	14.7	14.2	7.5	7.4

Table II. d_0 variation with n_f' and the TM_0 mode at $n_w'' = 1.457$, $t = 100\,\mu$m and $\lambda = 632.8$ nm.

n_f' / n_f''	2.0		3.0		4.0	
	TE_0	TE_{335}	TE_0	TE_{335}	TE_0	TE_{335}
0.01	92.6	—	50.1	75.3	36.7	52.6
0.05	92.4	—	50.1	75.4	36.7	52.6
0.1	91.7	—	50.1	75.4	36.7	52.6

cannot be recognized exist around the Brewster angle.

3. Measurement of n_f'

We consider the first valley appearing in the dependence of transmittance on d. The SOW is set as the sensor in the MPCVD chamber. A double-tubed coaxial-line type MPCVD system[7] is used for fabrication on the SOW sensor. Figure 8 shows the detail of the sensor. The material of the SOW is fused silica (T-4040, Toshiba Ceramics). t is 170 μm and l is 15 mm. The width of the part of the SOW on which the film is deposited, w, is 18 mm. A halogen lamp light is guided as input beams, and then output beam spectra are observed. Intensities of the spectrum from 400 to 800 nm are measured during the deposition. During one scan of measurement of the spectrum, d is regarded as constant because the spectrum is measured at 0.5 s per scan while the deposition rate of the films is very low at 0.05 nm/s. The changes in d are recorded using a crystal-oscillation-type thickness monitor, and then the thickness of the film on a Si substrate placed close to the SOW is measured using a needle-tactual-type thickness meter after the deposition. The change of d during the deposition is obtained by correcting the values of the crystal-oscillation-type thickness monitor with the value of the needle-tactual-type thickness meter. For further details, readers may refer to ref. 8. a-Si:H, Si_3N_4 and silicon rich SiN which has optical characteristics intermediate between those of the former two materials are used as films. For details of the fabrications, readers may refer to refs. 7, 12, 13, 14, and 15. Sample #1 is the a-Si:H film, #2 is the silicon rich SiN film and #3 is the Si_3N_4 film. For comparison, the value of n_f' is obtained from measurement of the film on the Si substrate placed close to the sensor by the ellipsometer. Further, n_f'' is obtained from the ultraviolet visible spectroscopy spectrum of the film on a fused silica substrate placed close to the sensor.

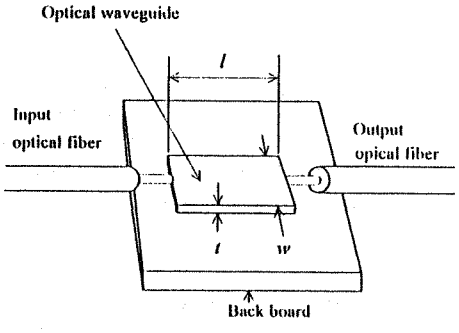

Fig. 8. Details of the SOW sensor.

We pointed out in §2.4 that the value of n_f'' must be considered for a film whose n_f' is smaller such as approximately 2.0 and whose n_f'' is larger such as approximately 0.1. For Si_3N_4, the absorption caused by the electron transition across the energy band does not exist in the visible light region (from 400 to 800 nm) in which it is clarified that E_0 is approximately 5 eV. Therefore, although the value of n_f' of Si_3N_4 is approximately 2.0 through the visible light region, n_f'' is regarded as 0. As clarified in Tables I and II, the value of n_f'' does not influence the value of d_0 in the region of our discussion, because the values of n_f' are from approximately 3 to 4 for the other two films. Therefore, for the three films discussed in this report, n_f'' can be any value from 0.01 to 0.1. We take the value of 0.029 which is obtained from the ultraviolet-visible spectroscopy spectrum for Sample #2 at 632.8 nm.

3.1 *Dependence of transmittance on d*

By the four-layer SOW simulation, the dependences of α_m on d are obtained for all the mode numbers of the potential guided light. The dependence of the transmittance T_m on d for each mode is calculated using

$$T_m = \exp(-\alpha_m \cdot l). \tag{3}$$

This procedure is performed for the TE and TM modes.

The incident light is smaller for higher modes according to the Gaussian distribution because the incident light from the light source is the Gaussian beam. Therefore, the coefficient G_m which is weighted for the mode number m is given as

$$G_m = \exp(-C \cdot m^2/M^2), \tag{4}$$

where M is the mode number of the maximum of the potential guided light. C is a constant. The value of M obtained from calculation is 569 for both the TE mode and the TM mode for $t = 170\,\mu$m.

The transmittance is defined as T_{TE} and T_{TM} to which the transmittance of the TE_m and TM_m modes are added as they are weighted for the mode number from 0 to M in

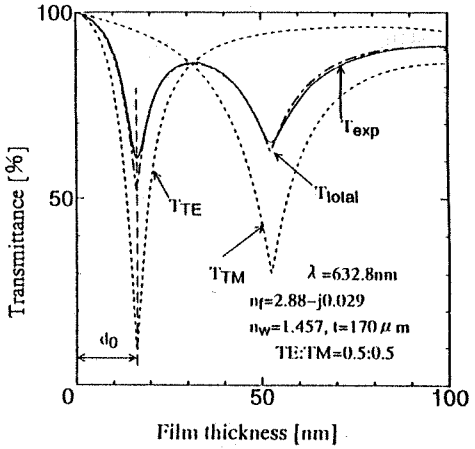

Fig. 9. Dependence of transmittance on d. T_{exp}: experimental values for sample #2; T_{TE} and T_{TM}: transmittance weighted by the mode number, by associating the mode number with the Gaussian distribution; T_{total}: total transmittance of T_{TE} and T_{TM} as 0.5:0.5.

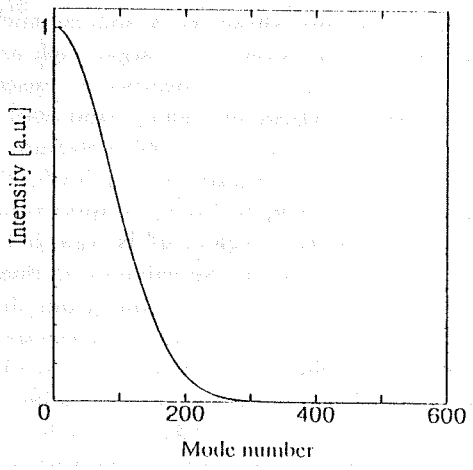

Fig. 10. Profile of the existence ratio of the transmittance weighted with the Gaussian distribution for the mode number.

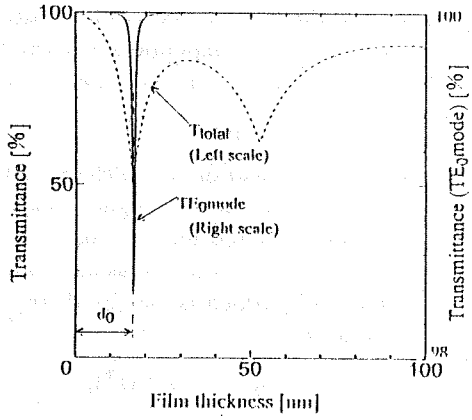

Fig. 11. Dependence of transmittance on d. T_{total}: total transmittance of T_{TE} and T_{TM} as 0.5:0.5; TE_0 mode: transmittance for the TE_0 mode.

accordance with the Gaussian distribution. T_{TE} and T_{TM} are shown as broken curves and the total transmittance T_{total} is shown as a dash-dotted curve when the existence ratio between T_{TE} and T_{TM} is assumed to be 0.5:0.5 for the addition of T_{TE} and $T_{TM} = 1$ in Fig. 9. C is 0.5×10^{-10}, by fitting of T_{total} to the transmittance T_{exp}, which is shown as the solid curve in Fig. 9 as the experimental result for Sample #2 at a wavelength of 632.8 nm. The profile of the existence ratio of the transmittance which is weighted with the Gaussian distribution for the mode number is shown in Fig. 10.

The first peak of α_m (refer to Figs. 2 and 5) is the first valley of T_{exp}, at which the value of the thickness is d_0. It is clarified that d_0 is the first valley of the TE mode from Fig. 9. The value of d_0 in T_{exp} is 16.3 nm.

From Tables I and II, the change of the value of d_0 is small through the mode numbers for the TE mode compared with the TM mode. Hence the error by misreading is smaller for the TE mode. In addition, d_0 of T_{TE} is smaller than that of T_{TM}; namely, the second valley of T_{total} in Fig. 9. n_f' for the thinner films can also be determined by considering the TE mode. Therefore, we obtain n_f' from the value of d_0 for the TE mode.

Figure 11 shows T_{total} and the transmittance for the TE_0 mode. It is clarified that d_0 corresponds to the first valley of the TE_0 mode from Fig. 11. From the calculation, it is confirmed that the values of d_0 of the transmittance for the TE_0 mode, T_{TE} and T_{total} correspond by the digit of 0.1 nm. Therefore, it is clarified that only the TE_0 mode has to be taken into account without considering higher modes. In this manner, the value of n_f' is 2.88.

Table III. n_f' from d_0 for the TE_0 mode, by the calculation and n_f' by ellipsometry, at $\lambda = 632.8$ nm.

Sample #	TE_0	Ellipsometer
1	3.45	3.49
2	2.88	2.89
3	1.80	1.81

Table III shows the values of n_f' determined using this method and the ellipsometer. The values determined using this method agree with those determined using the ellipsometer.

4. Distribution of the Refractive Index

From correspondence of the value of d_0 of the calculation for the TE_0 mode to the value of d_0 of the experiment, n_f' is obtained for the wavelength at every 50 nm between 400 nm and 800 nm. Figure 12 shows the measurement results for the three films which have different n_f'. The continuous values of the refractive index of the SOW are calculated by interpolating a quadratic function in the discontinuous values of the official refractive index data of T-4040. The measurement results of the film on the Si substrate placed close to the sensor with the ellipsometer at 632.8 nm, namely, the values in Table III, are also shown as + plots in Fig. 12.

From Fig. 12, it is clarified that the amount of fluctuation is especially large under 550 nm in Sample #1, while the amount of fluctuation is small in Samples #2 and #3. Figure 13 shows the dependence of d_0 on n_f' obtained by the four-layer SOW simulation. The solid curve is the result at a value of n_w' of 1.457 used for the experiments in this section. It is clarified from Fig. 13 that the error of n_f' becomes large when n_f' enlarges because the accuracy of d_0 by reading is constant. In the experiments, it is considered that the amount of fluctuation is large for the shorter wavelengths in Sample #1 as shown in Fig. 12 because the significant value of d_0 is the digit of 1/10 nanometer. The dependences of d_0 on n_f' are also shown in Fig. 13, when the values of n_w' are 1.522 (borosilicate glass) and 1.620 (bisphenol Z polycabonate[16]). It is clarified that the error caused by misreading at a large n_f' becomes smaller by using the smaller difference between n_w' and n_f'. Therefore, in this situation, the amount of fluctuation of n_f' is smaller when a SOW with a large n_w' is applied.

5. Conclusions

The transmittance of light guided through the SOW oscillates periodically with deposition of a silicon film on the SOW. The period of the oscillation becomes smaller when n_f' enlarges. Therefore, it was shown that the value

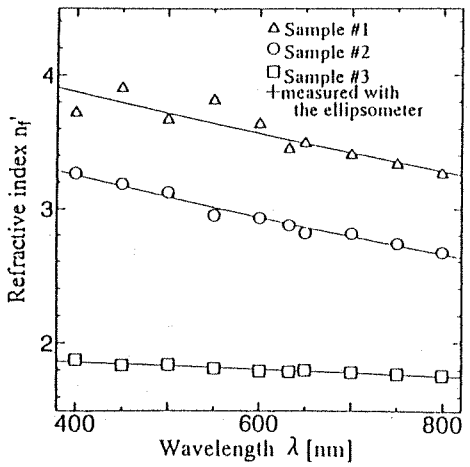

Fig. 12. Distributions of n_f'.

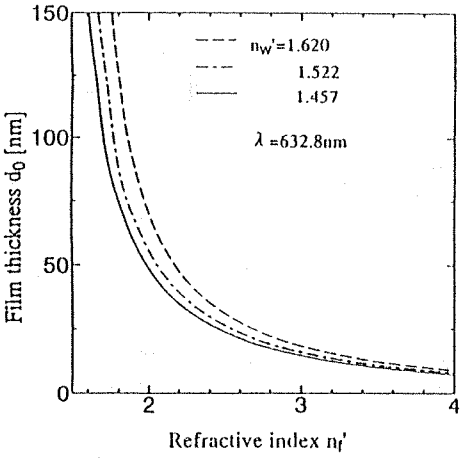

Fig. 13. Dependence of d_0 on n_f'. Broken curve: at $n_w' = 1.620$; dash-dotted curve: at $n_w' = 1.522$; solid curve: at $n_w' = 1.457$.

of n_f' can be measured by depositing a silicon thin film on a SOW whose refractive index and sizes are known. The peaks of α_m obtained from the calculation by considering all the modes of the four-layer SOW simulation, namely, the minimum film thickness d_0 by which the valleys appearing in the dependence of transmittance on d is given, correspond to d_0 for the TE_0 mode above a digit of 0.1 nm. Therefore, without considering the higher TE modes or the TM mode, it was clarified that n_f' with a thickness of 16.3 nm can be measured from the correspondence of the calculation result of the transmittance for the TE_0 mode only to the experimental value of the first valley appearing in the dependence of transmittance on d. Good agreement was obtained in comparison of the result of this method with that of the ellipsometry at a wavelength of 632.8 nm. Moreover, it was shown that the distributions of n_f' of silicon films are obtained at wavelengths of 400 to 800 nm. It was shown that the error caused by misreading d_0 can be reduced by using a SOW with a larger n_w'. As a result, the amount of fluctuation of n_f' can be reduced.

Acknowledgement

This work was supported by a Waseda University Grant for Special Research Projects in 1996 and by a Grant-in-Aid for Scientific Research from the Ministry of Education, Science, Sports and Culture.

1) M. Tatebe, T. Horiguchi, T. Kurashima and K. Ishihara: IEEE Optical Communication Conf. (1990) PD15.
2) S. Inaba, H. Kumazaki and K. Hane: Jpn. J. Appl. Phys. 34 (1995) 2018.
3) H. Tai and H. Tanaka: Opt. Lett. 12 (1987) 437.
4) Richard F. Caraon and Ted E. Batchman: Appl. Opt. 23 (1984) 2985.
5) Isamu Kato, Ryoichi Hara and Yasuyuki Sugiyama: Trans. IEE Jpn. J70-C (1987) 846.
6) I. Kato, Y. Sugiyama and K. Sugita: Trans. IEE Jpn. J71-C (1988) 68.
7) I. Kato, K. Mori and K. Sato: Trans. IEE Jpn. J75-C-I (1992) 630.
8) N. Takezawa and I. Kato: Jpn. J. Appl. Phys. 35 (1996).
9) R. Swanepoel: J. Phys. E 16 (1983) 1214.
10) R. W. Collins and B. Y. Yang: J. Vac. Sci. Technol. B 7 (1989) 1155.
11) J. N. Polky and L. M. Gordon: J. Opt. Soc. Am. 64 (1974) 274.
12) I. Kato and M. Yano: Trans. IEE Jpn. J69-C (1986) 662.
13) I. Kato, T. Ueda and K. Hatanaka: Trans. IEE Jpn. J69-C (1986) 662.
14) I. Kato, Y. Kohyama and K. Nogchi: Trans. IEE Jpn. J68-C (1985) 788.
15) I. Kato, K. Noguti and K. Numada: J. Appl. Phys. 62 (1987) 492.
16) T. Kurokawa, N. Takato and Y. Katayama: IEICE Tech. Rep. (1979) OQE79-107.

P1-31

Fabrication of SiN Film by Using Coaxial Line Type MPCVD System with a Longitudinal Magnetic Field

Xuantong Ying* Yoshinori Morita, Taro Kamiko, and Isamu Kato
Department of Electronics and Communication, School of Science and Engineering
Waseda University, 3-4-1 Ohkubo, Shinjuku-ku, Tokyo 169, Japan
* exchange professor from Fudan University, Shanghai 200433, P.R.China

A double tubed coaxial line type MPCVD (Microwave Plasma Chemical Vapor Deposition) system with a longitudinal magnetic field has been developed for high quality SiN film deposition. The deposition rate of the film was increased because of the confinement and the enhancement of the microwave plasma due to the electrical and magnetic interaction. The experimental results and discussion are reported

1. Introduction

SiN films have been widely used in integrated circuits as inter layer insulator, gate insulator etc. In order to deposit high quality SiN films with a reasonable deposition rate under low substrate temperature a double tubed coaxial line type MPCVD (Microwave Plasma Chemical Vapor Deposition) system with a longitudinal magnetic field has been developed.[1-4]

The plasma density could be increased and uniformed by the electrical and magnetic interaction. The magnetic field confines the plasma ions and electrons, depresses their diffusion from the center part to the wall of the discharge tube. Then a strong uniform and stable plasma could be remained during the deposition time. Therefore the dissociation of the source gas (SiH_4) and the deposition rate of SiN film could be increased comparing with those parameters without the magnetic field.

The experimental system, conditions, results and discussion are reported.

2.Experiment

The experimental system is shown as in Fig.1. The SiH_4 gas was mixed with N_2 plasma and dissociated on the end of the inner tube. The distance from the end of the discharge tube to the end of the inner tube is defined as z. The z could be -1.0~+1cm in our experiment.

A longitudinal magnetic field was applied on the microwave plasma by setting a coil with a current I on the cylindrical cavity in this system. A strong, uniform and stable plasma blew off into the deposition chamber. The high quality SiN film was deposited on the substrate. The distance between the substrate and the end of the discharge tube was 10 cm.

The experimental conditions are shown as in table 1

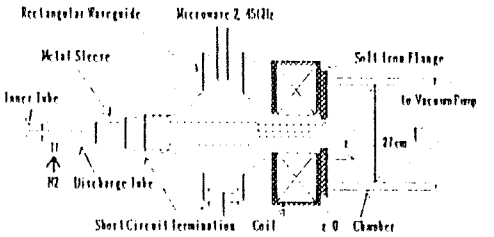

Fig. 1. Experimental Apparatus

Table 1 Experimental conditions

microwave input power	200 W
microwave reflection power	20 W
N_2 gas flux rate	115 ml/min
SiH_4 gas flux rate	5 ml/min
chamber pressure	3.4 mtorr
current in the coil	0-15 A
magnetic flux density at the center of the coil	0-2637 Gauss
position of the inner tube z	-1.0-1 cm
temperature of the substrate	R.T.

The plasma parameters like electron density and temperature were measured by a single probe.[5] The SiN film thickness and the deposition rate were measured and calculated by a needle thickness monitor. The film refractive index was measured by an ellipsometer. Other characteristics like the contents of N-H bonds, Si-H bonds and Si-N bonds were measured and calculated by the infrared absorption spectrum. The dangling bond density was measured by the electron spin resonance spectrum. The optical energy gap was measured by the UV absorption spectrum.

3.Experimental results and discussion

Fig. 2 shows the dependence of the electron density on the magnetic field at z=1cm. The electron density was increased with increasing of the magnetic field rapidly from about 600 Gauss to about 1000 Gauss because of the electrical and magnetic

interaction. The magnetic field confined the plasma ions and electrons, depressed their diffusion from the center part to the wall of the discharge tube. Then a strong uniform and stable plasma could be remained during the deposition time while the magnetic field kept around 1000 Gauss[4]. The electron density saturated when the magnetic field was over 1000 Gauss.

Fig.3 Shows the dissociation of the source gas SiH_4 vs. magnetic field. It is clear that when the magnetic field was kept around 1000 Gauss, the source gas was dissociated in the confined and enhanced plasma much more than that without the magnetic field. Therefore the SiN film deposition rate would be much high as shown in Fig. 4 in above mentioned confined and enhanced plasma.

All the characteristics of the film deposited in this new system with the longitudinal magnetic field, like refractive index ,the contents of N-H bonds, Si-H bonds and Si-N bonds, the dangling bond density and the optical energy gap did not change much comparing with those without the magnetic field. But the deposition rate could be increased much more.

The further detail is being investigated and will be reported later.

Aknowlegement:

This work was partially supported by The Grant-in-Aid for scientific Research from the Ministry of Education, Science, Sports and Culture. The authors would like to thank Mr. H. Yamamoto for his assistance in this work.

References:

[1] K.A.Budde, J. Rodgers, K. Pastor, C. Constantine, and D. Johnson, "Electron Cyclotron Resonance Plasma deposition of Silicon Nitride: Effefect of Very Low rf Substrate Bias," Appl. Phys. Lett., vol. 60, no. 21, pp. 2001-2003, May 1992.

[2] I. Kato, S. Wakana, and S. Hara, "Microwave Plasma CVD System to Fabricate a-Si Thin Films of Plasma," Jpn. J. Appl. Phys., vol. 22, no. 1, pp. L10-L12, Jan. 1983

[3] I. Kato, K. Noguchi, and K. Numada, "Preparation of Silicon Nitride Films at Room Temperature Using Doubled-Tubed Coaxial Line-Type Microwave Plasma Chemical Vapor Deposition System," J. Appl. Phys., vol. 62 , no. 2, pp.492-497, July. 1987.

[4] Y. Manabe and T. Mitsuyu, "Silicon Nitride Thin Films Prepared by the Electron Cyclotron Resonance Plasma Chemical Vapor Deposition method," J. Appl. Phys., vol. 66, no. 6 , pp. 2175-2180, Sept. 1989

[5] I. Kato, T. Sakamoto, and T. Shimoda: "Method of Probe Measurement in N_2/SiH_4 Microwave Plasma," Jpn. J. Appl. Phys., vol.33, no. 1A, pp.307-310, Jan. 1994

[6] I. Kato, T. Kamiko, Y. Morita, T. Ando, "Influence of Longitudinal Magnetic Field Applied to Coaxial Line Type Microwave Plasma (IV)," to be presented at 3rd International Conference , Jann. 21-24,1997. Nara-Ken New Public Hall Nara, Japan.

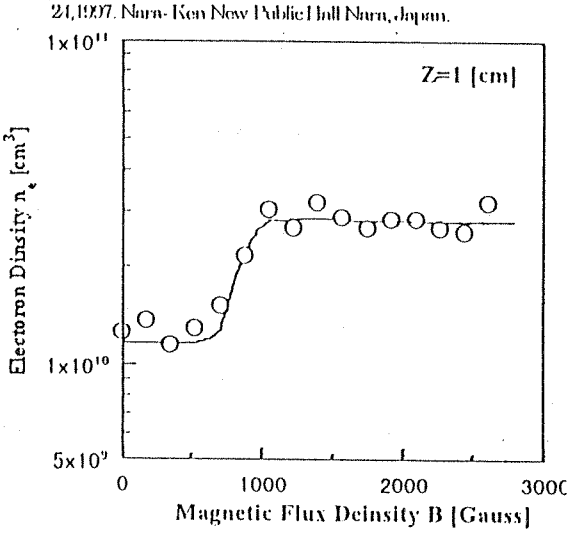

Fig2. Dependence of electron density on magnetic flux density

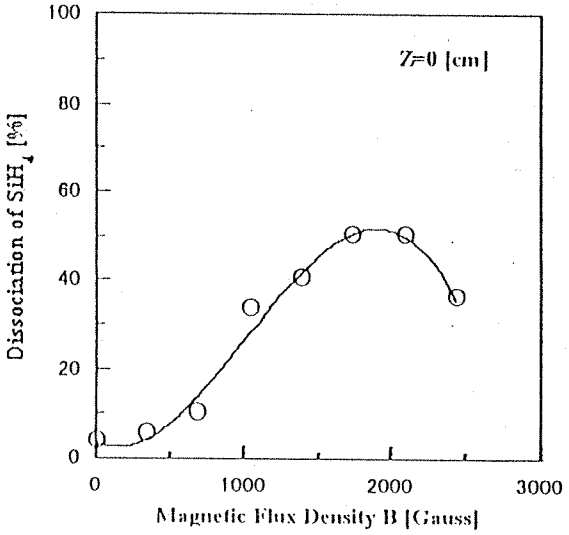

Fig 3. Dependence of dissociation of SiH_4 on magnetic flux density

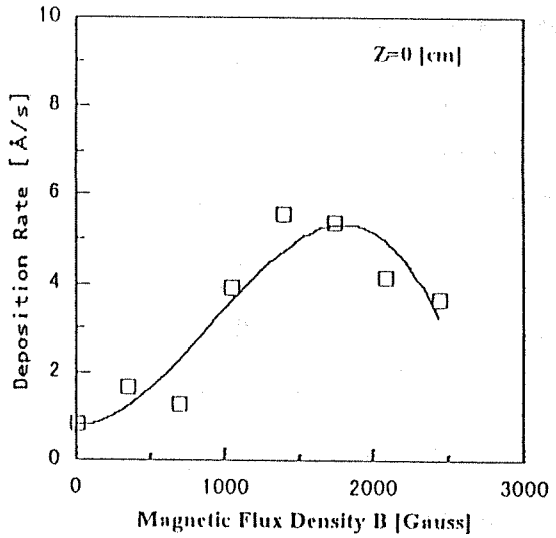

Fig.4 Dependence of deposition rate on magnetic flux density

P3-12

Influence of Longitudinal Magnetic Field Applied to Coaxial Line Type Microwave Plasma(IV)

Taro Kamiko, Yoshinori Morita, Tadahiko Ando and Isamu Kato

Department of Electronics and Communication, School of Science and Engineering, Waseda University, 3-4-1 Okubo, Shinjuku-ku, Tokyo 169, Japan

In the double tubed coaxial line type microwave plasma chemical vapor deposition system, a magnetic field along the gas flow is applied to the plasma, and the effects of applying longitudinal magnetic field to the plasma is considered. The spatial distributions of electron density in the discharge area are measured by a single probe method. It is determined that radial distribution of electron density at the discharge area is uniform, and the plasma inside of the discharge area extends keeping the density constant to the vicinity of the place where plasma blows off into the deposition chamber. Therefore, uniform and stable plasma which is proper for CVD system is generated by applying a magnetic field.

1. Introduction

In the double tubed coaxial line type microwave plasma chemical vapor deposition system, in order to generate the stable plasma in a wider range of gas pressure and with various kinds of gases, a magnetic field along the gas flow (longitudinal magnetic field) is applied to the discharge area, and the effects of applying longitudinal magnetic field to plasma have been considered by a single probe method. The plasma parameters of N_2 plasma have been measured in the deposition chamber and the effects of applying a magnetic field have been considered. And it was determined that the stability of the plasma is improved[1] and electron density can be increased by a few times with magnetic field over about 1000Gauss in the vicinity of the place plasma blows off into the deposition chamber[2]. In this report, the spatial distribution of plasma parameters in the radial and axial direction in the discharge area are measured by the single probe method and the effects of applying such a magnetic field are considered.

2. Experiment

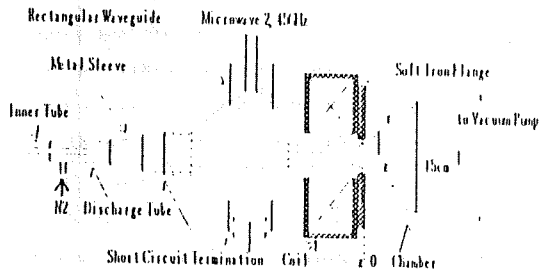

Fig. 1. Experimental Apparatus

Figure 1 shows experimental setup. The coil is set up around the discharge area, and a magnetic field along the gas flow is applied. Spatial distribution of electron density in the discharge area is measured by single probe method and the effect of applying such a magnetic filed is considered. The axial distance from the end of the discharge tube is defined as z and the radial distance from the center axis of the discharge tube is defined as r. The details of this system was reported in our previous work[3].

The experimental conditions are shown in Table I. An experimental condition in which a good quality of SiN thin film is fabricated when magnetic field is 0Gauss and SiH_4 gas flows in the inner tube is used. Single probe method is used in the measurement. The probe is a round plate which is 1mm in diameter. The surface of the probe is set up perpendicularly to the magnetic filed so that the influence of the magnetic field on the probe I-V characteristic is minimized. Points of the measurement are every 5mm between z = -15mm and z = 5mm, and at each z, r = 0,4,8mm.

Table I. Experimental Condition

Discharge Gas	N_2
N_2 Gas Flow Rate	50ml/min
Microwave Input Power	150W
Microwave Reflective Power	45W
Gas Pressure in Chamber	4.0mTorr
Coil Current	0～6A
Magnetic Field (at the center of the coil)	0～1986Gauss
Position of Inner Tube End	z = -20mm

3. Result and Discussion

Figure 2 shows the dependence of the electron density on magnetic field at z = 5mm.It is shown that electron density increases with increasing magnetic field from about 600Gauss to about 1000Gauss. Because the diffusion of the plasma toward the wall of the discharge tube is depressed, therefore, the decay of the plasma on the wall are depressed. The electron density saturates over

about 1000Gauss. Therefore, by applying a magnetic field over about 1000Gauss, electron density can be increased by a few times in the vicinity of the place the plasma blows off into the deposition chamber. And it can be said that those plasma is proper for CVD system because it is possible to fabricate films at a high rate. Figure 3 and 4 show the dependences of the electron density on magnetic field at z = 0,-10mm. Figure 2, 3 and 4 show electron density under about 600Gauss at z = 0 or 5mm are lower than that at z = -10mm, but over about 1000Gauss those electron densities are almost the same. The reason is as following. At z = -10mm electron density is high and stable regardless of magnetic flux density and doesn't fluctuate so much(as shown in Fig.4). On the contrary, at z = 0mm electron density is low and unstable, and fluctuates when magnetic flux density is under about 600Gauss (as shown in Fig.3), and the same tendency is shown at z = 5mm. Those fluctuation are suppressed by applying a magnetic field.

Figure 5 shows the dependence of electron density on r. The saturated value of the electron density vs. magnetic field are averaged when magnetic field is over about 1000Gauss. At each z, radial distribution of electron density is not the shape like as described as J_0 Bessel function but the shape like as trapezoid. Because the discharge is done by the microwave that propagates plasma as the fundamental mode of coaxial line. It means uniform plasma in radial direction can be generated.

The further details including the tendency of electron temperature will be reported later.

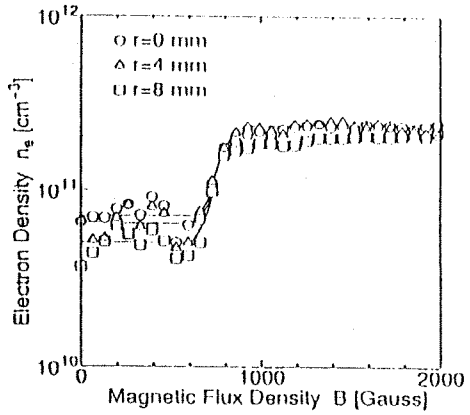

Fig. 2. Dependence of Electron Density on Magnetic Field (z = 5mm)

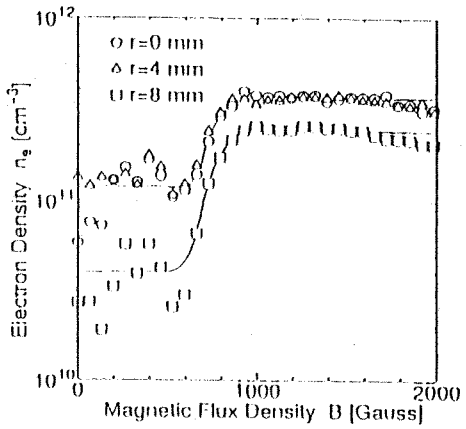

Fig. 3. Dependence of Electron Density on Magnetic Field (z = 0mm)

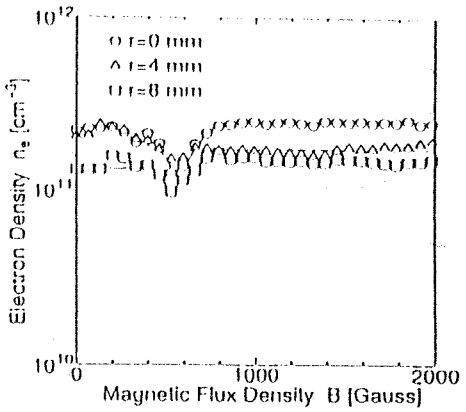

Fig. 4. Dependence of Electron Density on Magnetic Field (z = -10mm)

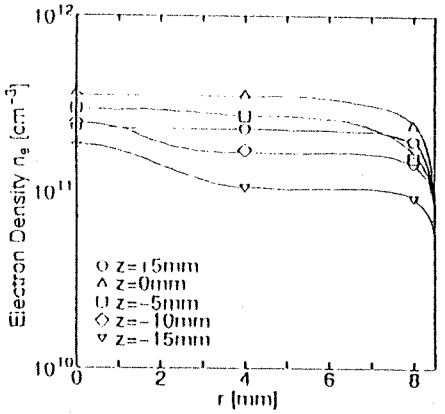

Fig. 5. Dependence of Electron Density on r (B ≧ 993 Gauss)

References

[1] T.Kamiko et al: The 57th Autumn Meeting of Jpn. Soc.Appl.Phys.,19p-ZV-15(1996)

[2] T.kamiko et al: The 13th Symposium on Plasma Processing, IAI-4(1996)

[3] T.Yamagishi et al: The 12th Symposium on Plasma Processing, I-A06(1995)

IVa-6

Separation of Film Surface Heating Effect and Ion Implanting Effect

Hirotaka Ogihara , Hidetaka Iizuka , Nobuyuki Koshiji and Isamu Kato

Department of Electronics and Communication , School of Science and Engineering , Waseda University , 3-4-1 Ohkubo , Shinjuku-ku , Tokyo 169 , JAPAN

Generally in a plasma CVD method , a substrate table is placed in the discharge plasma and films are fabricated under the ion bombardment. We have studied influences of the ion bombardment on a-Si:H films and clarified that an ion bombardment has a film surface heating effect and other effects (ion implanting effect) in films [1]. Even if the ion bombardment is increased , it is impossible to discuss whether film properties become good or not. In this paper , the film surface heating effect and the ion implanting effect of the ion bombardment are separately studied and discussed .

1.Introduction

We have developed the double tubed coaxial line type microwave plasma CVD (MPCVD) system to deposite a-Si:H films. In this paper , in order to study the ion implanting effects on a-Si:H films the dependence of the film properties on sheath voltage (V_{sh}) without heating substrate table and the dependence of the film properties on the substrate temperature (T_s) without the ion bombardment are measured [2]. The dependence of film properties on T_s is equivalent to that on the film surface heated by the ion bombardment effect. By subtracting the dependence of film properties on T_s from the dependence of film properties on V_{sh} , the ion implanting effect is left. Hence we try to put two axes together from the two figures of the dependence of Si concentration on T_s and V_{sh} , then the Si concentration in the film seems to be influenced by only the film surface heating effect. In the dependence of other film properties , two axes are put together in the same way and the film surface ion bombardment heating effect and the ion implanting effect have been separated.

2.Experiment

Figure 1 shows the configuration of the MPCVD system. The axial distance from the discharge tube end is defined as z. The substrate table area is 40 cm^2 and is placed at z=10 cm. Ar gas flow rate is 110 ml/min and SiH_4 gas flow rate is 30 ml/min. When DC substrate bias voltage (V_{dc}) is varied from +40 V to -80 V , V_{sh} can be controlled from 0 V to -95 V. The dependence of V_{sh} on V_{dc} has been measured by single probe method. The probe of 0.05 cm in diameter and 1 cm in length is used. The

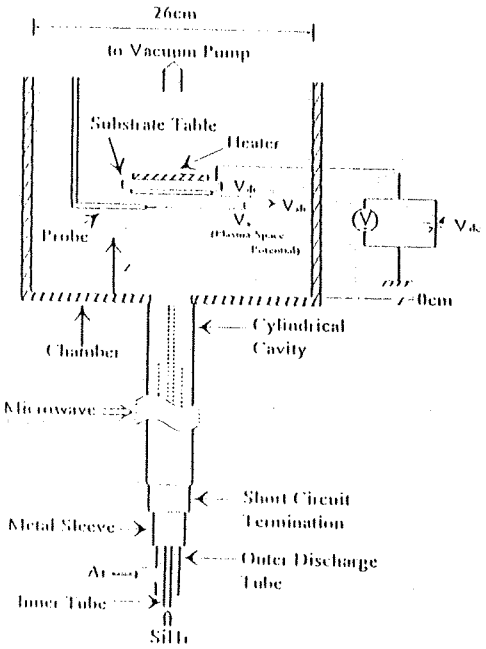

Fig.1 Configuration of the MPCVD system

measurement was performed at z=9 cm. In the case of the film property dependence measurement on T_s, V_{sh} is 0 V (namely V_{dc} is +40 V) and T_s is varied from R.T. to 250 ℃.

3.Result and Discussion

The dependence of Si concentration on T_s (at V_{sh}=0 V)and the dependence of Si concentration on V_{sh} (at T_s=30 ℃) are shown in Fig.2. In this figure the Si concentration at V_{sh} = 0 V and that at T_s = 30 ℃ must be the same because they are deposited at the same condition. Because the ion implanting dose not change the Si concentration of the film, considering only the film surface heating effect , we can adjust the unit of T_s axis to fit the Si concentration at T_s = 250 ℃ to that at V_{sh} = -95 V. By this way a linear relationship between T_s and V_{sh} is obtained as following experience equation.

$$T_s = -2.3158\ V_{sh} + 30$$

After two axes are put together in this way , the dependence of two other a-Si:H film properties on T_s and V_{sh} is shown in Fig.3 and Fig.4. The arrows in Fig.3 and Fig.4 , namely the difference of two curves , shows the amount of the ion implanting effect. The dependence of SiH concentration on T_s and V_{sh} is shown in Fig.3. From the figure the concentration of SiH bond increases by the ion implanting effect in the range of V_{sh} < -40 V because the hydrogen ions accelerated by V_{sh} are implanted in film. The dependence of dangling bond density on T_s and V_{sh} is shown in Fig.4. From the figure dangling bond density increases by the ion implanting effect because the Ar ions are implanted and cut bonds in film.

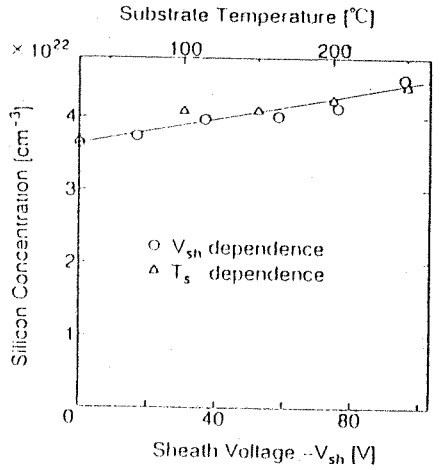

Fig.2. Dependence of Si concentration on T_s and V_{sh}

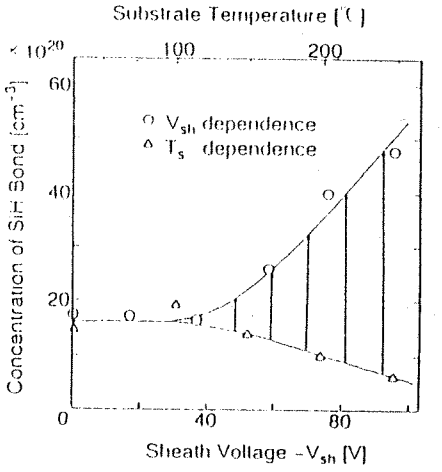

Fig.3. Dependence of SiH concentration on T_s and Vsh

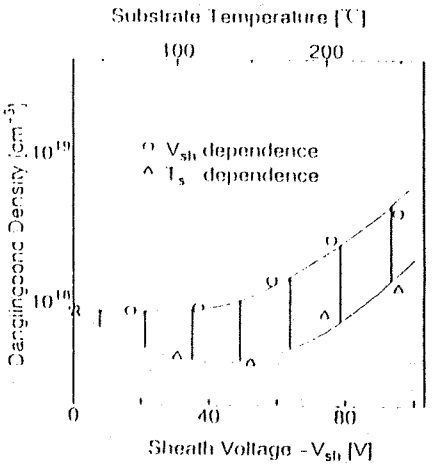

Fig.4. Dependence of dangling bond density on T_s and Vsh

References

[1]H.Kato,T.Yoneda and T.Matsushita:Trance.IEICE. C-II,J77,9,384-391(1994)

[2]M.Yamashita,H.Ogihara and I.Kato:*Proc. 13th Sympo.Plasma Processing*,109(1996)

P1-33

In situ Measurement of Change of Ultra Thin Films in Elapsed Time Using Optical Fiber Sensors

Naganori Takezawa, Nobuyuki Koshiji and Isamu Kato

Department of Electronics and Communication, School of Science and Engineering, Waseda University, 3-4-1 Ohkubo, Shinjuku-ku, Tokyo 169, Japan

An *in situ* measurement method of change of ultra thin a-Si:H films with passage of time by leaking from vacuum to atmospheric air will be shown. a-Si:H film with approximately 10 nm in thickness is deposited on the core of an optical fiber sensor whose part of the clad is removed. The film is changed by oxidation and the oxidation saturates in approximately 600 s. The larger attenuation of translated light maybe due to the change of defects by relaxation at the long wavelengths from 685 to 800 nm is observed.

1. Introduction

In thin film fabrication, the change of the films just after a leak by atmospheric air was not measured when fabrications were finished. The measurement of the surface oxidation layer of thin films was usually obtained by executing the etching of the surface and measurement of the X-ray photoelectron spectroscopy alternatively after leaking by atmospheric air and putting the films out of a fabrication chamber. In this case, the film surface oxidation progress measurement of change in elapsed time after the leak from vacuum to atmospheric air is not completed.

We have studied a method to measure the dependence of the light transmittance on the film thickness with depositing films on an optical fiber whose part of the clad is removed as a sensor for the measurement of the optical constants of ultra thin films deposited with the Plasma CVD. During the deposition of films in the plasma CVD system, the transmitted light which goes through the sensor decreases exponentially with periodic oscillation corresponding to the increase of film thickness. The reason is that the electric field strength concentrates periodically in the film. By removing the oscillation mathematically, we determined the optical energy gap[1]. Then, we also determined the refractive index from the value of the first valley in the oscillation or the period of the oscillation[2,3]. In our new method, we have been able to measure the optical energy gap of the ultra thin a-Si:H film with approximately 20 nm in thickness which is about 1/40 comparing with what in the conventional method and the refractive index of the ultra thin a-Si:H film with approximately 10 nm in thickness[1,2]. The sensitivity of the sensor is increased more by decreasing the diameter of the optical fiber and / or increasing the length of the film deposited part.

In this report, using this optical fiber sensor in the a-Si:H fabrication, we show an *in situ* measurement method of change of ultra thin films with passage of time just after the leak of atmospheric air.

2. Experimental Setup and the Optical Fiber Sensor

Our experimental setup - the double-tubed coaxial-line-type microwave plasma CVD

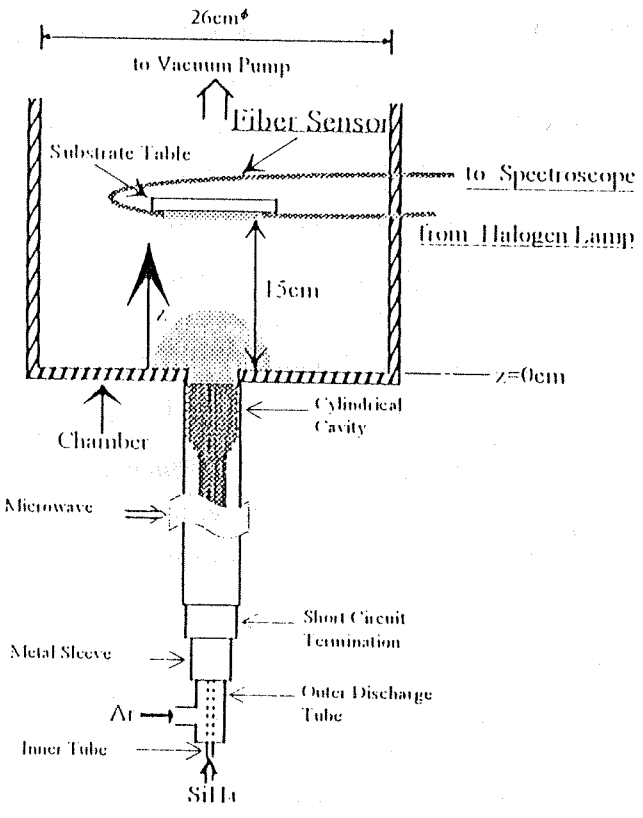

Fig. 1. Experimental setup. with our optical fiber sensor.

system is shown in Fig. 1[4]. As shown in Fig. 1, a-Si:H is fabricated from SiH_4 by using Ar plasma flowing from the bottom side of the system.

The optical fiber sensor is set on the substrate table in this chamber. The input port of the optical fiber is connected with a halogen lamp light source and the output port is connected with a spectrum analyzer. Transmitted light is measured in about 10 minutes after the fabrication.

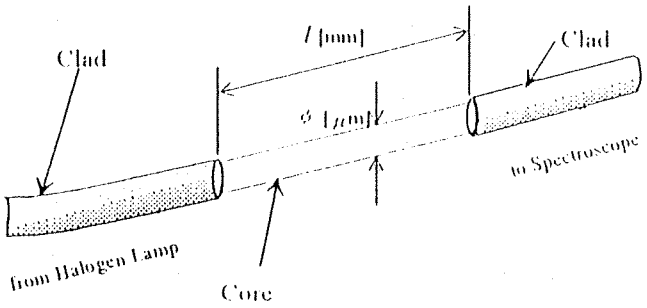

Fig. 2. Details of the optical fiber sensor.

Figure 2 shows the optical fiber sensor structure. This is a step index type optical fiber with silica core and polymer clad. The clad is removed for deposition of a-Si:H films. The length of the clad removed part is l [mm] and its diameter of the core is ϕ [μm].

3. Result and Discussion

Using the optical fiber sensor, whose length of the film deposited part l is 100 mm and diameter of the core ϕ is 110 μ m, a-Si:H film with approximately 10 nm in thickness is fabricated on the optical fiber sensor. The film change by oxidation is measured *in situ*. The period to take the leak of the CVD chamber from vacuum to atmospheric air is approximately 20 s.

Figure 3 shows the change of light transmittance through the optical fiber sensor with passage of time at wavelengths of 800, 750, 700 and 685 nm. From Fig. 3, it is clarified that the transmittance at every wavelength decreases after leaking the CVD system and it saturates in approximately 600 s. It is considered that the film is changed by oxidation and the oxidation saturates around 600 s. By comparing the rate of the change of transmittance among the wavelengths, it is clarified that the large rate of the change occurs at long wavelengths. It was reported that defects are changed by relaxation by the bias light in the region of 0.8 eV $< h\nu <$ 1.8 eV for a-Si:H because of the shift of the quasi-Fermi-level to the conduction band or an increase in the concentration of dangling-bond centers D^-[5,6]. The result in this experiment shows the similar tendency to the dependence of the absorption coefficient on energy owing to the change of defects described in above references. We consider that the similar phenomena occur by oxidation in the high energy side of the Urback tail region (1.5 eV < h ν < 1.8 eV). The more specific discussion will report at the presentation.

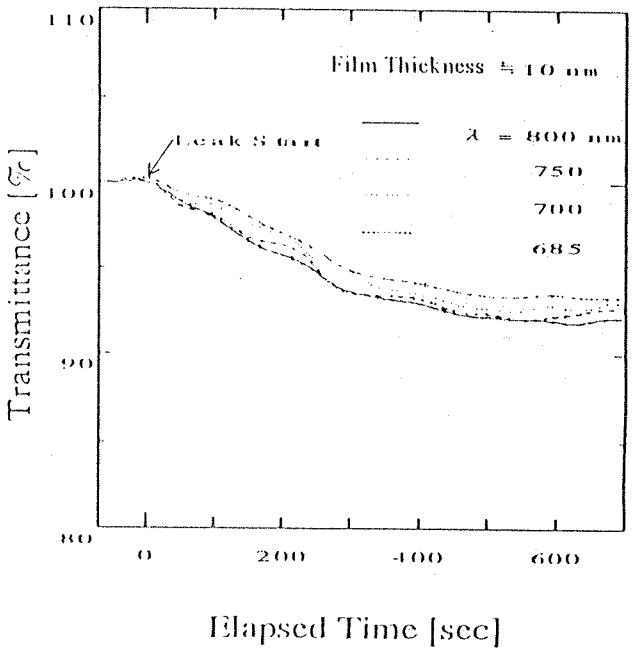

Fig. 3. Transmittance change with passage of time.

Acknowledgment

This work was supported by the Waseda University Grant for Special Research Project in 1996.

References

[1] N. Takezawa and I. Kato: Jpn. J. Appl. Phys. 35 (1996) 2826.

[2] S. Nojima, N. Takezawa, K. Hotta and I. Kato: *Extended Abstracts Spring Meeting of IEICE in 1995*, C (1995) p. 270 [in Japanese].

[3] S. Nojima, N. Takezawa, K. Hotta and I. Kato: *Proc. 12th Sympo. Plasma Processing*, ed. T. Makabe Div. Plasma Electronics, Jpn. Soc. Appl. Phys., Sendai, (1995) p. 325.

[4] I. Kato and M. Yano: Trans. IEE Jpn. J69-C (1986) 662.

[5] A. G. Kazanskii and E. P. Mifichevich: Sov. Phys. Semicond., 19 (1984) 323.

[6] S. Lee, S. Kumar, C. R. Wronski and N. Maley: J. Non-Cryst. Solids, 114 (1989) 316.

論　文

二重管式同軸線路形マイクロ波プラズマＣＶＤにおける N_2／ＳｉＨ$_4$プラズマのパラメータの空間分布

正　員　加藤　勇（早稲田大）
非会員　下田　毅（早稲田大）
非会員　山岸俊浩（早稲田大）

Spatial Distribution of Plasma Parameter in N_2/SiH_4 Plasma
in Double Tubed Coaxial Line Type Microwave Plasma CVD System

Isamu Kato, Member, Tsuyosi Shimoda, Non-Member,
Toshihiro Yamagishi, Non-Member (Wasada University)

We have comfirmed the new method of probe measurement in N_2/SiH_4 plasma. Using this method, we have measured the spatial distribution of plasma parameters such as electron temperature Te, electron density n_e, plasma space potential Vs, floating potential Vf and sheath voltage Vs-Vf with varying the gas flow rate of SiH_4 in the chamber of the double tubed coaxial line type microwave plasma CVD (MPCVD) system. In this paper, we report the spatial distribution of these plasma parameters in the chamber of this MPCVD system. And it is cleared that the plasma is very uniform in the chamber.

キーワード：マイクロ波プラズマ、プラズマパラメータ、シングルプローブ法、イオンボンバードメント、空間的アフターグロープラズマ

1．まえがき

プラズマを用いた化学気相堆積（ＣＶＤ）法の研究は現在盛んに行われており、水素化アモルファスシリコン（ａ－Ｓｉ：Ｈ）膜や窒化シリコン（ＳｉＮ）膜をはじめ各種の薄膜の作製に用いられている。一般に良く用いられている高周波プラズマＣＶＤ法では、電力が供給されているプラズマ（放電プラズマ）内で膜を作製しているため、膜表面は常にイオン衝撃にさらされているという問題が生じる。そこで筆者らは、イオン衝撃を抑えるために、マイクロ波を円筒キャビティ内に閉じ込めて、堆積室内には電力注入のないプラズマ（空間的アフターグロープラズマ）を生成できる二重管式同軸線路形マイクロ波プラズマＣＶＤ装置の研究開発を行ってきた[1]。また、本装置におけるプラズマは、イオンがマイクロ波の電界に追従できないためにイオン温度の低いコールドプラズマとなる。このような特長を持つ本装置の堆積室内においては、前述の空間的アフターグロープラズマ中で、またコールドプラズマ中で成膜が行われるので、膜表面へのイオンボンバードの少ない良質なａ－Ｓｉ：Ｈ膜やＳｉＮ膜が作製されることが期待できる。また、イオンボンバードがないことで膜表面が加熱されないため、低融点物質上に膜を堆積させることができる[2]。

また、多くの研究機関で行われているプラズマＣＶＤ法に関する研究は、ガス流量、ガス圧、電力などの外部から単独に直接制御可能な外部的プラズマパラメータを変化させて作製した膜の電子材料としての性質や、その応用上の良否について論じている。しかしながら、このような外部的プラズマパラメータは、装置の寸法や構造によって、その最適値が異なるので、これに基づいて、本質的な成膜機構を議論、解明することはできない。すなわち、電子温度、電子密度、プラズマ空間電位などの、外部から単独に直接制御できない内部的プラズマパラメータを測定し、これに基づいて、成膜機構を検討しなければならない。

このような内部的プラズマパラメータの測定には、ラングミュア・プローブ法が簡便かつ空間的分解能にすぐれた方法として知られている。しかしながら、シラン系ラジカルを含む反応性プラズマ中におけるプローブ測定では、プローブ上に膜が堆積して、その影響がプローブ電流電圧特性（I_p－V_p特性）に現れる。そこで、正常な測定を行うためには、新たな工夫を要する。筆者等はこれまでに、導電性膜である、良質なａ－Ｓｉ：Ｈ膜を堆積させることができるＡｒ／ＳｉＨ$_4$プラズマ中で、正常なプローブ測定を可能とする測定条件とその方法を明らかにしてきた[3]。その上で、二重管式同軸線路形マイクロ波プラズマＣＶＤ装置の堆積室内でのＡｒ／ＳｉＨ$_4$プラズマ中のプラズマパラメータの空間分布を測定により明らかにした[4]。

また、絶縁性膜であるＳｉＮ膜を堆積させることができるN_2／ＳｉＨ$_4$プラズマ中において従来のプローブ法によ

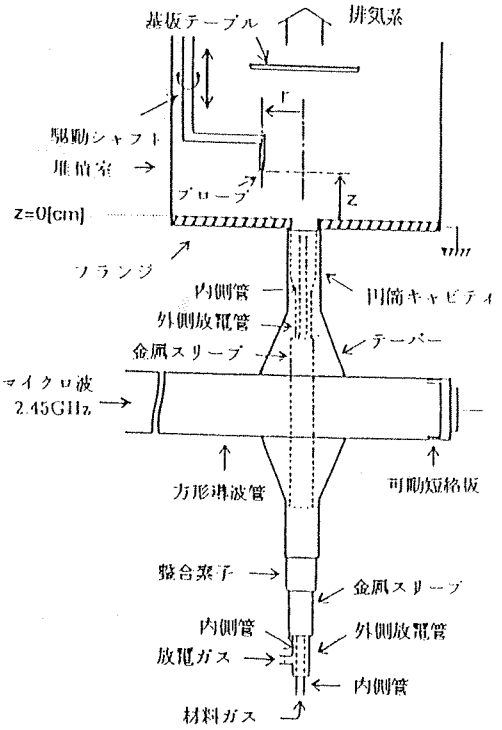

図1　二重管式同軸線路形マイクロ波プラズマCVD装置

Fig. 1 Double Tubed Coaxial Line Type Microwave Plasma CVD System

り測定を行う場合、Ar／SiH₄プラズマ中における測定と同様にプローブ表面にSiN膜が堆積してしまうため、正常なプローブI_p-V_p特性が得られないという問題が生じる。この問題を解決するために当研究室では、N_2／SiH₄プラズマ中での新しいプローブ測定法について明らかにしてきた[5]。本論文では、この方法を用いて、同装置の堆積室内におけるN_2／SiH₄プラズマ中の電子温度、電子密度、プラズマ空間電位などのプラズマパラメータの空間分布を、SiH₄ガス流量を変化させて測定した結果について報告することを目的とする。

2．実験

実験には、図1に示す二重管式同軸線路形マイクロ波プラズマCVD装置[6][7]を用いた。プラズマ生成条件として、マイクロ波電力を270［W］一定とした。外側放電管には放電ガスとしてN_2ガスを流し、ガス流量は140［ml/min］と一定とした。内側管には材料ガスとしてSiH₄ガスを流し、ガス流量は0～50［ml/min］まで変化させた。また比較のために、内側管にSiH₄ガスの代わりにN_2ガスを流し、ガス流量を0～50［ml/min］まで変化させた。なお、ガス流量の測定時の圧力は1［atm］とした。堆積室内のガス圧は、

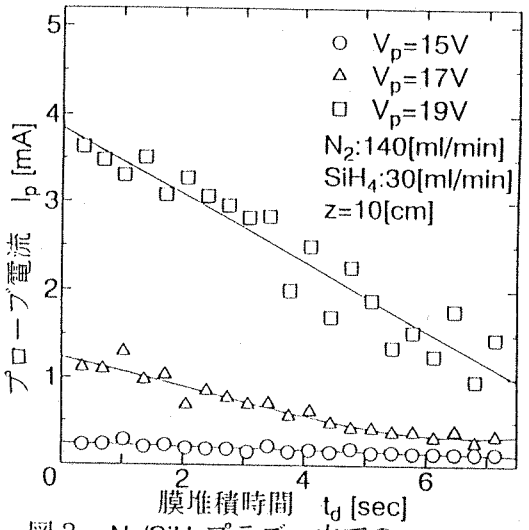

図2　N_2/SiH_4プラズマ中でのプローブ電流の膜堆積時間依存性

Fig. 2 Dependence of Probe Current on Film Deposition Time in N_2/SiH_4 Plasma

内側管に流すガス流量によって、3.3～4.3［mTorr］まで直線的に変化した。

本装置の堆積室は、内直径26［cm］の円筒形である。放電管端、すなわち堆積室のフランジの内壁面の位置から堆積室の軸方向への距離をz、中心軸からの径方向への距離をrと定義した（図1参照）。測定位置は、zは1.5～25［cm］の範囲で、rは0～10［cm］の範囲で変化させている。なお、内管端位置はチャンバー内に挿入されておらず、z＝-1.4［cm］の点とした。

3．プローブ測定法

前述のように、N_2／SiH₄プラズマのプローブ測定では、プローブ上にSiN膜が堆積するため、正常なI_p-V_p特性を得ることは単純にはできない。そこで、筆者等はN_2／SiH₄プラズマ中では図2のようにプローブ電流が膜堆積時間t_dとともに直線的に減少する領域があることに着目し、直線外挿をすることにより、膜が堆積していない場合（$t_d=0$）に得られる正常なI_p-V_p特性を得ることができることを明らかにしてきた[4]。

すなわち、N_2／SiH₄プラズマを発生させて、放電開始から一定時間間隔（340［ms］）でI_p-V_p特性を短時間（10［ms］）で測定する。取り込んだI_p-V_p特性から、あるプローブ電圧におけるプローブ電流の放電時間t_d依存性を求める（図2参照）。この図を用いて、放電時間に対するプローブ電流I_pの減少が直線となる領域より最小自乗法を用いて、放電時間が0秒での、すなわちプローブ上に膜が堆積していないときの正常なプローブ電流値I_{p0}を算出する。これを異なるプローブ電圧についても行い、正常な$I_{p0}-V_p$特性を得る。

さらに、プローブ上に堆積した厚さ45〔nm〕のSiN膜が、プローブに−200〔V〕の負バイアスを印加して、電子温度が13,000〔K〕、電子密度が5.0×10^{9}〔cm^{-3}〕の純N_2プラズマ中で約220秒間イオンボンバードを行えば除去できることを明らかにしている[13]。そこで、一連のプローブ測定ごとに、この条件でプローブ上に堆積したSiN膜の除去を行うことにより、同じプローブを繰り返し用いている。

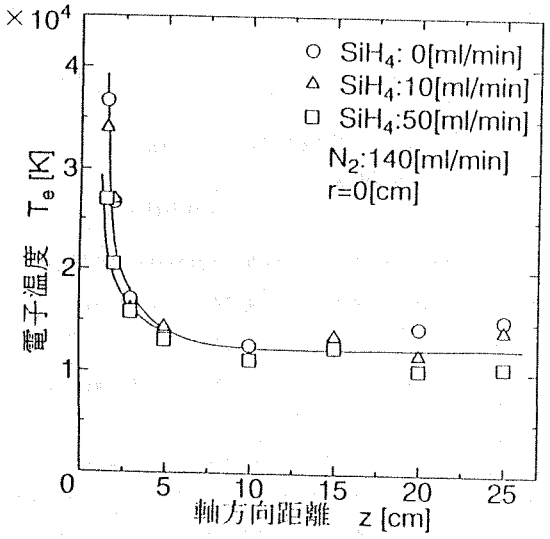

図3　電子温度のz依存性

Fig. 3 Dependence of Electron Temperature on z

4. 測定結果および考察

4.1 電子温度T_eの空間分布

図3に中心軸上（r＝0〔cm〕）の電子温度T_eの軸方向距離z依存性を示す。SiH_4ガス流量がいずれの場合も、T_eはzの増加に対して、放電管端（z＝0〔cm〕）付近で急激に減少した後、z＞5〔cm〕でほぼ一定となる。T_eの高い放電管端付近では、内側管を通して流したSiH_4分子または外側放電管を通って流出するN_2分子と電子との、電離や解離をともなう非弾性衝突周波数が高く、T_eの減少割合が大きいが、放電管端から離れT_eが低下すると、非弾性衝突断面積が小さくなるので、非弾性衝突周波数が減少し、T_eの減少割合は小さくなる。従って、SiH_4ガス流量を大きくすると高温部（z＜5〔cm〕）でT_eの減少は、よりすみやかに起こることになる。また低温部（z＞5〔cm〕）では、SiH_4ガス流量を大きくしてもT_eはほとんど変化しない。

図4にT_eの径方向距離r依存性を示す。T_eはrの増加に対して、z＝3〔cm〕では少し減少するが、z＝10〔cm〕ではほぼ一定となる。また、SiH_4ガスを増加させてもこの傾向はほとんど変化しない。図3、4より、z＞10〔cm〕の空間では、z、r方向にT_eは均一であることが分かる。

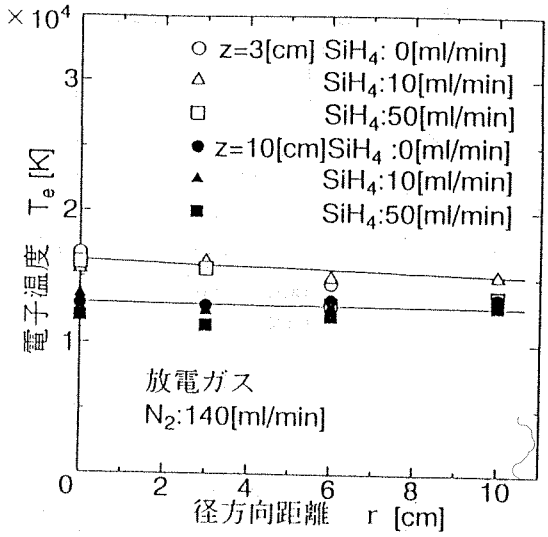

図4　電子温度のr依存性

Fig. 4 Dependence of Electron Temperature on r

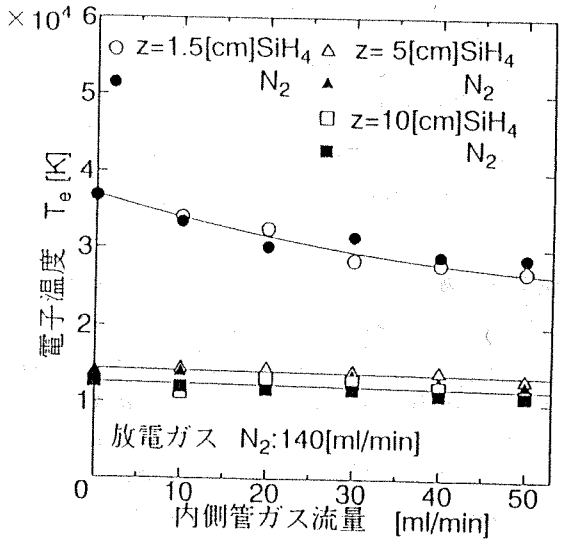

図5　電子温度の内側管ガス流量依存性

Fig. 5 Dependence of Electron Temperature on Gas Flow Rate of Inner Tube

図5にT_eのSiH_4ガス流量依存性を○（z＝1.5〔cm〕）、△（z＝5〔cm〕）、□（z＝10〔cm〕）プロットで示す。T_eは、前述のように放電管端付近のz＝1.5〔cm〕（T_eの高い領域）ではSiH_4ガス流量の増加にともない減少するが、z＞5〔cm〕（T_eの低い領域）ではSiH_4ガス流量を増加してもほぼ一定となっている。このことより、図3においてz＜5〔cm〕では2本の曲線とし、z＞5〔cm〕では1本の曲線としてある。したがって、SiH_4分子の解離のほとんどは、z＜5〔cm〕のT_eの高い領域で行われていること

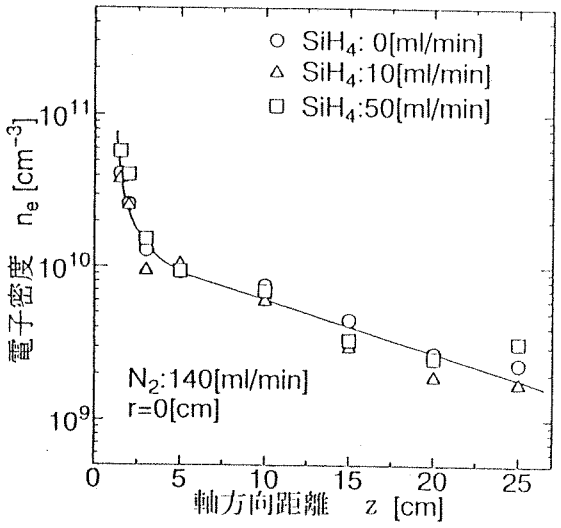

図6　電子密度のz依存性

Fig. 6 Dependence of Electron Density on z

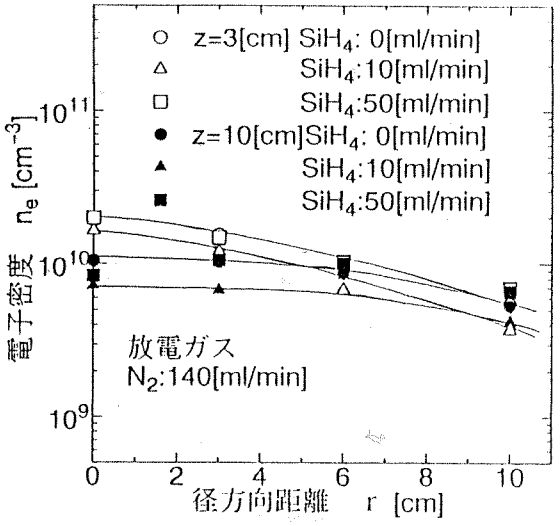

図7　電子密度のr依存性

Fig. 7 Dependence of Electron Density on r

が分かる。また、内側管にN₂ガス（●（z＝1.5[cm]）、▲（z＝5[cm]）、■（z＝10[cm]）プロット）を流して同様の測定を行った。図5から明らかなように両ガスにおいてほとんど変化がないことから、堆積室内において電子を冷却する効果はSiH₄とN₂では大きな違いはないことが分かる。

4．2　電子密度nₑの空間分布

図6に電子密度nₑのz依存性を示す。SiH₄ガス流量がいずれの場合も、nₑはzの増加に対して、放電管端付近で急激に減少した後、z＞5［cm］では、指数関数的に減少する。またSiH₄ガス流量を変化させてもnₑはほとんど変化しないことがわかる。

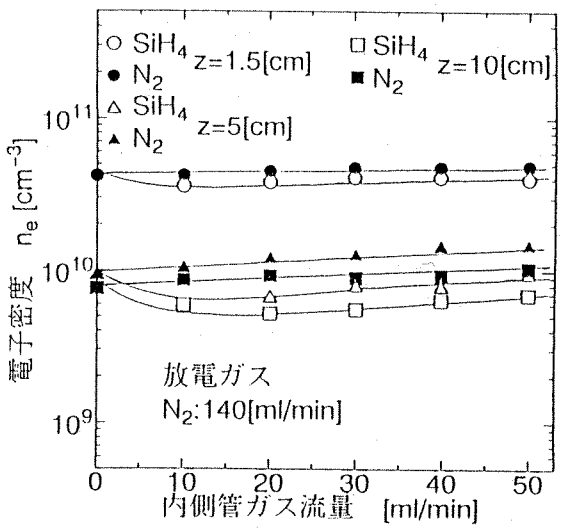

図8　電子密度の内側管ガス流量依存性

Fig. 8 Dependence of Electron Density on Gas Flow Rate of Inner Tube

図7にnₑのr依存性を示す。SiH₄ガス流量がいずれの場合もnₑはrの増加に対して、z＝3［cm］では減少するが、zが増加するほどr方向の均一性は良くなり、z＝10［cm］ではほぼ均一となる。

図8にnₑの内側管ガス流量依存性を示す。内側管に放電ガスと同じN₂を流したときは、zがいずれの場合にもnₑはN₂ガス流量の増加に対してわずかに増加するが大きな変化はない（黒プロット）。内側管にSiH₄ガスを流すと、zがいずれの場合にもnₑはいったん減少するが、その後SiH₄ガス流量を増加させるとわずかに増加する（白プロット）。しかしながら図6で述べたのと同様に、SiH₄ガス流量を変化させてもnₑは全体としては大きな変化はない。

4．3　空間電位V_sおよび浮動電位V_fの空間分布

図9にプラズマ空間電位V_sおよび浮動電位V_fのz依存性を示す。V_sは、zの増加に対して放電管端付近で急激に減少した後、z＞5［cm］で緩やかに減少する。V_fはzの増加に対して、全領域で緩やかに減少する。

図10にV_sおよびV_fのz＝10［cm］におけるr依存性を示す。V_sおよびV_fはr方向にほぼ均一となることがわかる。

図11（a）、（b）にそれぞれz＝1.5［cm］、10［cm］のときのプラズマ空間電位V_s及び浮動電位V_fの内側管ガス流量依存性を示す。V_sおよびV_fは、SiH₄ガスを加えることによって減少するが、SiH₄ガス流量を10［ml/min］以上に増加させても、ほとんど変化しない。また、内側管にN₂ガスを流した場合には、全領域でほとんど変化しない。

プラズマ中で成膜を行う際、基板を絶縁したときに基板とプラズマの間にできるシース電圧は、空間電位と浮動電位の差$V_s - V_f$で与えられる。なお、SiN膜のような絶

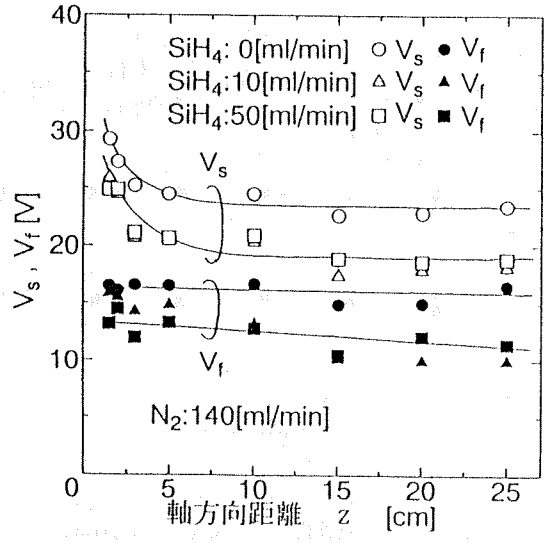

図9 空間電位・浮動電位のz依存性

Fig. 9 Dependence of Space Potential and Floating Potential on z

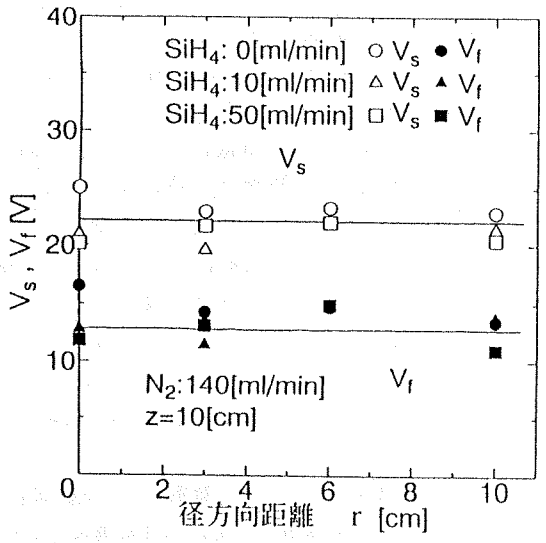

図10 空間電位・浮動電位のr依存性

Fig. 10 Dependence of Space Potential and Floating Potential on r

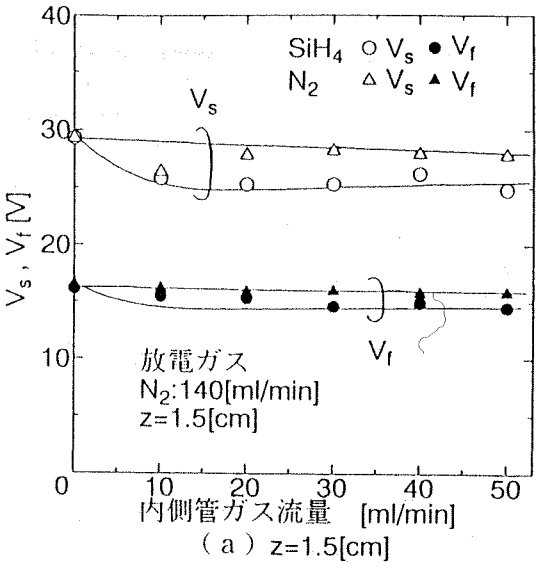

（a）z=1.5[cm]

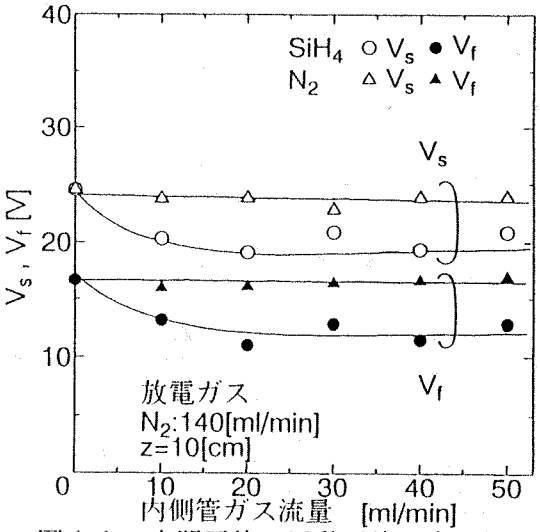

図11 空間電位・浮動電位の内側管ガス流量依存性（b）z=10[cm]

Fig. 11 Dependence of Space Potential and Floating Potential on Gas Flow Rate of Inner Tube

縁性の膜の場合には基板をアースしておいても成膜中の膜表面は絶縁状態にあることになる。従って、イオンは、このシース電圧によって加速され、膜に衝撃を与える。

図12に$V_s - V_f$のz依存性を示す。$V_s - V_f$はzの増加に対して放電管端付近で急激に減少した後、$z > 5$ [cm]でほぼ一定となる。また、SiH_4ガス流量を変化させても、ほとんど変化しない。さらに、$z \geq 10$ [cm]においては、$V_s - V_f$はr方向に均一であることも確認している。これらの結果から、$V_s - V_f$はSiH_4ガス流量にかかわらず、$z > 10$ [cm]の空間でz、r方向に均一であることが分かる。すなわち、この空間では、膜に与えられるイオン衝撃エネルギーは全膜面上で均一であることが分かる。また、$z > 10$ [cm]の空間では、図4、7の結果も合わせて考えると、内部的プラズマパラメータがr方向に均一となるので、均一なSiN膜が作製できると考えられる。さらに、図6の結果を考慮すると、基板位置をz方向に変化することにより、イオン衝撃エネルギーは変化させずに、電子密度のみを変化させて、すなわち衝撃を与えるイオンの数のみを変化させて成膜することが可能といえる。

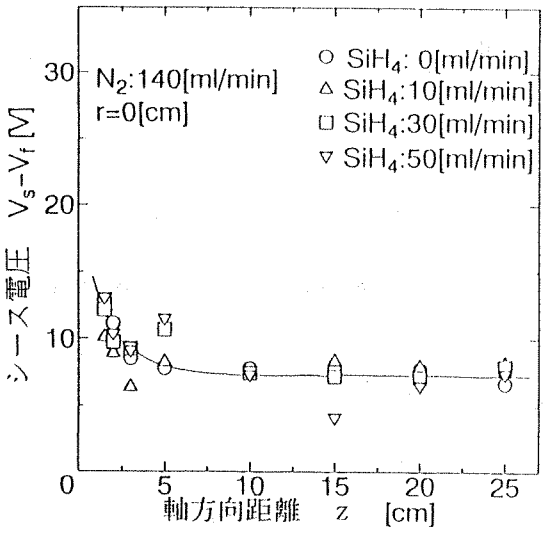

図12　シース電圧のz依存性

Fig. 12 Dependence of Sheath Voltage on z

5. まとめ

二重管式同軸線路形マイクロ波プラズマCVD装置の堆積室内におけるN_2／SiH_4プラズマのプラズマパラメータをSiH_4ガス流量を変化させて、シングルプローブ法により測定した。その結果、以下のことを明らかにした。

1. 電子温度は、zの増加に対して放電管端付近で急激に減少した後、$z>5$ [cm] でほぼ一定となる。また、rの増加に対しては、$z=3$ [cm] で緩やかに減少し、$z=10$ [cm] では一定となる。すなわち、$z>10$ [cm] では電子温度は空間的に均一であると考えてよいことが明らかとなった。

2. 電子温度は、SiH_4ガス流量の増加に対して、放電管端付近では減少するが、$z>5$ [cm] の空間では、ほとんど変化しない。これは、電子温度の高い放電管端付近では、SiH_4が解離されて電子の冷却効果が大きいが、電子温度の低い$z>5$ [cm] の空間では、非弾性衝突周波数が減少し電子がほとんど冷却されなくなるためである。

3. 電子密度は、zの増加に対して放電管端付近で急激に減少した後、$z>5$ [cm] で指数関数的に減少する。また、電子密度はrの増加に対して減少するが、zが増加するにしたがい、r方向の均一性はよくなり、$z>10$ [cm] ではr方向にほぼ均一となる。

4. 基板を絶縁したときのシース電圧V_s-V_fは、$z>10$ [cm] で空間的に一定となる。また、SiH_4ガス流量を変化させてもほとんど変化しない。すなわち、成膜中に膜に与えられるイオン衝撃エネルギーは、$z>10$ [cm] では、SiH_4流量によらず、かつ、空間的に一定であることが明らかになった。また、この時衝撃エネルギーは約7.5 [eV] であることを明らかにした。

謝辞　本研究の一部は、文部省科学研究費補助金の助成を受けて行われた。ここに改めて謝意を表する。

（平成7年8月23日受付、平成8年2月5日再受付）

文献

[1]加藤、加藤、阪本：電気学会放電研究会資料　ED-91-60 (1991)
[2]加藤、若葉：真空　26-7 (1983) 35
[3]加藤、白居、阪本：電気学会論文誌A 112 (1992) 355
[4]阪本、加藤：電気学会プラズマ研究会資料　EP-91-59 (1991) p. 11
[5]H. Kato, T. Sakamoto and T. Shimoda: Jpn. J. Appl. Phys., 33 (1994) 307
[6]加藤、上田、畑中：電気学会論文誌A 106 (1986) 391
[7]H. Kato, K. Hatanaka and T. Tatsumi: Bull. Sci. Engin. Res. Lab., Waseda Univ., 123 (1989) 1

加藤　勇

（正員）1944年7月26日生。1973年早稲田大学大学院博士課程修了。同大学助手、専任講師、助教授、1979～81年マニトバ大客員教授、1983年早稲田大学教授、現在に至る。マイクロ波プラズマCVD、光子光学、光子材料等に関する研究に従事。電子情報通信学会、応用物理学会、テレビジョン学会、IEEE会員。

下田　毅

（非会員）1970年1月9日生。1994年3月早稲田大学大学院理工学研究科電気工学専攻修士課程修了。マイクロ波プラズマに関する研究に従事。現在、日本電気中央研究所勤務。応用物理学会会員。

山岸　俊浩

（非会員）1970年3月28日生。1994年3月早稲田大学理工学部電子通信学科卒業。同年4月同大学院理工学研究科電気工学専攻修士課程入学、現在に至る。マイクロ波プラズマに関する研究に従事。応用物理学会会員。

論　文

RFバイアス印加同軸線路形マイクロ波プラズマCVDによるSiN膜の低温作製

森田　義則[†]　　加藤　勇[†]　　中嶋　達司[†]

Fabrication of SiN Films at Low Temperature Using RF Biased Coaxial-Line Type Microwave Plasma CVD

Yoshinori MORITA[†], Isamu KATO[†], and Tatsuji NAKAJIMA[†]

あらまし　イオン衝撃がSiN膜の特性に及ぼす影響を検討することを目的とする．本研究では，イオン衝撃効果を検討するのに適している2重管式同軸線路形マイクロ波プラズマCVD装置を用い，基板に印加するRFバイアスを変化させて，基板に入射するイオン密度を一定にしてイオン衝撃エネルギーのみを変化させた．RFバイアスを増加させると，膜密度は増加し水素含有量は減少したが，ダングリングボンド密度は増加した．前者はイオン衝撃により成膜中の膜表面が加熱されるためであり，後者はN^+イオン衝撃によりN^+イオンが膜中に打ち込まれ結合が切られるためである．また，基板温度を比較的低温である200°Cに上昇させて，かつ，RFバイアスを−175 V印加して成膜を行った結果，イオン衝撃による膜表面加熱と基板加熱の重畳効果により，膜密度が3 g/cm³，水素含有量が9 at.%となった．更に，基板を200°Cに加熱することによりN^+イオン衝撃のイオン打込みによるダングリングボンド密度の増加を抑制できた．また，本N_2/SiH_4プラズマにおいて，室温で成膜した場合に，RFバイアスが−70〜−80 Vで膜表面温度が約200°Cとなっていることを明らかにした．

キーワード　マイクロ波プラズマCVD，SiN膜，RFバイアス，イオン衝撃効果，膜表面加熱効果

1. まえがき

窒化シリコン(SiN)膜は，半導体デバイスの集積回路において，層間絶縁膜，ゲート絶縁膜，最終保護膜などに幅広く用いられており，その作製法には，熱CVD法，高周波プラズマCVD法，マイクロ波プラズマCVD法，電子サイクロトロン共鳴マイクロ波プラズマCVD法などがある．しかし，近年半導体デバイスプロセスにおいて薄膜の低温作製が要求されており，熱CVD法では900°Cと高温を必要とし，低温で薄膜を作製することができないことから，プラズマCVD法の研究が盛んに行われている．その中で，イオン衝撃下で成膜することにより低温で良質な膜が作製できるとの報告がなされている[1],[2]．しかしながら，イオン衝撃効果についての詳しい報告はない。これは，高周波プラズマCVD法では基板が放電プラズマ中に置かれており，イオン衝撃を変化させる(すなわちRFバイアスを変化させる）と電子温度，電子密度などの他のプラズマパラメータも大きく変化してしまい，イオン衝撃効果について検討するのには適さないこと，また電子サイクロトロン共鳴マイクロ波プラズマCVD法では，膜質が良くなる理由として，適度なイオン衝撃がもともとあるとしているので，イオン衝撃効果そのものを検討するのには適さないためと考えられる．

一方，我々が研究開発を進めてきている2重管式同軸線路形マイクロ波プラズマCVD装置は，マイクロ波の波長が短いことを生かしてマイクロ波および放電プラズマを所定の空間に閉じ込めることができるので，基板をマイクロ波電力の注入のない，電子温度の低い空間的アフターグロープラズマ中に設置することができる[3],[4]．これにより，イオン衝撃がかなり少ない状態で成膜することができる[3],[5]〜[7]．

本研究ではイオン衝撃がSiN膜の特性に及ぼす影響について検討を行うことを目的とする．イオン衝撃効果は基板に流入するイオン密度と基板前面のシース電圧の積で表される．そこで本研究では，まずイオン密度を変化させないで，基板前面のシース電圧のみを変化させることが可能であることを示す．そして，シース電圧（RFバイアス）のみを変化させることにより

† 早稲田大学理工学部電子通信学科，東京都
School of Science and Engineering, Waseda University, Tokyo, 169 Japan

SiN膜を作製し，SiN膜作製時におけるイオン衝撃効果について検討することとした．なお，SiN膜は絶縁膜であるので，直流バイアス法ではチャージアップが起こり，バイアスを印加したことにならないので，RFバイアス法を用いた[8],[9]．なお，成膜中の基板温度は室温と200℃とした．

2. 成膜装置および成膜条件

図1に成膜に用いたRFバイアス印加2重管式同軸線路形マイクロ波プラズマCVD (MPCVD) 装置の概略図を示す．本装置は，2重管式同軸線路形MPCVD装置にRFバイアス印加装置を取り付けたものである．まず，2重管式同軸線路形MPCVD装置について説明する．放電管は2重管構造となっており，溶融石英製の外側放電管 (outer discharge tube) に純N_2ガスを流して，マイクロ波により電離させ窒素プラズマを生成する．そして，ステンレス製の内側管 (inner tube) を用いてSiH_4ガスを放電管端まで導き，窒素プラズマ中に混入することによりSiH_4ガスを解離させている．窒素およびシラン系ラジカルは堆積室 (deposition chamber) 内に輸送され，基板 (substrate) 上にSiN膜を形成する．本装置ではマイクロ波は円筒キャビティ (cylindrical cavity) 内に閉じ込められているので，ここにマイクロ波電力が注入されている放電

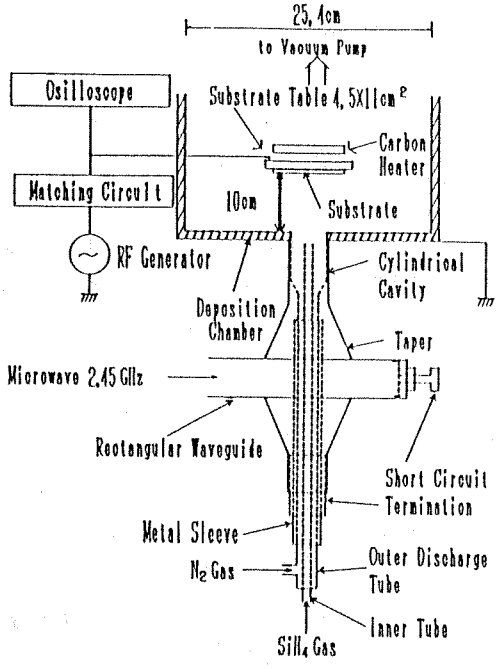

図1 実験装置概略図
Fig. 1 Schematic diagram of experiment system.

プラズマが生じる．そして，堆積室内にはマイクロ波の電力注入のない空間的アフターグロープラズマを生成することができる[3],[4]．この空間的アフターグロープラズマ中に基板を設置することにより，イオン衝撃がかなり少ない状態でSiN膜を作製することができる[3],[5]~[7]．2重管式同軸線路形マイクロ波プラズマCVD装置の詳細は文献[10]を参照して頂きたい．

次に，RFバイアス印加装置について説明する．周波数21.0 MHzの高周波は，整合回路 (matching circuit) を通して，内直径25.4 cmの堆積室内に導入され，堆積室とは電気的に絶縁してある大きさ4.5 cm×11.0 cmのステンレス製の基板テーブル (substrate table) に印加される．このように，RFバイアスを印加する基板テーブルを放電プラズマ領域外，すなわち空間的アフターグロープラズマ領域内に設置することにより，基板に高周波電力を印加しても，放電プラズマの状態を変化させずに基板にRFバイアスを印加することができる[8],[9]．RFバイアスとは，基板に高周波電力を印加したとき，基板に生じる自己バイアスである．基板テーブルの電位の測定には，整合回路の出力端に取り付けたオシロスコープ (osilloscope) により行った．印加する高周波の周波数が低いとイオンが高周波に追従可能となるため，高周波電圧がイオン衝撃効果に影響する[11]．しかし，ここで用いた高周波の周波数は21.0 MHzであり，イオンは高周波電界に追従できないために，イオンはRFバイアスのみによって膜表面で加速され膜表面に入射することになる．

次に，SiN膜の作製条件を示す．マイクロ波電力を270 Wとした．N_2ガス流量およびSiH_4ガス流量をそれぞれ140 ml/min, 15 ml/minとした．このときの堆積室内のガス圧は3.9 mTorrとなった．基板位置は放電管端から10 cmの位置に固定した．基板温度は室温と200℃とした．基板加熱にはカーボンヒータ (carbon heater) を用いた．印加した高周波の電力を0 Wから約70 Wまで増加させることにより，基板電位を+4 Vから−175 Vまで変化できた．我々はこれまでに純窒素プラズマにおいてRFバイアスを変化させて，RFバイアスがプラズマに与える影響について電気単針法および発光分光分析を用いて検討を行ってきた．但し，実験条件は，SiH_4ガス流量を0 ml/minとし，基板温度は室温で，他の条件はSiN膜の作製条件と同じとした．その結果，RFバイアスを印加しても基板近傍(放電管端から9 cm離れた点) で電気探針のイオン飽和

電流が変化していないことから，イオン密度，すなわち電子密度がRFバイアスを印加しても変化していないことを明らかにしてきた[12]．また，このことと基板近傍でラジカルの発光強度がRFバイアスを印加するとわずかに変化していることから，基板近傍で電子温度はわずかに増加するが，その増加割合は4%以下であるので，空間的アフターグロープラズマの状態はRFバイアスを印加してもほとんど変化していないことを明らかにしてきた[12]．N_2/SiH_4プラズマにおいても，同様と考えられる．すなわち，基板にRFバイアスを印加することにより，マイクロ波放電により生成された空間的アフターグロープラズマの状態をほぼ変化させずに，基板前面のシース電圧のみを変化させることができる．シース電圧とは基板前面のシース端でのプラズマ空間電位と基板電位との差であり，この電圧によりイオンが加速される．前述のように空間的アフターグロープラズマ中では，基板をフローにしたとき，シース電圧はかなり小さいと考えられるので，RFバイアスにより，イオンが加速されるものとして以後，検討を進めることにする．

膜厚測定には触針式膜厚計を用いた．屈折率測定には波長632.8 nmの光源のエリプソメータを用いた．赤外吸収分光スペクトルと膜厚より，N-H結合，Si-H結合，Si-N結合のストレッチングモードの積分吸収強度を求め，それぞれの赤外吸収強度に比例係数$2.8\times10^{20}\,cm^{-2}$[13]，$1.4\times10^{20}\,cm^{-2}$[14]，$9.2\times10^{18}\,cm^{-2}$[15]を掛けることにより，N-H結合の形で含まれる水素含有量，Si-H結合の形で含まれる水素含有量，窒素含有量を求めた．全水素含有量はN-H結合の形で含まれる水素含有量とSi-H結合の形で含まれる水素含有量の和として求めた．電子スピン共鳴スペクトルと膜厚より，ダングリングボンド密度を求めた．屈折率と窒素含有量を用いて，Lorentz-Lorenzの関係式よりSi/N比，膜密度，Si含有量を求めた[16]，[17]．紫外可視吸収スペクトルと膜厚より，光学エネルギーギャップを求めた[18]．

3. 実験結果および考察

図2に堆積速度のRFバイアス依存性を示す．図から，堆積速度はRFバイアスを増加させると，いずれの基板温度においても減少することがわかる．これは，後述するが，イオン衝撃により，成膜中の膜表面が加熱され，膜がち密になったことと，膜がスパッタリングを受けたためである．また，基板温度を室温から200℃に上昇させると，膜表面反応が促進されて膜がよりち密になるので，堆積速度は減少する．

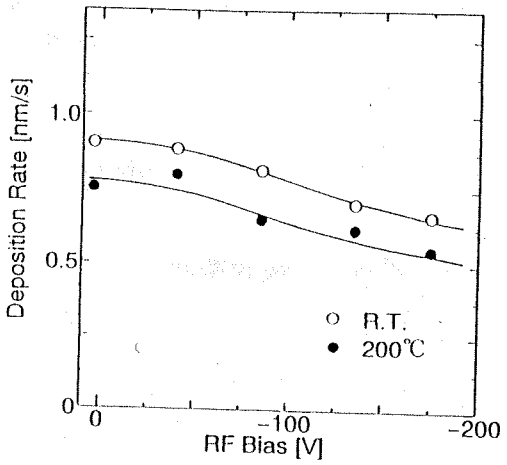

図2 堆積速度のRFバイアス依存性
Fig. 2 Dependence of deposition rate on RF bias.

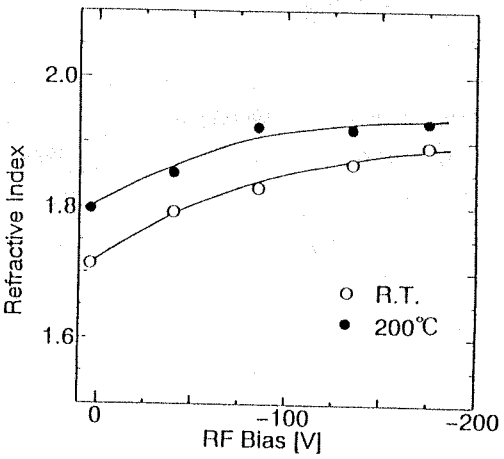

図3 屈折率のRFバイアス依存性
Fig. 3 Dependence of refractive index on RF bias.

図3に屈折率のRFバイアス依存性を示す．図から，屈折率はRFバイアスを増加させると，いずれの基板温度においても増加することがわかる．また，基板温度を増加させると屈折率は増加する．これは，膜密度の増加が主な原因である．なお，基板温度を200℃でRFバイアスを−175 V印加すると，屈折率は熱CVD法で作製した膜の値（2.0〜2.1）[17]に近づくことがわかる．

図4に水素含有量のRFバイアス依存性を示す．図から，N-H結合，Si-H結合の形で含まれる水素含有量はRFバイアスを増加させると，いずれの基板温度においても減少することがわかる．RFバイアスを印加すると，膜表面に入射するイオンが加速され膜表面の原子と衝突して格子振動を起こして，膜表面が加熱

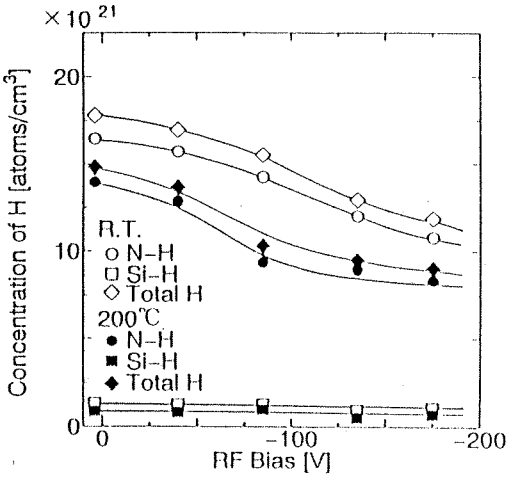

図4 水素含有量のRFバイアス依存性
Fig. 4 Dependence of concentration of H on RF bias.

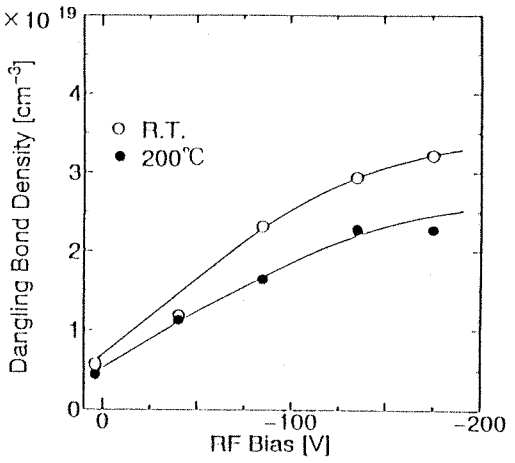

図5 ダングリングボンド密度のRFバイアス依存性
Fig. 5 Dependence of dangling bond density on RF bias.

される(膜表面加熱効果)．これにより，膜表面での反応が促進されるので，水素が脱離して，膜中に取り込まれる水素量は減少する．また，図から，基板温度を200℃に加熱すると，更に膜の表面反応が促進され，N-H結合，Si-H結合の形で含まれる水素含有量は減少していることがわかる．また，基板温度を200℃でRFバイアスを−175 V印加すると，イオン衝撃による膜表面加熱と基板加熱の重畳効果により，膜中の全水素原子数は，膜の全原子数に対して9%まで減少し，熱CVD法で作製した膜の値(4〜7%) [19]とほぼ同程度までに水素含有量を低減できることがわかる．

図5にダングリングボンド密度のRFバイアス依存性を示す．図から，RFバイアスを増加させるに従い，どの基板温度においてもダングリングボンド密度は増加することがわかる．RFバイアスを増加すると，膜の表面加熱により基板温度を上昇させたときと同様に，膜表面反応が促進されてダングリングボンド密度が減少するとも考えられるが，実際には増加した．これは窒素系イオンが膜表面に打ち込まれ結合が切られるためである[20]．マススペクトルメータによる分析によると，N_2^+ イオンは N^+ イオンの14倍あるが，膜に打ち込まれるのは質量の軽いほうの N^+ イオンが主と考えられる(このことについては後に更に検討を加える)．また，図から，基板温度を200℃に上昇させることにより，膜の表面反応が促進されダングリングボンド密度は減少していることがわかる．基板温度が室温でRFバイアスを増加させるとダングリングボンド密度が増加してしまったが，基板温度を200℃に上昇させることにより，イオン衝撃によるダングリングボンド密度の増加を抑制できることがわかる．しかしながら，熱CVD法で作製した膜のダングリングボンド密度は 4×10^{15}〜1×10^{18} cm^{-3} [21]程度であり，本装置で作製した膜の値より小さい．また，いずれの基板温度においてもRFバイアスを増加させると，ダングリングボンド密度は増加する．従って，ダングリングボンド密度の小さい膜を作製するには，イオン衝撃を避けて成膜する必要がある．

図6に窒素含有量，シリコン含有量のRFバイアス依存性を示す．図から，RFバイアスを増加させると，どの基板温度においても窒素含有量，シリコン含有量は増加することがわかる．これは，RFバイアスを増加させるに従い，基板温度を上昇させたときと同様な効果(膜表面加熱効果)が生じて，膜の表面反応が促進されて，ち密な膜となったためである．また，図から，基板温度を200℃に加熱すると，膜の表面反応が更に促進され，室温の場合より窒素含有量，シリコン含有量が増加することがわかる．窒素含有量の増加割合はシリコン含有量の増加割合より大きい．マススペクトルメータによる分析によると窒素系イオンとシラン系イオンとはほぼ同量である．しかしながら，前述のように，質量の軽い N^+ イオンは膜に打ち込まれて膜中に残るので，窒素含有量の増加割合が大きくなると考えられる．

また，本実験による窒素含有量，シリコン含有量が一番大きい基板温度が200℃でRFバイアスを−175 V印加して作製した膜を熱CVD法で作製した膜と比較すると，窒素含有量は 5.7×10^{22} atoms/cm^3 で熱CVD法で作製した膜の値 (5.3×10^{22} atoms/cm^3) [21]

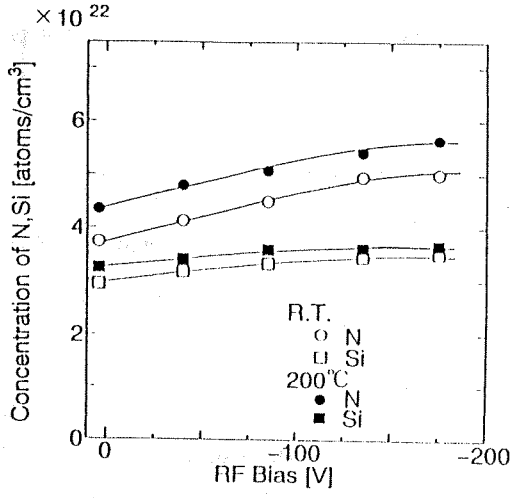

図6 窒素含有量、シリコン含有量のRFバイアス依存性
Fig. 6 Dependence of concentration of N and Si on RF bias.

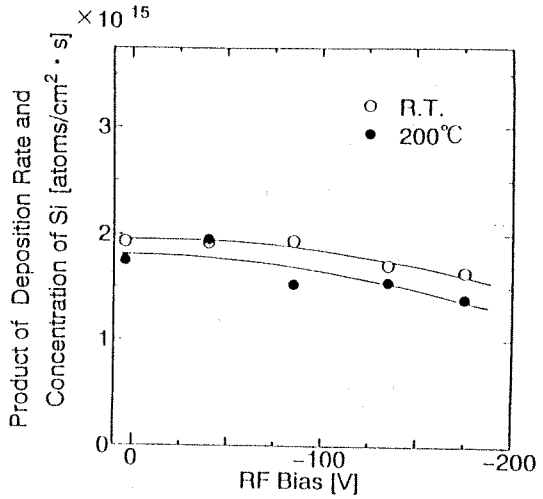

図7 堆積速度とシリコン含有量の積のRFバイアス依存性
Fig. 7 Dependence of product of deposition rate and concentration of Si on RF bias.

より大きい．これは，イオン衝撃によるN^+イオンの打込みによると考えられる．一方，シリコン含有量は3.7×10^{22} atoms/cm^{3}で熱CVD法で作製した膜の値(4.0×10^{22} atoms/cm^3) [21]に近づいている．これは，イオン衝撃による膜表面加熱効果により膜が緻密化したためと考えられる．

図7に堆積速度とシリコン含有量の積のRFバイアス依存性を示す．図から，RFバイアスを増加させると堆積速度とシリコン含有量の積，すなわち単位時間単位面積当たりに膜となるシリコン原子数は，RFバイアスを増加させると減少することがわかる．これはイオン衝撃によりスパッタリングを生ずるためと考えられる．ここで，シラン系イオンが膜に衝突してSiをスパッタしたとしても，そのイオン中のSiが膜として残るので，結果的にスパッタリングは起きないことになる．しかしながら，ほぼ同質量のN_2^+イオンはSiのスパッタリングを生ずることになる．

図8に堆積速度と窒素含有量の積のRFバイアス依存性を示す．図から，RFバイアスを増加させても堆積速度と窒素含有量の積，すなわち，単位時間単位面積当たりに膜となる窒素の原子数は，RFバイアスを増加させてもほぼ一定であることがわかる．シリコンの原子の場合と同様に，単位時間単位面積当たりに膜となる窒素の原子数も，イオン衝撃によるスパッタリングにより減少するとも考えられるが，実際にはほぼ一定であった．これは，前述のように，窒素系イオン(主としてN^+イオン) が膜中に打ち込まれる分だけ減少が抑えられることによると考えられる．すなわち，イオンラジカルより中性ラジカルが多いことを考慮すると，シラン系イオンは膜表面加熱効果に寄与し，N_2^+イオンは膜表面加熱効果とSiのスパッタリングに寄与する．また，N^+イオンは膜中に打ち込まれ，膜の窒素含有量を増加する効果があるが，膜中の結合を切り，ダングリングボンド密度を増加させる効果もあることになる．

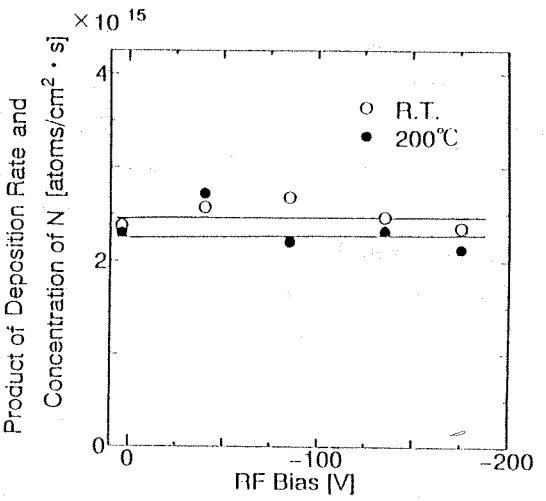

図8 堆積速度と窒素含有量の積のRFバイアス依存性
Fig. 8 Dependence of product of deposition rate and concentration of N on RF bias.

図9にSi/N比のRFバイアス依存性を示す．図から，RFバイアスを増加させると，どの基板温度においてもSi/N比は減少することがわかる．これは，イオン衝撃により膜表面の温度が上昇したために薄膜形成に寄与するシラン系ラジカルと窒素系ラジカルの付着確

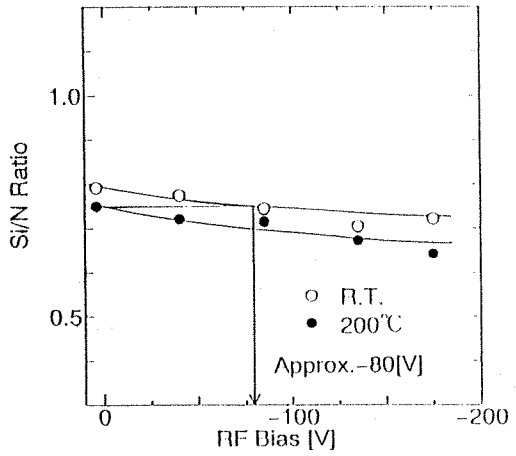

図 9 Si/N 比の RF バイアス依存性
Fig. 9 Dependence of Si/N ratio on RF bias.

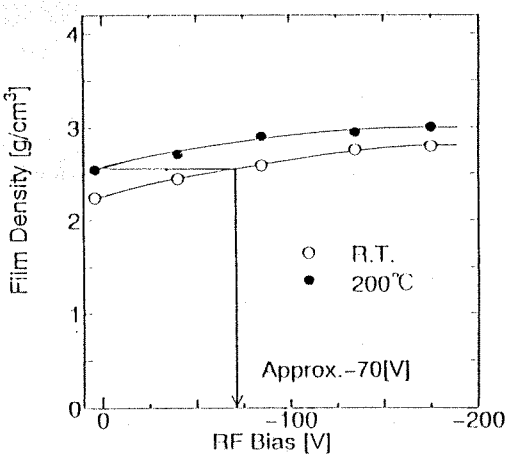

図 10 膜密度の RF バイアス依存性
Fig. 10 Dependence of film density on RF bias.

率の比が温度により変化したため [16] と，窒素系イオンがイオン衝撃により膜表面に，より多く打ち込まれるためである．また，図から，基板温度を上昇させると，Si/N 比は減少していることがわかる．これは薄膜形成に寄与するシラン系ラジカルと窒素系ラジカルの付着確率が温度により異なることを示すものである [16]．また，RF バイアス印加により，窒素リッチな膜となることが示されている．

基板温度が室温で RF バイアスが約−80 V で作製した膜の Si/N 比と基板温度が 200℃で RF バイアスがほぼ 0 V で作製した膜の Si/N 比が一致することから，イオン衝撃による膜表面加熱効果により，基板温度が室温で RF バイアスが約−80 V のとき，膜表面温度が約 200℃となっていると考えられる．

図 10 に膜密度の RF バイアス依存性を示す．図から，RF バイアスを増加させると，どの基板温度においても膜密度は増加することがわかる．これは，RF バイアスを増加させると，基板温度を上昇させたときと同様に成膜中の表面での構造緩和が促進されたためである．この膜密度の増加が，図 2 で堆積速度が RF バイアスの増加に対して減少した主な理由である．また，基板温度を 200℃にすると，更に膜の構造緩和が促進され，膜密度が増加する．基板温度が 200℃で RF バイアスがほぼ 0 V の場合の膜密度は，基板温度が室温で RF バイアスが約−70 V の場合の膜密度と一致する．従って，この場合，RF バイアスが約−70 V で，膜表面温度が約 200℃となっていると考えられる．図 9 における同様の考察では RF バイアスが約−80 V で約 200℃になっているが，実験誤差を考えれば両者は良く一致しているといえる．イオン衝撃効果には膜表面加熱効果ばかりでなく，イオン打込み効果，スパッタリング効果などがあるが，膜表面加熱効果について言えば，この場合 RF バイアスが−70〜−80 V で膜表面が約 200℃となっていると考えてよいことになる．

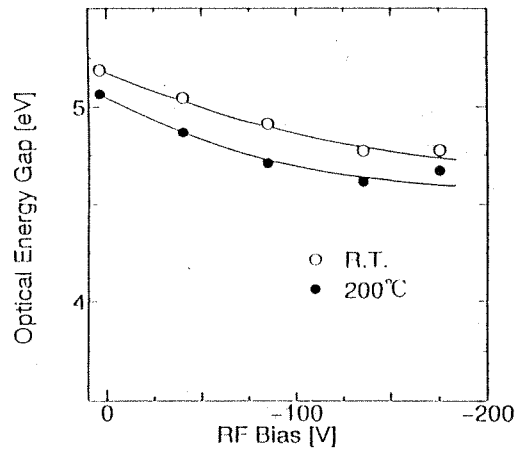

図 11 光学エネルギーギャップの RF バイアス依存性
Fig. 11 Dependence of optical energy gap on RF bias.

基板温度を 200℃で RF バイアスを−175 V 印加すると，イオン衝撃による膜表面加熱効果と基板加熱の効果が重畳するので，膜密度は 3.0 g/cm³ となり，非常に緻密な膜となっており，熱 CVD 法で作製した膜の膜密度 (2.8〜3.1 g/cm³) [17] と同程度の値となることがわかる．

図 11 に光学エネルギーギャップの RF バイアス依存性を示す．図から，RF バイアスを増加させると，どの基板温度においても光学エネルギーギャップは減少することがわかる．また，基板温度を上昇させると光学エネルギーギャップは減少することがわかる．熱

CVD法では光学エネルギーギャップは約5.1 eVであり，本装置で室温で成膜した場合とほぼ一致している．RFバイアスを印加すると最小で4.7 eVとやや低下する．しかしながら，電子サイクロトロン共鳴マイクロ波プラズマCVDで成膜した場合3 eV程度のものもあり[22]，本実験における値の減少割合は小さいといえる．

4. むすび

2重管式同軸線路形マイクロ波プラズマCVD装置を用いて，基板にRFバイアスを印加することにより基板に入射するイオン密度を一定にしてイオン衝撃エネルギー(RFバイアス)のみを変化させて，SiN膜を作製して以下のことを明らかにした．

(1) RFバイアスを増加させることにより，水素含有量は減少し，膜密度は増加する．これは，イオン衝撃による膜表面加熱効果のためである．

(2) シラン系イオンは膜表面加熱効果に寄与し，N_2^+イオンは膜表面加熱効果とSiのスパッタリングに寄与する．また，N^+イオンは膜中に打ち込まれ，窒素含有量を増加する効果があるが，膜中の結合を切り，ダングリングボンド密度を増加させる効果もある．

(3) 基板温度を比較的低温である200°Cに上昇させて，かつ，RFバイアスを−175 V印加することにより，堆積速度0.55 nm/s，屈折率1.93，水素含有量9 atomic%，膜密度3.0 g/cm³の膜が作製できた．

(4) 膜表面加熱効果はイオンの種類および密度によって変化するものであるが，本N_2/SiH_4プラズマ(電子温度約12,000 K，電子密度約5×10^9 cm^{-3}) [23]では，基板を加熱しないで室温で成膜した場合に，RFバイアスが−70〜−80 Vで膜表面温度が約200°Cとなるという，結果を得た．

今後，窒素ガスとシランガス流量を変化させて，同様な実験を行い，最適条件を明らかにすると共に，電子温度，電子密度等の内部的プラズマパラメータの詳細な測定を行い，堆積機構について検討を進める．また，本SiN膜が半導体デバイス作製に適応できるかどうかを検討するため，電気的特性も測定する予定である．

謝辞 本研究の一部は文部省科学研究費の補助を得て行ったものである．

文献

[1] S. Matuo and M. Kiuchi, "Low Temperature Chemical Vapor Deposition Method Utilizing an Electron Cyclotron Resonance Plasma," Jpn. J. Appl. Phys., vol. 22, no. 4, pp. L210-L212, April 1983.

[2] K. A. Buckle, J. Rodgers, K. Pastor, C. Constantine, and D. Johnson, "Electron Cyclotron Resonance Plasma Deposition of Silicon Nitride: Effect of Very Low rf Substrate Bias," Appl. Phys. Lett., vol. 60, no. 21, pp. 2601-2603, May 1992.

[3] I. Kato, S. Wakana, and S. Hara, "Microwave Plasma CVD System to Fabricate α-Si Thin Films of Plasma," Jpn.J. Appl.Phys., vol. 22, no. 1, pp. L40-L42, Jan.1983.

[4] 下田 毅, 加藤 勇, "空間的アフターグロープラズマのプラズマパラメータ," 第40回応物春季予稿集, 分冊1, no. 29p-X12, p. 8, March 1993.

[5] I. Kato, S. Wakana, S. Hara, and H. Kezuka, "Microwave Plasma CVD System for the Fabrication of Thin Solid Films," Jpn. J. Appl. Phys., vol. 21, no. 8, pp. L470-L472, Aug. 1982.

[6] 加藤 勇, 若菜伸一, "新しいマイクロ波プラズマ化学気相堆積装置," 真空, vol. 26, no. 7, pp. 628-636, June 1983.

[7] 清田幸弘, 加藤聖隆, 加藤 勇, "マイクロ波プラズマCVDにおいてプラズマ粒子衝撃がSiN膜特性に与える影響," 信学技報, vol. 8, no. 240, Oct. 1987.

[8] 伊藤高已, 加藤聖隆, 加藤 勇, "RFバイアス印加マイクロ波プラズマCVDによるSiN薄膜の作成," 信学論(C-II), vol. J74-C-II, no. 1, pp. 21-25, Jan. 1991.

[9] K. Suzuki, K. Ninomiya, S. Nishimatsu, and S. Okudaira, "Radio-Frequency Biased Misrowave Plasma Etching Technique: A Method to Increase SiO_2 Etch Rate," J. Vac. Sci. Technol. B, vol. 3, no. 4, pp. 1025-1034, July/Aug. 1985.

[10] I. Kato, K. Noguchi, and K. Numada, "Preparation of Silicon Nitride Films at Room Temperature Using Doubled-Tubed Coaxial Line-Type Microwave Plasma Chemical Vapor Deposition System," J. Appl. Phys., vol. 62, no. 2, pp. 492-497, July 1987.

[11] 古村雄二, 筑根敦弘, "プラズマシリコン窒化膜," プラズマ材料科学ハンドブック, 日本学術振興会プラズマ材料科学第153委員会編, pp. 343-347, オーム社, 東京, 1992.

[12] 加藤聖隆, 加藤 勇, 中島秀文, "RFバイアス印加マイクロ波プラズマCVD法によるSiN膜の低温作成," 第4回マイクロエレクトロニクスシンポジュウム, 東京, pp. 209-212, May 1991.

[13] A. Morimoto, Y. Tsujimura, M. Kumeda, and T. Shimizu, "Properites of Hydrogenated Amorphous Si-N Prepared by Various Methods," Jpn. J. Appl. Phys., vol. 24, no. 11, pp. 1394-1398, Nov. 1985.

[14] C. J. Fang, K. J. J. Gruntz, L. Ley, M. Cardona, F. J. Demond, G. Müller, and S. Kalbitzer, "The Hydrogenated of a-Ge: H and a-Si: H as Determined by IR Spectroscopy, Gas Evolution and nuclear Reaction Techniques," J. Non Cryst. Solids, vol. 35 and 36, pp. 255-260, Jan./Feb. 1980.

[15] H. Watanabe, K. Katoh, and M. Yasui, "Electrical Properties of Glow Discharge Amorphous SiN_x: H Thin Films," Thin Solid Films, vol. 106, no. 4, pp. 263-

273, Aug. 1983.
[16] 加藤 勇, 幸山裕亮, 野口一人, "同軸線路形マイクロ波プラズマ装置によるSiN膜の作成," 信学論 (C), vol. J68-C, no. 10, pp. 788-795. Oct. 1985.
[17] 吉見武男, "プラズマシリコン窒化膜の基本特性," 薄膜ハンドブック, 日本学術振興会薄膜第131委員会編, pp. 236-243, オーム社, 東京, 1983.
[18] J. Tauc, R. Grigorovici, and A. Vancu, "Optical Properities and Electronic Structure of Amorphous Germanium," Phys. Status Solid, vol. 15, no. 2, pp. 627 637, June 1966.
[19] V. J. Kapoor and R. S. Bailley: "Hydrogen related Memory Traps in Thin Silicon Nitride Films," J. Vac. Sci. Technol. A, vol. 1, no. 2, pp. 600 603, April-June 1983.
[20] 伊藤尚巳, 中島秀文, 中山厚紀, 加藤聖隆, 加藤 勇, "窒化シリコンの膜特性に与えるプラズマ粒子衝撃効果," 第37回応物春季予稿集, 分冊2, no. 30a-ZD-5, p. 711, March 1990.
[21] 藤田静雄, 佐々木昭夫, "シリコン窒化膜の最近の研究," 応用物理, vol. 54, no. 12, pp. 1250-1266, Dec. 1985.
[22] Y. Manabe and T. Mitsuyu, "Silicon Nitride Thin Films Prepared by the Electron Cyclotron Resonance Plasma Chemical Vapor Deposition method," J. Appl. Phys., vol. 66, no. 6 pp. 2475-2480, Sept. 1989.
[23] I. Kato, T. Sakamoto, and T. Shimoda: "Method of Probe Measurement in N_2/SiH_4 Microwave Plasma," Jpn. J. Appl. Phys., vol. 33, no. 1A, pp. 307-310, Jan. 1994.

(平成7年9月27日受付, 8年1月12日再受付)

森田 義則

平4早大・理工・電子通信卒. 現在, 同大学院博士課程在学. マイクロ波プラズマCVDの研究に従事. 応用物理学会会員.

加藤 勇 (正員)

昭42早大・理工・電子通信卒. 昭48同大学院博士課程了. 同年工博. 同年早大勤務. 昭53同大助教授. 昭54～56マニトバ大客員教授, カナダ国立研究会議の研究費を受け共同研究ならびに研究指導. 昭58同大教授, 現在に至る. マイクロ波プラズマCVD, 光子工学, レーザ工学, 電子物性工学, 計測工学, 光子材料, プラズマ・エレクトロニクス, 光・量子エレクトロニクス, 半導体薄膜工学などの研究に従事. 電気工学会, 応用物理学会, テレビジョン学会, 日本真空協会, IEEE各会員.

中嶋 達司

平6早大・理工・電子通信卒. 現在, 同大学院修士課程在学. マイクロ波プラズマCVDの研究に従事. 応用物理学会会員.

Electronics and Communications in Japan, Part 2, Vol. 79, No. 5, 1996
Translated from Denshi Joho Tsushin Gakkai Ronbunshi, Vol. 79-C-II, No. 1, January 1996, pp. 1-7

Dependence of Plasma Parameters on Electric Potential of Electrode in Microwave Plasma

Isamu Kato, Toru Matsushita, and Makoto Yamashita

School of Science and Engineering, Waseda University, Tokyo, Japan 169

SUMMARY

The authors have been studying the double-tubed coaxial line-type microwave plasma chemical vapor deposition (MPCVD). The discharge tube of the present MPCVD is a dual-tube structure made of a fused quartz outer discharge tube and stainless steel inner tube. The authors have discovered that the ion bombardment energy can be controlled without varying the electron densities and temperature by changing the potential of the substrate placed in a spatial after-glow plasma. In the present research, it is found that the ion bombardment energy can also be controlled by changing the potential of the inner tube placed in the discharge plasma. However, the electron densities and temperature have exhibited a tendency different from the one when the substrate potential is varied. Hence, a theoretical calculation has been carried out on the electron densities and temperature based on Maxwell-Boltzmann distribution. It is found that a different tendency can be explained from the fact that the electrons successively vanish on the deposition chamber wall from the higher-energy side as the plasma spatial potential is reduced from about 13 V to 4 V so that the electron velocity distribution is modified.

Key words: Substrate potential; inner tube potential; ion collision; plasma parameters; Maxwell-Boltzmann distribution.

1. Introduction

Hydrogenized amorphous silicon (a-Si:H) films are used as the electronic and photonic materials for thin-film transistors and solar cells. The plasma chemical vapor deposition (CVD) method often is used for fabrication of the a-Si:H film since the method can be used for a large surface area and is a low-temperature process. Although it is necessary to control the plasma in order to control the film quality, few studies on the plasma have been carried out. In the plasma CVD, the problem on the ion collision cannot be considered separately. We have developed a double-tube coaxial-line-type microwave plasma CVD (MPCVD) with which the film can be grown in a spatial after-glow plasma with less ion bombardments by trapping the discharge plasma in a specified region. They have been engaged in research on the ion bombardments [1-5]. In these studies, we have discovered that the ion bombardment energy can be controlled without changing the ion flux density incident on the substrate if the dc bias voltage applied to the substrate placed in the spatial after-glow plasma is varied [1].

In the present research, the plasma parameters are measured by varying the potential of the stainless inner tube placed in the discharge plasma in the MPCVD apparatus to find out if the ion bombardment energy can be controlled in the same way as varying the potential of the substrate placed in the spatial after-glow plasma. As

ISSN8756-663X/96/0005-0058

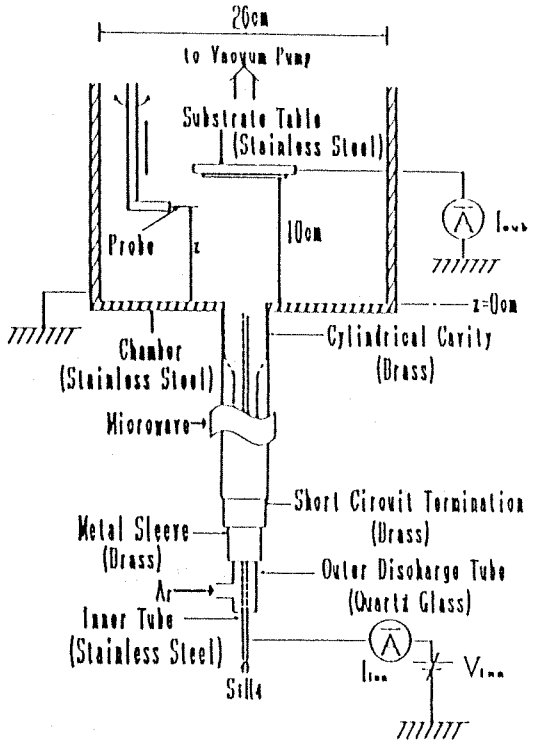

Fig. 1. Schematic diagram of experimental system.

a result, it is found that the ion bombardment energy can be controlled when the inner tube potential is varied. However, there is different tendency in the plasma parameters if the substrate potential is varied or if the inner tube potential is varied. Therefore, a theoretical study is carried out to find the reason for the difference.

2. Experiment

Figure 1 shows the schematic of the MPCVD equipment used in the experiment. The discharge section of the equipment is a dual-tube configuration made of a fused quartz outer discharge tube and a stainless inner tube. Ar gas flows in the outer discharge tube while SiH_4 gas flows in the inner tube. The microwave at 2.45 GHz generated in a magnetron propagating in a rectangular waveguide is led to the metallic cylindrical cavity. In the cavity region, Ar gas is discharged by the microwave power. SiH_4 gas is guided to the end of the discharge tube by the stainless inner tube and is mixed with Ar plasma where it collides with the particles of Ar plasma and is dissociated. In the present MPCVD equipment, the microwave power is confined within the cavity. Within the deposition chamber, a spatial after-glow plasma, in which no microwave power is injected, is formed by the flow and diffusion. For the details of the present equipment, the readers are referred to [2], [3], and [4]. We have been carrying out research by changing the substrate potential with the inner tube and the deposition chamber wall grounded [1]. In the present research, however, the substrate and the deposition chamber wall are grounded and the inner tube potential is varied. Here, the inner tube potential is V_{inn}, the substrate potential is V_{sub}, the current flowing in the inner tube is I_{inn}, the current in the substrate is I_{sub}, and the distance along the axial direction from the end of the discharge tube is z (see Fig. 1).

The experimental conditions are described below. The microwave power is 150 W. The substrate is placed at $z = 10$ cm. If V_{inn} exceeds ± 40 V, the glowing condition in the spatial after-glow plasma changes. Therefore, the dc discharge occurs between the inner tube and the deposition chamber wall and the power is injected into the plasma. Further, when V_{inn} exceeds -30 V, the inner tube is sputtered by Ar ions and the metal atoms ejected from the stainless inner wall attach to the discharge tube so that the condition of the microwave discharge changes. Hence, in this research, V_{inn} was varied in the range between -30 V and $+40$ V where no dc discharge occurs and the inner tube is not sputtered. Then V_{sub} was 0 V. By means of the single-probe method, the measurement of the plasma parameters was carried out in the pure Ar plasma (Ar gas flow: 110 ml/min) and in the AR/SiH_4 plasma under the conditions identical to the time of fabrication of the a-Si:H film (Ar gas flow: 110 ml/min, SiH_4 gas flow: 30 ml/min). A cylindrical probe with a diameter of 0.05 cm and a length of 0.3 cm was used. The measurement was carried out at the locations of $z =$ 3, 5, 7, and 9 along the center axis of the deposition chamber.

The probe measurement in Ar/SiH_4 plasma which is a reactive plasma cannot be carried out in a usual way because a film deposits on the surface of the probe. We have established the probe measurement method that can also be carried out in Ar/SiH_4 plasma [5]. In the present research, this method is used for measurement in Ar/SiH_4 plasma.

In this paper, the V_{sub} dependence of the electron density, electron temperature, plasma spatial potential, and I_{sub} was measured again in order to test repeatability. The results agreed well with those reported earlier. Also, the V_{sub} dependence of I_{inn} was not measured previously but was measured here for the first time.

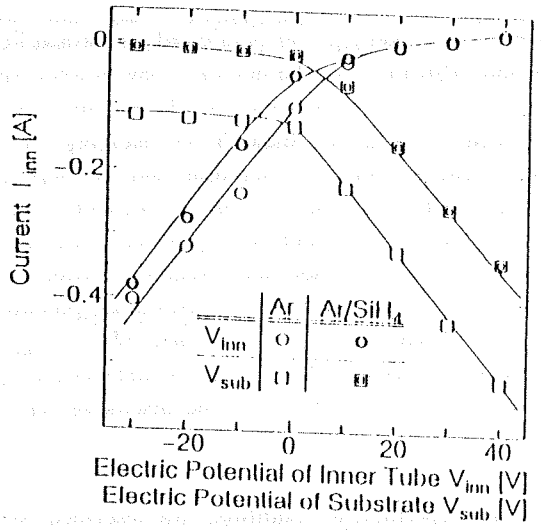

Fig. 2. Dependence of I_{inn} on V_{inn} and V_{sub}.

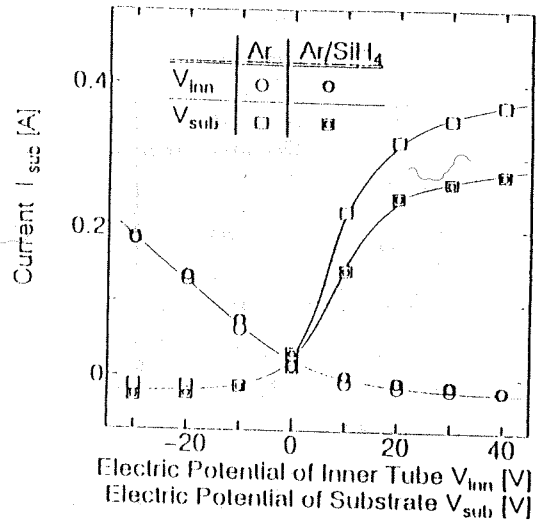

Fig. 3. Dependence of I_{sub} on V_{inn} and V_{sub}.

3. Results and Discussions

Figure 2 shows the V_{sub} dependence and V_{inn} dependence of I_{inn}. The electron current is taken positive. From the figure, it is found that I_{inn} changes little in the negative region of a varying V_{sub} and that it decreases rapidly in the positive region of V_{sub}. The reason why I_{inn} does not change in the negative region of V_{sub} is that the sheath voltage of the inner tube surface does not change. The reason why I_{inn} decreases rapidly in the positive region of V_{sub} is that the sheath voltage of the inner tube surface increases rapidly. On the other hand, when V_{inn} is varied, I_{inn} increases rapidly and then is saturated for an increasing V_{inn}. The reason why I_{inn} increases rapidly is that the sheath voltage of the inner tube surface decreases rapidly and I_{inn} is saturated because the variation of the sheath voltage of the inner tube surface decreases. From the figure, it is found that the V_{sub} dependence and the V_{inn} dependence of I_{inn} are almost symmetric.

Next, let us discuss the reason why I_{inn} increases in both cases as SiH_4 gas is mixed. First, it is clear from the schematic of the equipment in Fig. 1 that the surface area of the inner tube is smaller than those of the inner wall of the deposition chamber and of the substrate table. The gas flow is upward in Fig. 1 as is the Ar plasma. When SiH_4 gas is mixed, Ar ions are used for the dissociation of SiH_4 and are decreased due to the charged transfer. As a result, the silan ions and hydrogen ions are increased. These ions, which are lighter in weight than the Ar ions, are carried upward by the gas flow and at the same time are more likely to reach the inner wall of the deposition chamber and the substrate table by diffusion. Hence, the ion current in the inner tube is decreased while I_{inn} increases. However, if V_{inn} is varied to exceed about 15 V, the results with a mixed SiH_4 gas coincide with those without it. This is because the ion current decreases so that the electron current is dominant, which does not depend on the type of ions.

Figure 3 shows the V_{sub} dependence and the V_{inn} dependence of I_{sub}. Similar to the case in Fig. 2, the electron current is positive in Fig. 3. As V_{sub} is increased, I_{sub} increases slowly for V_{sub} of less than -10 V while it increases rapidly in the region between -10 V and 20 V and then is saturated. On the other hand, when V_{inn} is increased I_{sub} decreases rapidly and then is constant. From the figure, it is found that the V_{sub} dependence and the V_{inn} dependence of I_{sub} are almost symmetric.

From Figs. 2 and 3, it is found that the ion bombardment energy can be controlled by varying the inner tube potential (V_{inn}) as well as by that of the substrate potential (V_{sub}).

Next, the results of the probe measurement are shown. Figure 4 depicts the V_{sub} dependence and the V_{inn} dependence of the plasma spatial potential (V_s) at $z = 3$ cm. When V_{sub} is increased, V_s increases slightly in the negative region of V_{sub} and increases rapidly in the positive region of V_{sub}. On the other hand, V_s increases rapidly if V_{inn} is increased. Similar results are obtained at other measurement locations.

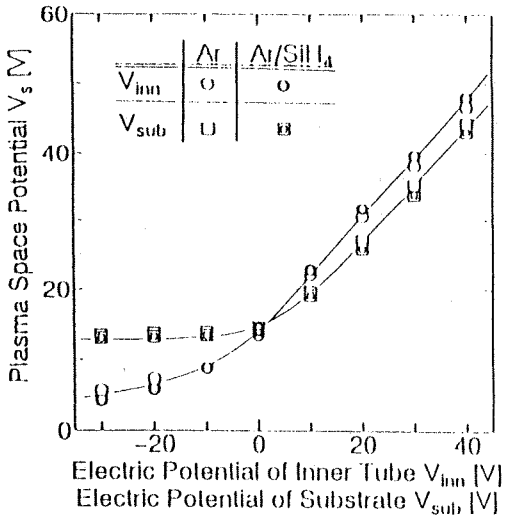

Fig. 4. Dependence of V_s on V_{inn} and V_{sub}.

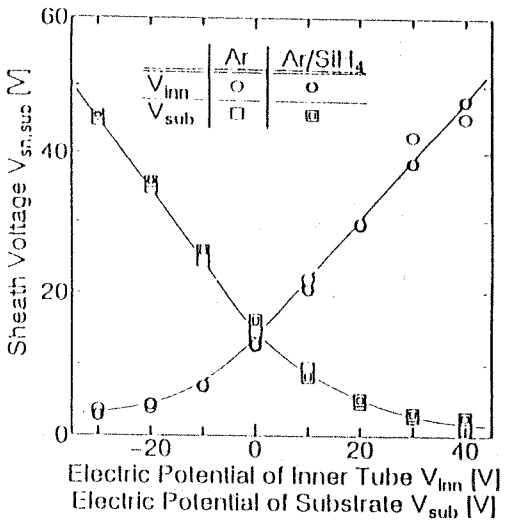

Fig. 5. Dependence of $V_{sh,\,sub}$ on V_{inn} and V_{sub}.

When V_{sub} is negative, the decreasing gradient of V_s becomes smaller and the decrease is only up to about 13 V. On the other hand, if V_{inn} is negative, V_s continues decreasing up to about 4 V. This is because the inner tube is placed in the discharge plasma with high electron density and temperature so that V_{inn} affects V_s strongly, whereas the substrate is in the spatial after-glow plasma in which the electron density and temperature are low.

The sheath voltage ($V_{sh,\,sub}$) on the surface of the substrate can be obtained by taking the difference between V_s and V_{sub} at the edge of the sheath. Since the sheath thickness is several millimeters, it is necessary to carry out the measurement at a location several millimeters from the substrate. However, since the gradient of V_s in the z direction is small, the value of V_s at the sheath edge can be approximated by the value of V_s at z = 9 cm [1]. Hence, by taking the difference between V_s and V_{sub} at z = 9 cm, $V_{sh,\,sub}$ is derived. Figure 5 shows the results. Since V_{sub} is 0 V, the V_{inn} dependence of $V_{sh,\,sub}$ is identical to the V_{inn} dependence of V_s. From the figure, it is found that $V_{sh,\,sub}$ decreases as V_{sub} is increased. This result indicates that the ion bombardment energy decreases as V_{sub} is increased. On the other hand, $V_{sh,\,sub}$ decreases as V_{inn} is decreased. This result indicates that the ion bombardment energy decreases as V_{inn} is decreased. From the above results, it is found that the ion bombardment energy can be controlled by changing V_{inn}.

The ion bombardment energy can be reduced to about 3 eV when V_{inn} is -30 V. When V_{sub} is +40 V,

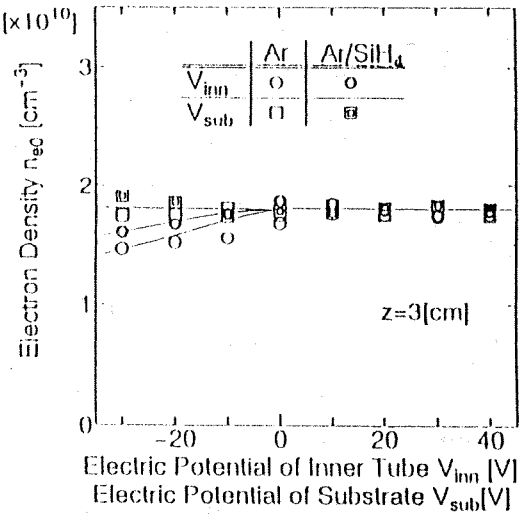

Fig. 6. Dependence of n_{e0} on V_{inn} and V_{sub}.

the ion bombardment energy can be reduced to about 3 eV. However, the electric field that can repel the ions cannot be formed by varying V_{sub} or V_{inn}.

Figure 6 shows the V_{sub} dependence and the V_{inn} dependence of the electron density (n_{e0}) at z = 3 cm. It is found from the figure that n_{e0} does not change with V_{sub}. On the other hand, if V_{inn} is varied, n_{e0} increases slightly as V_{inn} approaches 0 V from a negative value. There is no change for a positive V_{inn}. Similar results are obtained at other measurement locations.

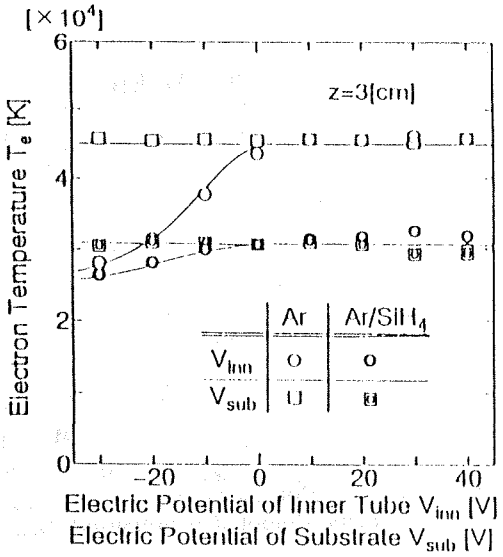

Fig. 7. Dependence of T_e on V_{inn} and V_{sub}.

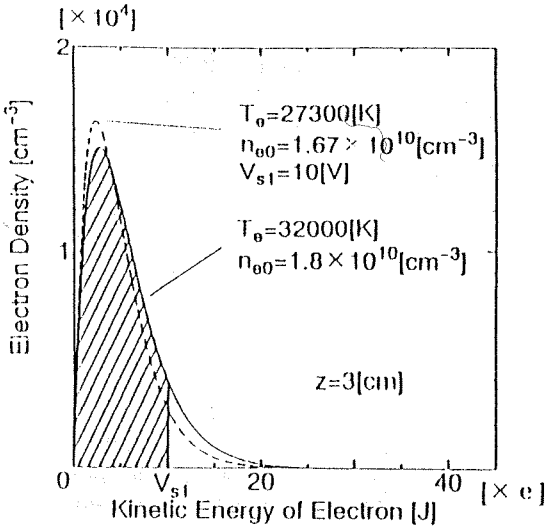

Fig. 8. Maxwell-Boltzmann's distribution.

Figure 7 shows the V_{sub} dependence and the V_{inn} dependence of the electron temperature (T_e) at $z = 3$ cm. From the figure, it is found that T_e does not change as V_{sub} is varied. On the other hand, if V_{inn} is varied, T_e increases as V_{inn} approaches 0 V from a negative value. No change is observed for a positive value of V_{inn}. The results are similar at other measurement locations.

It is found also from the figure that T_e of Ar/SiH_4 plasma is lower than T_e of the pure Ar plasma. This is due to the increases of nonelastic collision, the dissociation of SiH_4 because Ar/SiH_4 plasma is generated mixing Ar plasma with SiH_4 [5].

In the foregoing, it became clear that the potential (V_{inn}) of the electrode in the discharge plasma and the potential (V_{sub}) of the electrode in the spatial after-glow plasma have similar effects on V_s. On the other hand, it was found experimentally that n_{e0} and T_e do not change when V_{sub} is varied while they decrease as V_{inn} is increased in the negative direction in the negative region. The reason for the different tendencies will be discussed.

The velocity distribution of the electrons is, in general, Maxwell-Boltzmann:

$$n_e(v)=4\pi n_{e0}\left(\frac{m_e}{2\pi kT_e}\right)^{3/2} v_2 \exp\left(-\frac{m_e v^2}{2kT_e}\right) \qquad (1)$$

where k is Boltzmann's constant, m_e is the electron mass, T_e is the electron temperature, v is the electron velocity, n_{e0} is the total electron density, and $n_e(v)$ is the density of the electrons with a velocity of v. Since

$$\frac{1}{2} m_e v^2 = eV \qquad (2)$$

Eq. (1) becomes

$$n_e(V)=8\pi n_{e0}\left(\frac{m_e}{2\pi kT_e}\right)^{3/2}\frac{eV}{m_e}\exp\left(-\frac{eV}{kT_e}\right) \qquad (3)$$

where e is the elementary change and V is the voltage. If the sheath voltage or V_s of the wall surface of the deposition chamber is sufficiently large, most of the electrons are repelled back at the wall. As V_s is decreased, the electrons following Maxwell-Boltzmann distribution reach the wall of the deposition chamber successively in the order of higher-electron energy and vanish by recombination with ions at the wall surface.

The solid line in Fig. 8 is the velocity distribution of the electrons obtained by substitution of the experimental data of n_{e0} and T_e to Eq. (3) when V_s is sufficiently large ($V_{inn} > 0$). The values at $z = 3$ cm were used as the experimental data. Next, when V_s is decreased and is V_{s1} in the figure, the electrons with kinetic energy of less than eV_{s1} are repelled by the sheath voltage whereas other electrons with a larger kinetic energy can be separated from the sheath voltage and vanish at the wall of the deposition chamber. Hence, the electron density n'_{e0} when V_s is V_{s1} is the integration of the hatched region in Fig. 8 and is given by

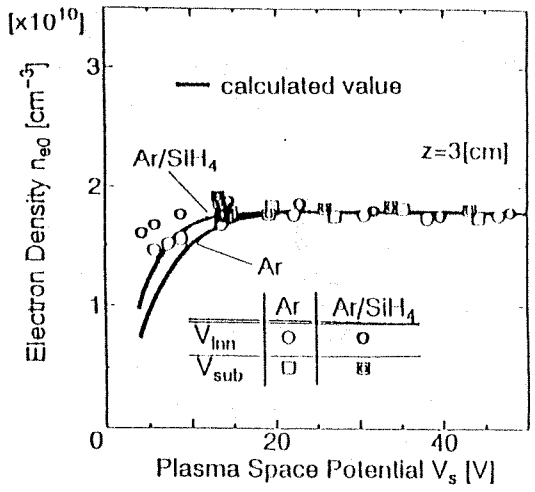

Fig. 9. Comparison of calculated values with experimental values of n_{e0}.

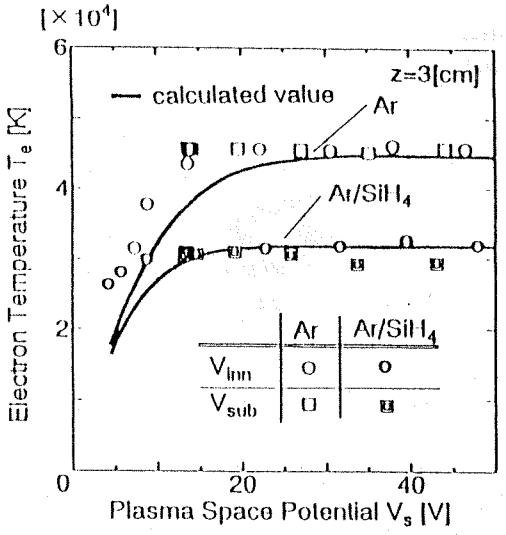

Fig. 10. Comparison of calculated values with experimental values of T_s.

$$n'_{e0}=\int_0^{V_{s1}} n_e(V)dV \tag{4}$$

The electron group with the distribution of the hatched region in Fig. 8 is diffused while colliding with other particles and then becomes another Maxwell-Boltzmann distribution indicated by the dotted line in Fig. 8. Let T_e be the electron temperature of the redistribution. Then, $n_e(V)'$ is given by

$$n_e(V)'=8\pi n'_{e0}\left(\frac{m_e}{2\pi kT_e}\right)^{3/2}\frac{eV}{m_e}\exp\left(-\frac{eV}{kT_e}\right) \tag{5}$$

Then, the energy of the total electrons in the plasma is preserved. Hence,

$$\int_0^{V_{s1}} n_e(V)eV\,dV=\int_0^{\infty} n_e(V)'eV\,dV \tag{6}$$

holds. By solving Eq. (5) and Eq. (6) simultaneously, T_e can be obtained as a first-order approximation.

Figure 9 shows the comparison of the electron density derived from Eq. (4) with the experimental data. On the other hand, Fig. 10 shows the electron temperature derived by solving Eq. (5) and Eq. (6) simultaneously, compared with the experimental data. In both figures, it is found that the experimental findings that n_{e0} and T_e become small if V_s is small ($V_{inn} < 0$) can be explained by the theory described above.

In Figs. 9 and 10, the numerical and experimental results have the identical tendencies that n_{e0} and T_e decrease as V_s is decreased. The results of the theoretical calculations indicate that the reduction is larger. The reaction described above takes place only at the wall surface of the deposition chamber but not in the entire space of the deposition chamber. In the theoretical calculations, however, the calculation was under the assumption that the high-energy electrons in the entire space arrive at the wall of the deposition chamber where it then vanishes. Therefore, the numerical results are smaller than the experimental results. From the above results, when V_{sub} is varied, there is little change in n_{e0} and T_e. This is because V_s decreases only up to about 13 V with a negative value of V_{sub} (as shown in Fig. 4) and the extinction of the electrons at the wall of the deposition chamber is negligible so that the velocity distribution of the electrons does not change. On the other hand, if V_{inn} is varied, n_{e0} and T_e vary. This is because V_s decreases to about 4 V as V_{inn} is negative (as shown in Fig. 4) and the electrons on the higher-energy side vanish by a large amount so that the electron density decreases and the electron temperature is reduced.

4. Conclusions

In a double-tubed coaxial-line microwave plasma CVD system, the plasma parameters were measured while the substrate potential (V_{sub}) and the inner tube

potential (V_{inn}) are varied. The following results can be reported.

(1) The plasma spatial potential (V_s) increases slightly as V_{sub} is increased with a negative value and increases suddenly when V_{sub} is positive. When V_{inn} is increased, V_s increases rapidly. When V_{sub} is varied in the negative region, V_s decreases only to about 13 V. If V_{inn} is varied in the negative region, V_s decreases to about 4 V.

(2) When V_{sub} is increased, the ion bombardment energy can be reduced. When V_{inn} is decreased, the ion bombardment energy can be reduced.

(3) When V_{sub} is varied, the electron density (n_{e0}) and the electron temperature (T_e) do not change. If V_{inn} is increased in the negative direction, n_{e0} and T_e decrease.

(4) The variations of n_{e0} and T_e in item (3) can be explained from the fact that, if V_s is decreased, the electron density decreases due to extinction of the electrons with higher energy in Maxwell-Boltzmann distribution successively on the wall of the deposition chamber so that the average energy of the total electrons in the plasma decreases.

(5) As a method to control the ion bombardment energy, the one varying the substrate potential generally is used. When the substrate is grounded, or the substrate happens to be grounded, the ion bombardment energy can still be controlled by varying the potential of another electrode (inner tube) in the microwave plasma.

V_{sub} is varied in the fabrication of the a-Si:H film and in future V_{inn} will be varied in the fabrication for comparison.

REFERENCES

1. I. Kato, T. Yoneda, and T. Matsushita. Influence of ion bombardment on a-Si:H films fabricated by plasma CVD. Trans. I.E.I.C.E. (C), **J77-C-II**, No. 9, pp. 384-391 (Sept. 1994).
2. I. Kato, S. Wakana, and S. Hara. Microwave plasma CVD system to fabricate a-Si thin films out of plasma. Jpn. J. Appl. Phys., **22**, No. 1, pp. L40-L42 (Jan. 1983).
3. I. Kato and S. Wakana. A new microwave plasma chemical vapor deposition system. Vacuum, **26**, No. 7, pp. 628-636 (July 1983).
4. I. Kato and M. Yano. Fabrication of a-Si:H thin films in and out of plasma coaxial line-type microwave plasma CVD. Trans. I.E.I.C.E. (C), **J69-C**, No. 5, pp. 662-668 (May 1986).
5. I. Kato, T. Usui, and T. Sakamoto. Spatial distribution of plasma parameters in microwave plasma chemical vapor deposition. Trans. Inst. Elect. Eng. of Japan (A), **112**, No. 5, pp. 355-362 (May 1992).

AUTHORS (from left to right)



Isamu Kato graduated in 1967 from the Department of Electronic Communications, Waseda University, where he received his Dr. of Eng. degree in 1973. In 1973, he joined the faculty of Waseda University where he was promoted to Associate Professor in 1978. From 1979 to 1981, he was a Visiting Professor at the University of Manitoba. He has supervised research and participated in joint research with the Canadian National Research Council. In 1983, he was promoted to Professor. He has been engaged in research on photonic engineering, laser engineering, electron physics, metrology, photonic materials, plasma electronics, optical and quantum electronics, and semiconductor thin-film techniques. He is a member of the Institute of Electrical Engineers of Japan, the Applied Physics Society, the Institute of Television Engineering, the Japan Vacuum Society, and IEEE.

Toru Matsushita graduated in 1993 from the Department of Electronic Communications, Waseda University, where he received his M.S. degree in 1995. He has been engaged in research on microwave plasma CVD. At present, he is with Hitachi Central Research Laboratory, Storage Research Department. He is a member of the Applied Physics Society.

Makoto Yamashita graduated in 1994 from the Department of Electronic Communications, Waseda University, where he is working toward his M.S. degree. He has been engaged in research on microwave plasma CVD. He is a member of the Applied Physics Society.

Jpn. J. Appl. Phys. Vol. 35 (1996) pp. 2826–2832
Part 1, No. 5A, May 1996

Optical Energy Gap Measurement of Semiconductor Ultrathin Films Using Optical Waveguides

Naganori TAKEZAWA and Isamu KATO

Department of Electronics and Communication, School of Science and Engineering, Waseda University, Tokyo 169, Japan

(Received January 10, 1996; accepted for publication January 29, 1996)

Measurement of the optical energy gap (E_0) using a slab optical waveguide (SOW) has been studied. With increasing hydrogenated amorphous silicon (a-Si:H) film thickness, transmittance was found to decrease with periodic oscillation. It has been clarified that the oscillation is caused by the change of the field strength distribution of a guided mode in a-Si:H according to the increase of a-Si:H film thickness, using the four-layer structure SOW simulation. By removing the oscillation due to the dependence of transmittance on a-Si:H film thickness, the influence of the oscillation on the values of E_0 can be eliminated. As a result, it has been demonstrated that E_0 of a-Si:H with thickness on the order of 1/40 that of samples used in the conventional method can be measured. It has been clarified that sufficient absorption to determine E_0 of a-Si:H ultrathin films is obtained because the sensitivity of the sensor is increased by changing the size of the SOW.

KEYWORDS: interference fringe, ultrathin film, optical energy gap, band gap, slab optical waveguide, a-Si:H

1. Introduction

The optical energy gap (E_0) is used as one of the factors in the evaluation of semiconductors. E_0 is obtained from the dependence of transmittance on the wavelength for semiconductor films, by ultraviolet-visible spectroscopy. In conventional methods of measurement, a transmitted spectrum is obtained by irradiating ultraviolet-visible light perpendicularly onto a film surface. The spectrum is a curve with interference fringes due to multiple reflection between boundaries of the semiconductor. The fringes are removed by interpolating a curve which goes through the center of the fringes. Using the resultant spectrum without fringes, E_0 is obtained using an expression in which E_0 is proportional to the square root of the absorption coefficient.[1,2] In these methods, when films are sufficiently thick, it is easy to determine the curve which goes through the center of the fringes because there are many fringes and their amplitude is small. Absorption by the semiconductor is high, so that error in the determination of E_0 is low. On the other hand, when films are thin, it is difficult to determine the curve which goes through the center of the fringes because there are few fringes and their amplitude is high. The absorption is also low. Consequently, error in the determination of E_0 becomes appreciable. Therefore, the conventional methods require thick semiconductor films of approximately 1 μm.[3]

We have developed a measurement method for E_0 of ultrathin hydrogenated amorphous silicon (a-Si:H) semiconductor film, using an optical fiber where the clad of a middle section is removed.[4] In this method, the a-Si:H film is deposited on the core of the optical fiber section without the clad. In this region, some of the guided light is absorbed by the a-Si:H film. It has been found that even if the semiconductor film is thin, absorption sufficient to determine E_0 can be obtained by increasing the length of the part from which the clad is removed (the bare part of the core). However, a problem that the semiconductor film is deposited nonuniformly on the core of the optical fiber arises in this method.

Based on the above, we devised a new measurement method in which a slab optical waveguide (SOW) is used as a sensor instead of the clad-removed optical fiber. By depositing the semiconductor only on the surface of the SOW sensor, the problem of nonuniform deposition of semiconductor film is overcome.

First, the experimental results show that with increasing a-Si:H film thickness, transmittance decreases with oscillation. This phenomenon is analyzed by simulation of the four-layer structure SOW of air, a-Si:H, optical waveguide and air. The absorption coefficient of the four-layer SOW was found to peak periodically since the electric field strength distribution of a guided mode around the a-Si:H layer becomes maximum according to the a-Si:H film thickness.

Next, two curves, one of which is an exponential curve which goes through each maximum oscillation in the dependence of transmittance on the deposited a-Si:H film thickness and the other of which is an exponential curve which goes through each minimum, are determined in order to remove the oscillation. The method for obtaining the exponential function without the oscillation, which is the arithmetic mean of the above two curves and goes through the point at which transmittance is 1 with deposited film thickness of 0 nm, is described. Using this method, E_0 of ultrathin films can be determined in a range of thickness which could not be measured by conventional methods.

Finally, the dependences of E_0 on the width of the part on which the a-Si:H film is deposited, the length, and the thickness of the optical waveguide are discussed based on results of experiments in which each of the parameters of the SOW sensor are changed.

2. Experimental Conditions and the SOW Sensor

Figure 1 shows our experimental setup. The chamber of the microwave plasma chemical vapor deposition (MPCVD) system is shown. a-Si:H is fabricated using Ar and SiH_4 plasma flowing from the left-hand side of the system. The SOW sensor is set at the position of the substrate to be fabricated in this chamber. Guided white

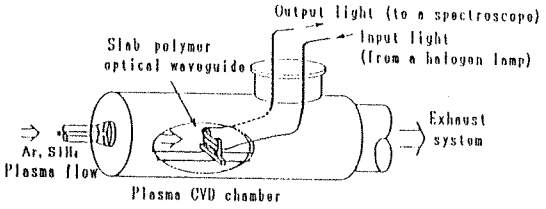

Fig. 1. Experimental setup.

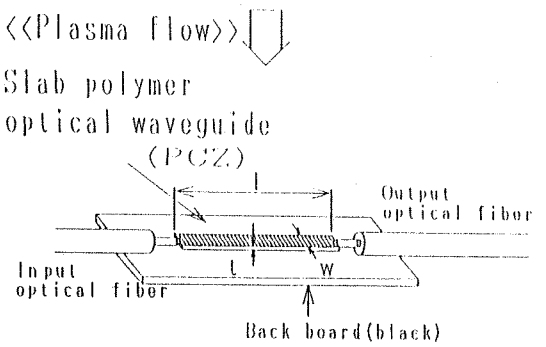

Fig. 2. Details of the slab optical waveguide (SOW) sensor.

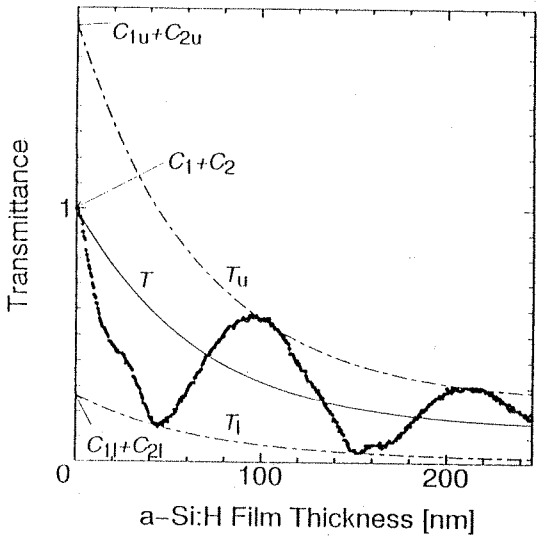

Fig. 3. Dependence of transmittance on the a-Si:H film thickness. •: experimental values; upper broken line T_u: upper transmittance through the maxima; lower broken line T_l: lower transmittance through the minima; solid line T: transmittance without oscillation.

light is irradiated, and during the deposition, absorption spectra which change continuously are measured.

Figure 2 shows the SOW sensor. The material of SOW is bisphenol Z polycarbonate (PCZ).[5] The width of the part of the SOW sensor on which film is deposited is defined as w mm, its length is defined as l mm, and the thickness of SOW is defined as $t\,\mu$m. The step index optical fibers with the 400 μm silica core and the polymer clad are attached to the two ends of the SOW sensor to guide input and output beams. An acrylic resin board is used as the back board to prevent deposition of semiconductor films onto the back of SOW. The color of the board is black in order to reduce the amount of stray light guided through the board. Although this is not shown in Fig. 2, the joints between SOW and optical fibers, and the two remaining sides of SOW are covered with foil to prevent deposition of semiconductor films. A halogen lamp is used as a light source.

3. Experiment

To fabricate a-Si:H, the double-tubed coaxial-line-type MPCVD system has been used.[6] In the chamber, the intensity of the ultraviolet-visible spectrum from 500 to 800 nm through the optical waveguide system is first measured before the semiconductor is deposited on the SOW sensor. Second, a-Si:H film is fabricated on the SOW sensor. The intensities of the ultraviolet-visible spectrum are measured at fixed time intervals. During the measurement, the film thickness does not change, because the intensity is measured quickly at approximately 0.5 s per scan while the deposition rate of a-Si:H is very low at approximately 0.05 nm/s. Third, transmittance spectra are obtained from the ratio of the spectrum intensity before the deposition to those measured for each film thickness. Finally, from the transmittance spectra, the dependence of $(\alpha h\nu)^{1/2}$ (where α is the absorption coefficient, h is Planck's constant and ν is frequency) is obtained.[7] Then, E_o is determined from the linearity part of the curve which is expressed as

$$(\alpha h\nu)^{1/2} = B(h\nu - E_o), \tag{1}$$

where B is a constant.

The thickness of the a-Si:H film on the SOW sensor is determined in the following manner. At the time of fabrication, a glass substrate and crystal-oscillation-type thickness monitor are placed close to the SOW sensor. During the fabrication, the a-Si:H film thickness is measured, and the change of the deposition rate is recorded. After the fabrication, the a-Si:H film thickness on the glass substrate is measured with a needle-tactual-type thickness meter. The results measured using the thickness monitor are corrected relative to the a-Si:H film thickness on the glass substrate. Then, the film thickness at each measurement of the transmittance spectrum is determined.

4. Oscillation in the Dependence of Transmittance on the Film Thickness

An example of the measured result is shown in Fig. 3. The plot of the experimental values (•) reveals the dependence of transmittance on the a-Si:H film thickness obtained using the SOW sensor with $l = 50$ mm, $t = 78\,\mu$m and $w = 0.8$ mm at the wavelength of 632.8 nm. In Fig. 3, with increasing a-Si:H film thickness, transmittance decreases exponentially with oscillation.

The reason for the oscillation is investigated in terms of the dependence of field strength distribution near a-Si:H on the film thickness, by the SOW simulation in the TE guided mode. Figure 4 shows the profile of the four-layer structure of SOW of air, a-Si:H, optical waveguide and air. The effective complex refractive index and field strength distribution are obtained from solutions of an eigenvalue equation for a transversely guided mode.[8]

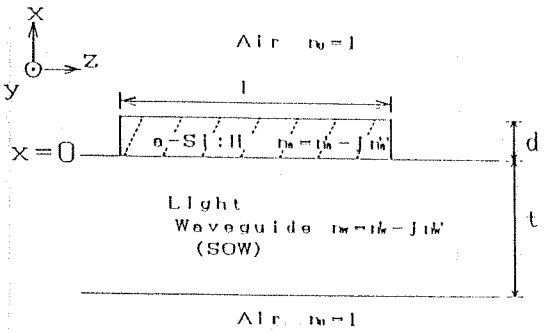

Fig. 4. Structure of waveguide with the a-Si:H film.

The complex refractive index of SOW n_w and complex refractive index of a-Si:H n_a used in the simulation are obtained in the following manner.

First, ultraviolet-visible spectra of two SOW films which have different thicknesses are measured. A reflection coefficient and absorption coefficient are calculated using

$$T_i = T_0 \exp(-\alpha_w t_i) \quad (i = 1 \text{ or } 2) \tag{2}$$

$$(1 - R)^2 = T_0, \tag{3}$$

where T_i is the transmittance of each SOW film, i is the sample number, T_0 is the transmittance when absorption of SOW is 0, α_w is the absorption coefficient, t_i is the thickness of each SOW film and R is the reflection coefficient. The multiple reflection is neglected in the approximation here.

The real part of n_w is obtained using

$$R = (n_w' - 1)^2/(n_w' + 1)^2, \tag{4}$$

where n_w' is the real part of n_w, and the refractive index of air is 1.

The imaginary part of n_w is obtained using

$$n_w'' = \lambda/2\pi \cdot \alpha_w, \tag{5}$$

where n_w'' is the imaginary part of n_w, and λ is wavelength.

The real part of n_a is measured using an ellipsometer. The imaginary part of n_a is obtained using eq. (5), similarly to n_w''.

n_w, obtained in the above manner, is $1.62 - j2.09 \times 10^{-5}$, and n_a is $2.90 - j0.07$.

We next studied the dependence of the absorption coefficient on the a-Si:H film thickness, obtained from the imaginary part of the effective complex refractive index of the four-layer structure SOW.

When the a-Si:H film thickness d is 0 nm, we observe the TE_0 mode. The dependence of the absorption coefficient of the four-layer structure SOW on the a-Si:H film thickness when the thickness of SOW t is constant at 95 μm, is shown in Fig. 5. The absorption coefficient reaches a peak when the a-Si:H thickness d is around 20 nm, 150 nm and 280 nm with a period of approximately 130 nm.

Considering the results described above, we examine the electric field strength distributions observed at the a-Si:H film thicknesses d of around 20 nm and around 150 nm.

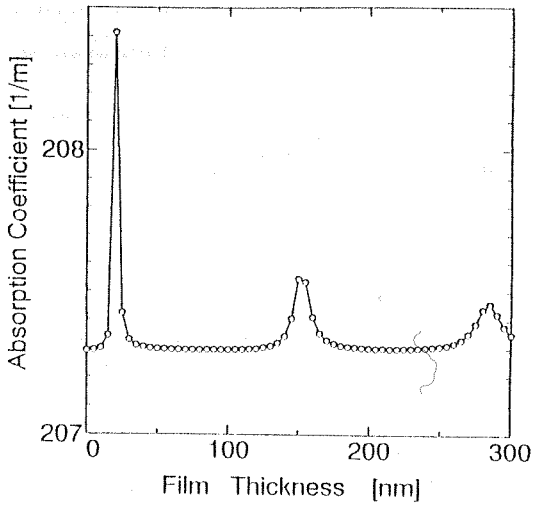

Fig. 5. Dependence of absorption coefficient on the a-Si:H film thickness for TE mode.

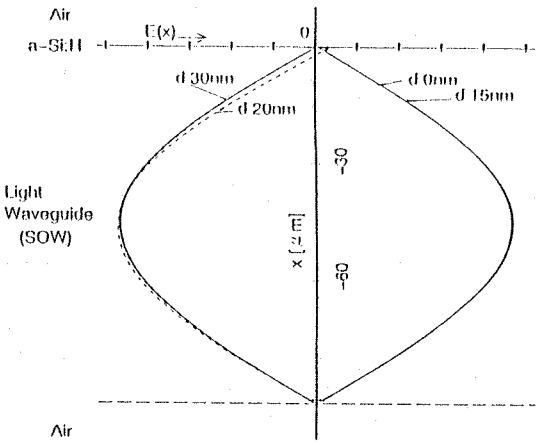

Fig. 6. Field strength distributions of TE mode obtained by the SOW simulation. $d = 0$, 15, 20 and 30 nm.

The field strength distributions throughout the entire optical waveguide at d of 0, 15, 20 and 30 nm are shown in Fig. 6. The line $x = 0\,\mu$m corresponds to the boundary between the a-Si:H layer and the optical waveguide layer in Fig. 4. In Fig. 6, although the direction of the electric field is reversed between $d = 15$ nm and 20 nm, the field distributions seem to be in the TE_0 mode throughout the entire waveguide including the a-Si:H layer. The details of the field distributions around $x = 0\,\mu$m for $d = 0$, 15, 19 and 20 nm are shown in Fig. 7. d increases in the positive direction along the x axis, and the boundary between air and a-Si:H is shown as the dashed line. The field distribution is in the TE_0 mode up to $d = 19$ nm according to both Figs. 6 and 7. For $d = 20$ nm, the direction of the electric field is reversed in Fig. 6, but not in Fig. 7. The number of antinodes of the electric field increases in Fig. 7.

The expanded view of the field distributions for thicker a-Si:H layers with $d = 130$, 140, 150 and 160 nm is shown in Fig. 8. A new antinode of the electric field is observed between $d = 140$ nm and $d = 150$ nm. Here, the electric field in the a-Si:H layer becomes maximum. Therefore,

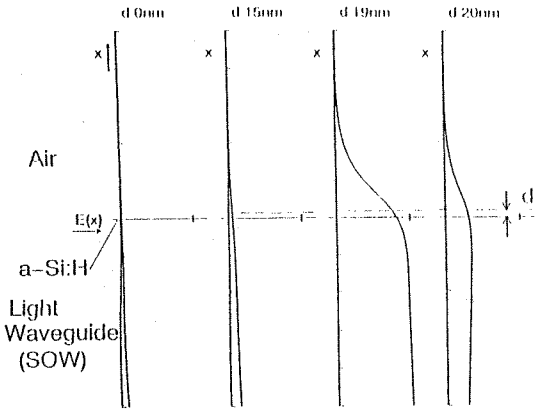

Fig. 7. Field strength distributions, at $d = 0$, 15, 19 and 20 nm.

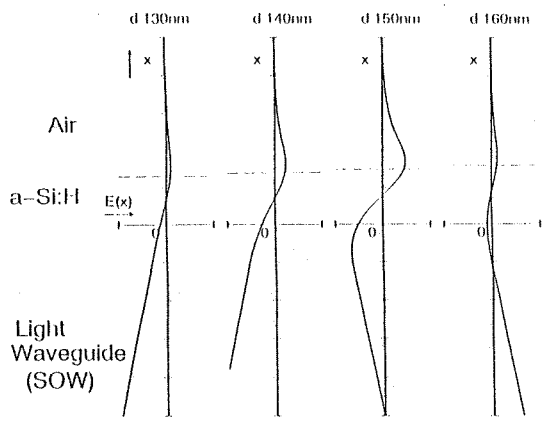

Fig. 8. Field strength distributions, at $d = 130$, 140, 150 and 160 nm.

in Fig. 5, the antinodes of the electric field in the a-Si:H layer are generated with a period of approximately 130 nm at approximately $d = 20$, 150, and 280 nm, at which the electric field in the a-Si:H layer becomes maximum. Because the absorption coefficient of a-Si:H is very large compared with that of the optical waveguide, the absorption must be large when amplitude of the field in the a-Si:H is high. From Figs. 7 and 8, as the amplitude of the field in the a-Si:H becomes high at $d = 19$ nm and $d = 150$ nm, the absorption of the four-layer SOW shows peaks.

When d is 0 nm, we observe the TE_n mode, and investigation in the same manner as described above reveals the same tendency. It has been confirmed that the absorption coefficient reaches a peak at almost the same thicknesses as shown in Fig. 5 as the a-Si:H film thickness increases.

The slab waveguide simulation of the four-layer structure clarified the following. As the a-Si:H film thickness increases from 0 nm, the field strength distribution in the a-Si:H film changes to the mode which has antinodes of the electric field. With each increase of the number of antinodes, the field strength distribution in the a-Si:H layer shows a maximum. As a result, oscillation occurs in the dependence of transmittance on the a-Si:H film thickness, as shown in Fig. 3, because the absorption coefficient of the entire optical waveguide becomes maximum periodically.

5. Method for Removing the Oscillation of Transmittance

The dependence of transmittance on the a-Si:H film thickness at each wavelength shows almost the same tendency as in Fig. 3.

The curve from which the oscillation in the dependence of transmittance on the deposited film thickness was removed at a certain wavelength goes through the point of transmittance of 1 at the thickness of 0 nm, $(d, T) = (0, 1)$, and is expressed as an exponential function with absorption coefficient α. There is light which passes through the optical waveguide without interacting with the deposited film, in addition to light which is absorbed into the deposited film on the optical waveguide in this measurement method. The ratio of light which passes through the optical waveguide to the total amount of light is defined as the constant C_1, and the ratio of light which is absorbed into the deposited film is defined as the constant C_2. In Fig. 3, even if d becomes infinite, the transmittance approaches the constant C_1 asymptotically instead of approaching 0. Therefore, in our measurement method, the transmittance T is given by the expression below when the oscillation is removed.

$$T = C_1 + C_2 \exp(-\alpha d). \tag{6}$$

From eq. (6), when $d = 0$,

$$C_1 + C_2 = 1. \tag{7}$$

The function T_u which goes through the maxima of the oscillation and function T_l which goes through the minima are expressed as

$$T_u = C_{1u} + C_{2u} \exp(-\alpha_u d) \tag{8}$$

$$T_l = C_{1l} + C_{2l} \exp(-\alpha_l d). \tag{9}$$

The relationship among T, T_u and T_l is defined as

$$T = (T_u + T_l)/2. \tag{10}$$

Substituting eqs. (8) and (9) into eq. (10) yields,

$$C_1 + C_2 \exp(-\alpha d) = \{C_{1u} + C_{1l} + C_{2u} \exp(-\alpha_u d) + C_{2l} \exp(-\alpha_l d)\}/2. \tag{11}$$

For eq. (11) to hold for every d,

$$\alpha = \alpha_u = \alpha_l. \tag{12}$$

From eqs. (6), (8), (9), (10) and (12),

$$C_1 = (C_{1u} + C_{1l})/2 \tag{13}$$

$$C_2 = (C_{2u} + C_{2l})/2. \tag{14}$$

From eqs. (7), (13) and (14),

$$C_1 + C_2 = (C_{1u} + C_{1l} + C_{2u} + C_{2l})/2 = 1. \tag{15}$$

Substituting the maxima (T_{u1}, d_2), (T_{u2}, d_4) and the minima (T_{l1}, d_1), (T_{l2}, d_3) into eqs. (8) and (9), applying eq. (12), C_{1u}, C_{1l}, C_{2u} and C_{2l} are given as functions of α alone. Substituting C_{1u}, C_{1l}, C_{2u} and C_{2l} obtained above into eq. (15), the function wherein the 1 on the right-hand side is transposed to the other side is defined

as $f(\alpha)$. Therefore,

$$f(\alpha) = 0. \tag{16}$$

The values of the maxima and minima are obtained from the experimental values in Fig. 3. The values of C_{1u} and C_{1l} are also estimated roughly from the same figure. Substituting these values into eq. (8), the approximate value of α_u is determined. On calculating $f(\alpha)$ by varying α, it becomes clear that there is only one value of α which satisfies eq. (16) in the range of α above 0 and below the value of two orders larger than α_u. Then, using the Newton-Raphson method for eq. (16) with α_u as the initial value, the value of α is obtained. T, T_u and T_l are determined using the value of α, and are also shown in Fig. 3. The values of $C_1 + C_2$, $C_{1u} + C_{1l}$ and $C_{2u} + C_{2l}$ when $d = 0$, obtained from eqs. (6), (8) and (9), and using eq. (12), are also shown in Fig. 3. It is clear that T_u passes through each maximum of the experimental values (•) and T_l passes through each minimum. Furthermore, it is clear that T almost passes through the middle of the experimental values (•). The same procedure to remove the oscillation is used at each wavelength. Figure 9 shows the experimental values (•) of the dependence of transmittance on the wavelength at the a-Si:H film thickness of 203.7 nm. The dependence of transmittance on the wavelength obtained from T, T_u and T_l at each wavelength is also shown in the same figure (○ is T, upper ◇ is T_u and lower ◇ is T_l). From Fig. 9, it is clear that even if the abscissa is converted to wavelength the curves obtained from T_u and T_l go through the maxima and minima of the experimental values (•). The wavelength of 632.8 nm taken from Fig. 3 is also shown as the dashed line in Fig. 9.

Next, Fig. 10 shows the same data, with ordinate of $(\alpha h\nu)^{1/2}$ and abscissa of $h\nu$, translated from the experimental values (•) and ○ plots in Fig. 9. E_o is obtained by extrapolating the straight line represented by eq. (1).

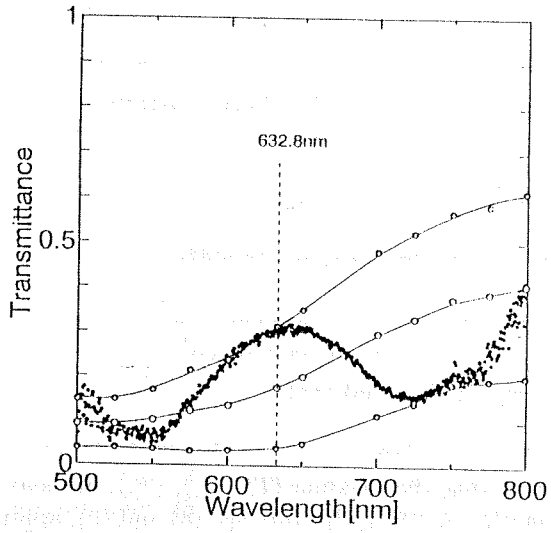

Fig. 9. Dependence of transmittance on wavelength. •: from experimental values; ○: transmittance without oscillation; upper ◇: upper transmittance Tu; lower ◇: lower transmittance T_l. The data at the wavelength of 632.8 nm taken from Fig. 3 are also shown as the dashed line.

6. Dependence of E_o on the Film Thickness

Next, the dependence of E_o on the a-Si:H film thickness, obtained using the SOW sensor, is shown in Fig. 11. The values with the transmittance oscillation removed (○), as well as those without removal of the transmittance oscillation (△) for comparison are shown. From Fig. 11, it is clear that E_o is influenced significantly by the transmittance oscillation, and the errors in △ plots are marked. On the other hand, it is clear that E_o approaches a constant value when the a-Si:H film thickness is more than approximately 65 nm because the errors become small when the oscillation is removed. The value of E_o is approximately 1.8 eV which agrees with the value measured by the conventional method[4] for an a-Si:H film on the order of 1 μm thick.

After removing the influence of the transmittance oscillation, the increase of E_o with a-Si:H thickness less than 65 nm in ○ plots of Fig. 11 shows that absorption sufficient for determining E_o cannot be obtained in this range of film thickness.

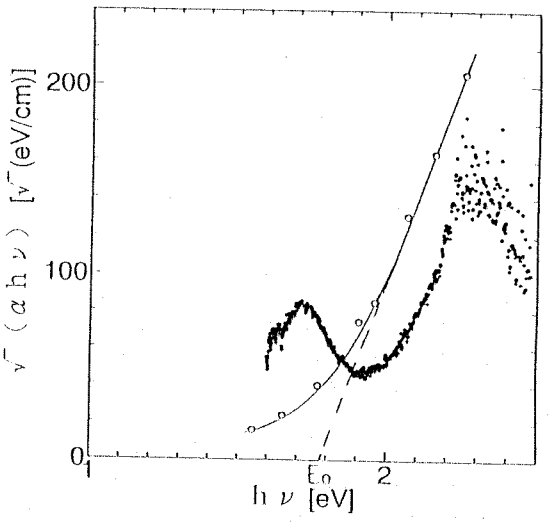

Fig. 10. $(\alpha h\nu)^{1/2}$ versus photon energy $h\nu$ translated from the plots in Fig. 9. •: from experimental values; ○: from transmittance without oscillation; dashed line: fitting straight line of eq. (1).

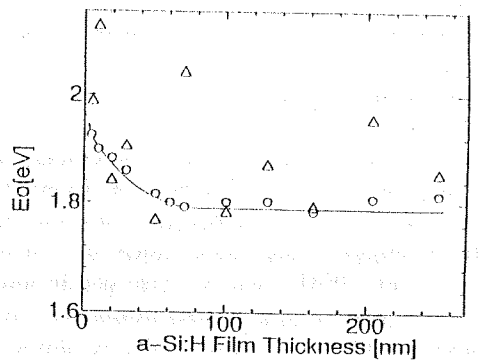

Fig. 11. Dependence of E_o on the a-Si:H film thickness. ○: with the procedure to remove the oscillation and △: without the procedure to remove the oscillation.

7. Characteristics of E_o in Case of Changing the Dimensions of the SOW Sensor

We change the width and length of the SOW section on which film is deposited and the thickness of SOW, and investigate the dependence of E_o on the a-Si:H film thickness.

7.1 *Width of the SOW section with deposited film*

The dependence of E_o on the a-Si:H film thickness for various widths of the SOW section with a-Si:H film deposition w is shown in Fig. 12. It is clear that E_o takes the same constant value at almost the same thickness when the width is 1 mm and 5 mm. Therefore, it is clear that the sensitivity of the sensor is not influenced if the range of w variation is small.

7.2 *Length of the SOW section with deposited film*

The dependence of E_o on the a-Si:H film thickness for various lengths of the SOW section with a-Si:H film deposition l is shown in Fig. 13. At $l = 100$ mm, E_o takes a constant value for a-Si:H film thickness d more than approximately 35 nm. At $l = 50$ mm, E_o takes the same constant value when d is more than 65 nm. Therefore, it is clear that even if the a-Si:H film is extremely thin, E_o can be determined when l is sufficiently long. It is considered that sufficient absorption for the determination of E_o is obtained because the interaction distance between a-Si:H and guided light becomes longer when l becomes longer. Also, it is clear that the products of the minimum values of the thickness d needed to determine E_o and l in two samples are almost the same.

7.3 *Thickness of SOW*

The dependence of E_o on the a-Si:H film thickness for various thicknesses of SOW t is shown in Fig. 14. At $t = 30\,\mu$m, E_o has a constant value when the a-Si:H film thickness d is more than approximately 20 nm. At $t = 78\,\mu$m, E_o has the same constant value when d is more than approximately 65 nm. From this result, it is clear that E_o can be determined when t is sufficiently thin. When t becomes thin, the amount of light which passes through the optical waveguide without interacting with the a-Si:H film decreases (corresponding to the decrease of C_2 in eq. (6)). Therefore, sufficient absorption is obtained to determine E_o because the effective absorption coefficient increases.

In our investigation using the conventional method for E_o with various thicknesses of the deposited film, the a-Si:H film thickness is required to be more than approximately 750 nm,[4] whereas a film thickness of approximately 20 nm is sufficient to measure E_o in our method. In other words, the E_o measurement of a-Si:H is accomplished with thickness on the order of 1/40 that required in the conventional method.

8. Conclusions

For the optical energy gap measurement of a-Si:H ultrathin films, we proposed a new method of using a SOW as the sensor.

(1) It has been shown experimentally that with increasing a-Si:H film thickness, transmittance decreases with periodic oscillation. It was clarified analytically that this phenomenon occurs because the field strength distribution of the guided modes at the a-Si:H layer periodically becomes maximum with increase of the film deposition thickness, so that the absorption coefficient of the entire waveguide including the a-Si:H film exhibits peaks periodically.

(2) The method for removing the oscillation in the dependence of transmittance on the a-Si:H film thickness has been described, and it has been shown that the

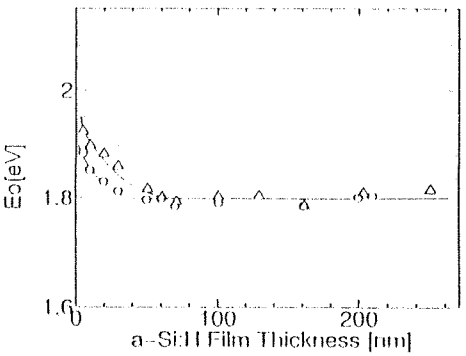

Fig. 13. Dependence of E_o on a-Si:H film thickness with variation of the length of the SOW section with film deposition l. o: $l = 100$ mm, $t = 87\,\mu$m and $w = 1$ mm; △: $l = 50$ mm, $t = 78\,\mu$m and $w = 0.8$ mm.

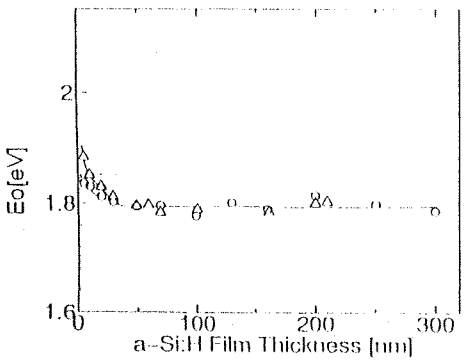

Fig. 12. Dependence of E_o on the a-Si:H film thickness with variation of the width of the SOW section with film deposition w. o: $w = 5$ mm, $l = 100$ mm and $t = 90\,\mu$m; △: $w = 1$ mm, $l = 100$ mm and $t = 87\,\mu$m.

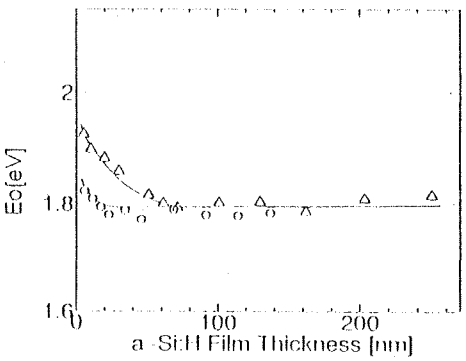

Fig. 14. Dependence of E_o on a-Si:H film thickness with variation of the thickness of SOW t. o: $t = 30\,\mu$m, $l = 48$ mm and $w = 2.4$ mm; △: $t = 78\,\mu$m, $l = 50$ mm and $w = 0.8$ mm.

exponential function which passes through the point of transmittance of 1 at the film thickness of 0 nm, with oscillation removed, can be obtained. It has been clarified that the influence of the oscillation in the dependence of E_0 on the wavelength can be removed, and E_0 can be determined in a range of thin films which could not be measured previously by conventional methods.

(3) To increase the sensitivity of the SOW sensor, we need only increase the length of the SOW section with film deposition l and/or decrease the thickness of the SOW sensor t. The width of the SOW section with film deposition w is not related to the sensitivity of the sensor in the range of width studied in this work (approximately from 1 to 5 mm).

(4) E_0 can be determined for a-Si:H film thicker than approximately 20 nm (approximately 1/40 the thickness required in the conventional method) when the SOW sensor (the material is PCZ, t is 100 μm, l is 100 mm and w is 5 mm) is used.

This method is an *in situ* measurement method in which the a-Si:H film is not exposed to air, while in the conventional methods air exposure is unavoidable. This is an especially important issue for ultrathin films which are easily affected by oxidation.

Acknowledgement

This work was supported by the Waseda University Grant for Special Research Project in 1995 and in part by the Grant-in-Aid for Scientific Research from the Ministry of Education, Science, Sports and Culture. The authors thank Mr. Hotta, a graduate student, for his assistance in the experiments and simulations.

1) J. Tauc, R. Grigorovici and A. Vancu: Phys. Status Solidi **15** (1966) 627.
2) P. J. Zanzucchi, C. R. Wronski and D. E. Carlson: J. Appl. Phys. **48** (1977) 5227.
3) R. Swanepoel: J. Phys. E **16** (1983) 214.
4) N. Takezawa and I. Kato: Jpn. J. Appl. Phys. **32** (1993) L1474.
5) T. Kurokawa, N. Takato and Y. Katayama: IEICE Tech. Rep. (1979) OQE79-107.
6) I. Kato and M. Yano: Trans. IEE Jpn. **J69-C** (1986) 662.
7) R. V. Kruzelecky, C. Ukah, D. Racansky and S. Zukotynski: J. Non-Cryst. Solids **103** (1988) 234.
8) J. N. Polky and L. M. Gordon: J. Opt. Soc. Am. **64** (1974) 274.

INFLUENCE OF LONGITUDINAL MAGNETIC FIELD APPLIED TO COAXIAL LINE TYPE MICROWAVE PLASMA (II)

同軸線路形マイクロ波プラズマへの縦磁界印加の影響 (II)

Taro KAMIKO, Toshihiro YAMAGISHI, Yoshinori MORITA and Isamu KATO
神子太郎、山岸俊浩、森田義則、加藤勇

Department of Electronics and Communication
School of Science and Engineering, Waseda University,
3-4-1 Ohkubo, Shinjuku-ku, Tokyo 169, Japan
早稲田大学理工学部電子通信学科、〒169　東京都新宿区大久保3-4-1

Abstract The magnetic field along the gas flow (the longitudinal magnetic field) is applied to the discharge area in the double tubed coaxial line type microwave plasma chemical vapor deposition system and the effect of the applied longitudinal magnetic field to pure N_2 plasma is considered as follows. The probe I-V characteristic is stabilized by applying the magnetic field over about 1000[Gauss]. When the magnetic flux density is about 1000[Gauss], the electron temperature and the electron density increase due to the effect of the electron cyclotron resonance. The effect of the applied longitudinal magnetic field doesn't vary over about 1000[Gauss] regardless of the magnetic flux density. In the vicinity of the place where plasma blows off into the deposition chamber, one can increase n_e at z=1.5[cm] by about ten times and can increase n_e at z=0[cm] by about three times. Therefore this plasma is proper for CVD because it is possible to fabricate films at high rate.

1. Introduction

In order to generate the stable plasma in a wider range of the gas pressure and with various kinds of gases, the coil is set up around the discharge tube of the double tubed coaxial line type microwave plasma chemical vapor deposition system. The magnetic field along the gas flow is applied to the discharge area. The plasma parameters are measured by the single probe method, and the effects resulted from depression of the diffusion of plasma in the radial direction are investigated.[1]~[5] In this report, the plasma parameters in the discharge area have been measured. And the discharge mechanism is examined in detail.

2. Experiment

In this system, the microwave electric field in the discharge area is the fundamental mode of the coaxial line and runs parallel with the gas flow, namely, with the applied magnetic field. Therefore the electron cyclotron resonance (ECR) doesn't fundamentally occur. The axial distance from the end of the discharge tube is defined as z and the radial distance from the center axis of the discharge tube is defined as r. For further details of this system, see ref. [2].

The experimental condition is shown in the Table 1. With the N_2 gas flow rate 50 [ml/min], letting SiH_4 gas flow, SiN films is fabricated. The experiment is made on pure N_2 plasma. The magnetic flux density (B) is the value at the center of the coil. The single probe method is applied in the measurement. At z=1.5[cm] in the deposition chamber, a probe of 0.05[cm] in

diameter and 1.0[cm] in length is used, where the gas flow rate is 30,40 and 50[ml/min]. At z=0 and -1.5[cm] in the vicinity of the dischage area, a probe of 0.05[cm] in diameter and 0.1[cm] in length is used, where the gas flow rate is 50[ml/min]. The probe is set up perpendicularly to the gas flow, namely, to the magnetic field in some way like bending the tip of the probe perpendicularly. It is confirmed that the results of the measurements agree with each other regardless of the probe length. The end of the inner tube is set up at z=-2.0[cm]. It is the same position when SiN films are fabricated.

Table 1: Experimental Condition

Microwave Input Power	150	[W]
Microwave Reflective Power	45	[W]
N_2 Gas Flow Rate	30,40,50	[ml/min]
Gas Pressure in Chamber	2.4,3.2,4.0	[mTorr]
Position of Probe	z=1.5,0,-1.5[cm],	r=0[cm]
Coil Current	0~6	[A]
Magnetic Flux Density	0~1986	[Gauss]

3. Result and Discussion

First, we consider the results of the measurement in the deposition chamber, namely, at z=1.5[cm]. The dependences of the electron temperature (T_e) and the electron density (n_e) on B are shown in Fig. 1 and 2.

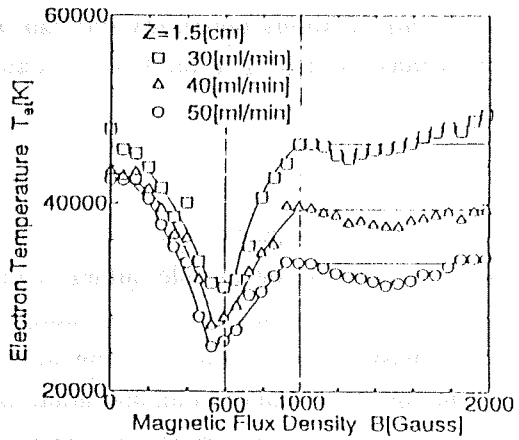

Figure 1: Dependence of Electron Temperature on Magnetic Flux Density

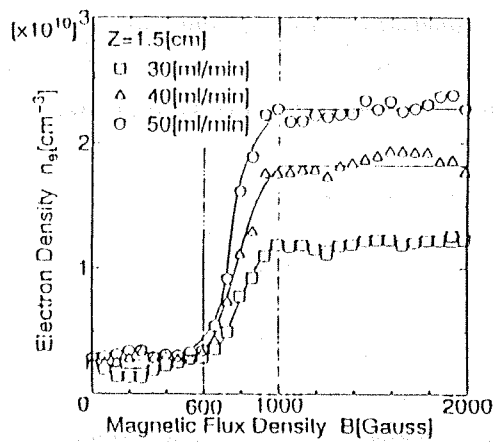

Figure 2: Dependence of Electron Density on Magnetic Flux Density

With increasing B from 0 to about 600[Gauss], T_e decreases and n_e keeps constant. The reason is as follows. The diffusion of electrons toward the wall of the discharge tube is depressed by applying the longitudinal magnetic field, the decay of electrons on the wall decreases, and in order to keep the balance of the generation and the decay of the plasma, the generation of electron must decrease. Therefore, T_e decreases. This reason is as follows. It becomes difficult that the microwave electric power penetrates the center of the plasma as n_e increases in the vicinity of the wall of the discharge tube.

With increasing B from about 600[Gauss] to about 1000[Gauss], both T_e and n_e increase and are saturated at about 1000[Gauss]. This is the effect of ECR. It occurs not at the resonance magnetic field 875[Gauss] but at about 1000[Gauss]. For further details about this, see ref. [2].

With increasing B over about 1000[Gauss], T_e and n_e keep constant. The reason is as follows. The dependence of the electron diffusion coefficient ($D_\perp$) in the radial direction on B is given

by

$$D_\perp = \frac{D}{1 + \omega_c^2/\nu^2} \qquad D = \frac{kT_e}{m_e\nu} \qquad \omega_c = \frac{eB}{m_e}$$

where k is Boltzmann constant, e is quantum of electricity, ν is collision frequency and m_e is electron mass. The result of this calculation is shown in Fig. 3.

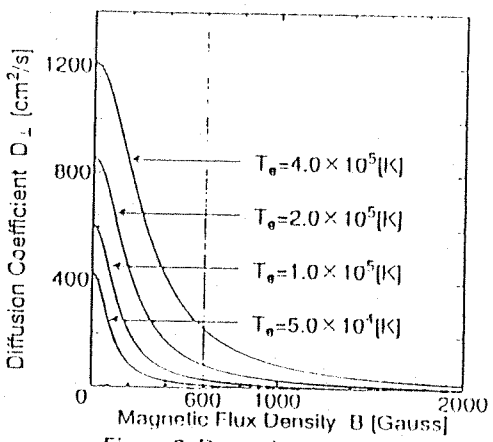

Figure 3: Dependence of $D_\perp$ on B

In this figure, $D_\perp$ decreases rapidly with increasing B from 0[Gauss] to about 600[Gauss], and decreases gradually with increasing B over about 600[Gauss]. That is to say, the effect that the diffusion of electrons is depressed increases rapidly under about 600[Gauss], and that increases gradually over about 600[Gauss]. The reason for T_e and n_e areconstant with increasing B over about 1000[Gauss] is as follows. The effect that the diffusion of electrons is depressed increases gradually and the effect of ECR decreases at the same time. And in this figure, the tendency that the slope of the curve around 0[Gauss] is nearly zero correspond with the tendency of the dependence of T_e on B which is shown previously.

In addition, n_e at z=1.5[cm] increases by about ten times applying the magnetic field (as shown Fig. 2).

Next, we will consider the results of the measurement in the vicinity of the discharge area, namely, at z=0,-1.5[cm]. The dependences of T_e and n_e on B are shown in Fig. 4 and 5.

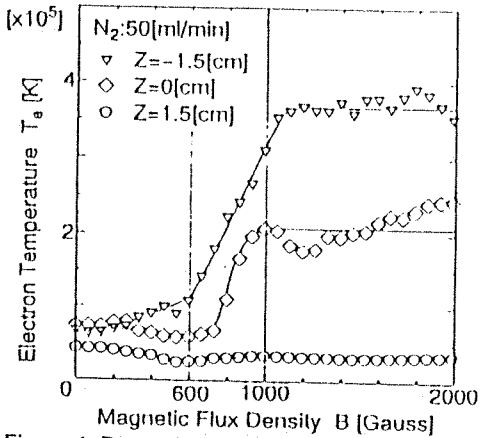

Figure 4: Dependence of Electron Temperature on Magnetic Flux Density

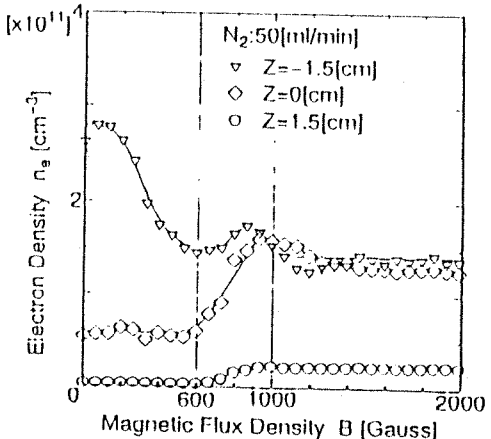

Figure 5: Dependence of Electron Density on Magnetic Flux Density

In case of z=0[cm], the results are as follows. With increasing B from 0[Gauss] to about 1000[Gauss], T_e decreases and n_e keep constant. With increasing B from about 600[Gauss] to about 1000[Gauss], both T_e and n_e increase due to the effect of ECR. And with increasing B

over about 1000[Gauss], both of them keep constant. This tendency is same as the tendency at z=1.5[cm].

In addition, n_e at z=0[cm] increases by about three times applying the magnetic field.

In case of z=-1.5[cm], the results are as follows. With increasing B from 0[Gauss] to about 600[Gauss], T_e increases a little and n_e decreases rapidly. This tendency is different from the tendency at z=1.5 and 0[cm]. The reason is as follows. The radial distribution of n_e in the discharge tube varies from the shape of zero degree Bessel function to the shape like trapezoid with increasing B and therefore n_e at r=0[cm] decreases. In addition, the distance from the end of the inner tube is only 0.5[cm] and many of the electrons can't reach the shadow of the inner tube due to depression of the diffusion of electrons. The reason why T_e increases is that most of the electrons which reach the shadow of the inner tube have high energy.

With increasing B from about 600[Gauss] to about 1000[Gauss], both T_e and n_e increase due to the effect of ECR. And with increasing B over about 1000[Gauss], both of them keep constant. This tendency is same as the tendency at z=1.5 and 0[cm].

It follows from what has been said that the effect of the applied longitudinal magnetic field doesn't vary over about 1000[Gauss] regardless of B.

In addition, it is confirmed that the probe I-V characteristic is stabilized by applying the magnetic field over about 1000[Gauss].

4. Conclusions

The magnetic field along the gas flow is applied to the discharge area, and the effects of the applied longitudinal magnetic field are considered as follows.

(1) The probe I-V characteristic is stabilized by applying the magnetic field over about 1000[Gauss].

(2) When B is about 1000[Gauss], T_e and n_e increase due to the effect of ECR.

(3) The effect of the applied longitudinal magnetic field doesn't vary over about 1000[Gauss] regardless of B.

(4) In the vicinity of the place where plasma blows off into the deposition chamber, one can increase n_e at z=1.5[cm] by about ten times and can increase n_e at z=0[cm] by about three times. Therefore this plasma is proper for CVD because it is possible to fabricate the films at high rate.

Acknowlegement

This research was supported in part by the Grant-in-Aid for Scientific Research from the Ministry of Education, Science and Culture of Japan.

Reference

[1] T.Yamagishi et al:The 55th Autumn Meeting of Jpn.Soc.Appl.Phys.,19p-ZV-15(1994)

[2] T.Yamagishi et al:The 12th Symposium on Plasma Processing,I-A06(1995)

[3] T.Yamagishi et al:The 42nd Spring Meeting of Jpn.Soc.Appl.Phys.,28p-TE-1(1995)

[4] T.Yamagishi et al:The 56th Autumn Meeting of Jpn.Soc.Appl.Phys.,27p-M-9(1995)

[5] T.Kamiko et al:The 56th Autumn Meeting of Jpn.Soc.Appl.Phys.,27p-M-10(1995)

INFLUENCE OF LONGITUDINAL MAGNETIC FIELD APPLIED TO COAXIAL LINE TYPE MICROWAVE PLASMA (III)

同軸線路形マイクロ波プラズマへの縦磁界印加の影響（III）

Toshihiro YAMAGISHI, Taro KAMIKO, Yoshinori MORITA and Isamu KATO
山岸俊浩、神子太郎、森田義則、加藤勇

Department of Electronics and Communication
School of Science and Engineering, Waseda University.
3-4-1 Ohkubo, Shinjuku-ku, Tokyo 169, Japan
早稲田大学理工学部電子通信学科、〒169 東京都新宿区大久保3-4-1

Abstract The magnetic field along the gas flow (the longitudinal magnetic field) is applied to the discharge area in the double tubed coaxial line type microwave plasma chemical vapor deposition system and the electron density (n_e) is measured in the Ar plasma. The effects of the applied magnetic field to the Ar plasma are investigated. The results are as follows. With increasing the magnetic flux density (B), n_e in the deposition chamber has a peak but n_e in the vicinity of the discharge area doesn't vary remarkably. In the vicinity of the discharge area, in any B, n_e at the center of the discharge tube is higher than that at the point which is away from the center of the discharge tube, because the plasma decays on the wall of the discharge tube by bipolar diffusion. Moreover the radial distribution of n_e varies from the shape which is described as J_0 Bessel function to the shape like trapezoid, because the diffusion of the charged particles toward the wall of the discharge tube is depressed by applying the magnetic field.

1. Introduction

The plasma parameters have been measured in the double tubed coaxial line type microwave plasma chemical vapor deposition system. The plasma parameters in the deposition chamber, that is to say, in the spatial afterglow plasma have been measured, and the effects of the applied magnetic field to Ar plasma have been investigated[1]-[5]. In this report, the spatial distribution of the electron density (n_e) are measured when the magnetic field is applied to Ar plasma. From the results of this measurement, the discharge mechanism in this system is investigated from the effects of the applied magnetic field to Ar plasma.

2. Experiment

Fig. 1 shows the configuration of this system. For further details of this system, see reference (2). Table 1 shows the experimental condition.

The n_e is measured by a single probe method. The cylindrical probe of 0.05[cm] in diameter and of 1.0 or 0.1[cm] in length is used. The probe is set perpendicularly to the magnetic force line. The axial distance from the end of the discharge tube is defined as z and the radial distance from the center axis of the discharge tube is defined as r.

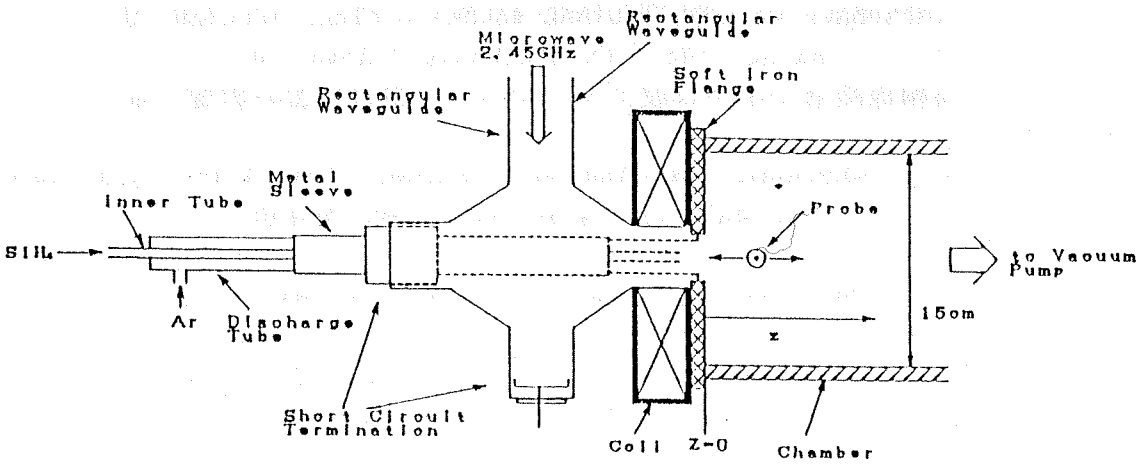

Fig. 1 Experimental Apparatus

Table 1. Experimental Condition

Microwave Input Power	100 [W]
Microwave Reflective Power	30 [W]
Ar Gas Flow Rate	30 [ml min]
Gas Pressure in Chamber	2.6 [mTorr]
Position of Probe	z -1.0~+1.5 [cm]
	r 0, 0.3 [cm]
Coil Current	I=0~6 [A]
Magnetic Flux Density(Center)	B 0~1986 [Gauss]

3. Result and Disccusion

Fig. 2 shows the dependence of n_e on magnetic flux density (B) at z=+1.5[cm]. The B is the value at the center of the coil. It shows that n_e increases gradually with B increased from 0 to about 700[Gauss] because the radial diffusion of the charged particles is depressed by applying the magnetic field. Then, n_e increases rapidly and peaks out at about 1200[Gauss]. This is the effect of the electron cyclotron resonance. With B increased further, n_e decreases because of the decay of the effect of the electron cyclotron resonance.

Fig. 3 shows the dependence of n_e on B at z=0[cm]. It shows that the dependence of n_e has the same tendency as Fig. 2 (z=+1.5[cm]). However, n_e increases by about 2.5 times compared with n_e at z=+1.5[cm], because the point of the measurement (z=0[cm]) is nearer to the discharge plasma area than the point of z=+1.5[cm].

Fig. 4 shows the dependence of n_e on B at z= -1.0[cm] as parameter is r. With B increased, both n_e at r=0 and 0.3[cm] decrease and then are constant. The reason why n_e decreases is as follows. With B increased, the radial distribution of n_e varies from the shape which is described as Jo Bessel

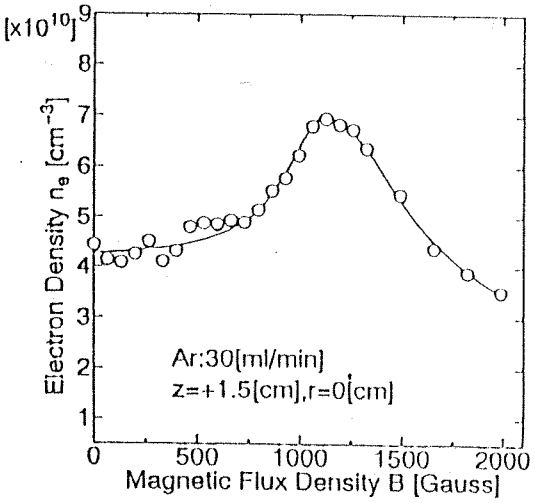

Fig.2 Dependence of Electron Density on Magnetic Flux Density

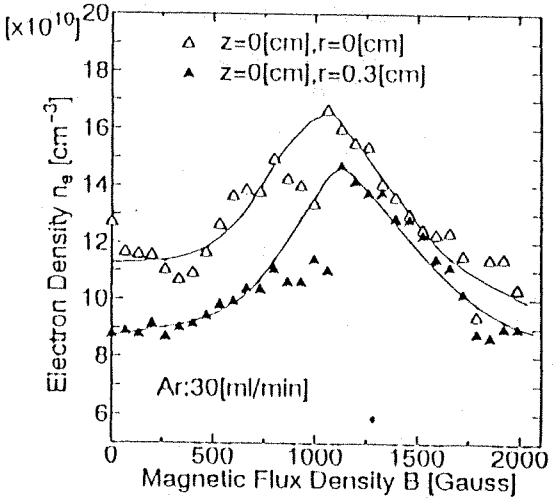

Fig.3 Dependence of Electron Density on Magnetic Flux Density

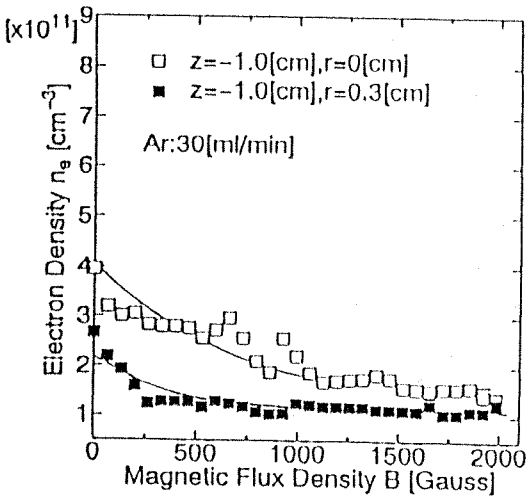

Fig.4 Dependence of Electron Density on Magnetic Flux Density

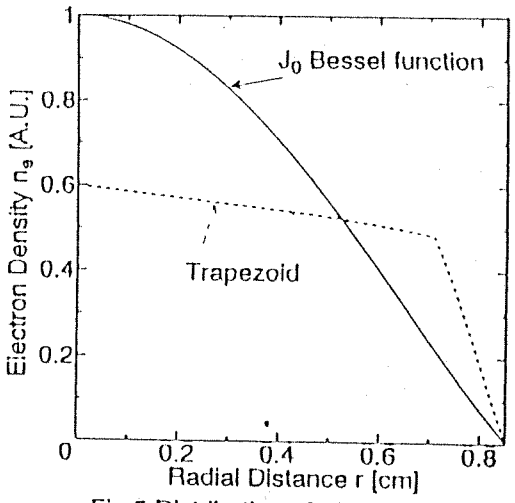

Fig.5 Distribution of Electron Density on Radial Distance

function to the shape like trapezoid (as shown in Fig. 5), because the diffusion of the charged particles toward the wall of the discharge tube is depressed by applying the magnetic field, and it becomes defficult that the microwave electric power penetrates to the center of the plasma, and in the vicinity of the wall the rate of ionization increases. The value of both n_e at r=0 and 0.3[cm] becomes higher than that at z=0[cm], because the point of the measurement (z=-1.0[cm]) is nearer to the discharge area than the point of z=0[cm].

Moreover, Fig. 3 and 4 show that n_e at r=0.3[cm] is lower than that at r=0[cm] regardless of B. These results show that n_e decreases as the point

of the measurement is nearer to the wall of the discharge tube, because the plasma decays on the wall of the discharge tube by the surface recombination. That is to say, the radial distribution doesn't have a dimple in the center of the plasma, because the volume recombination doesn't occur on account of the low pressure. As B is increased, the difference between n_e at r=0[cm] and that at r=0.3[cm] decreases (as shown in Fig.3 and 4). This shows that the radial distribution of n_e varies from the shape which is described as J0 Bessel function to the shape like trapezoid, and shows that the conclusions mentioned above is valid.

4. Conclusions

(1) At z=11.5 and 0[cm], with B increased, the tendency of n_e has a peak at about 1200[Gauss], because of the effect that the diffusion of the charged particles is depressed by applying the magnetic field and the effect of the electron cyclotron resonance.

(2) At z=0 and 1.0[cm], n_e at r=0.3[cm] is lower than that at r=0[cm]. It shows the natural result that n_e decreases as the point of the measurement is nearer to the wall of the discharge tube, because the plasma decays on the wall of the discharge tube by the surface recombination.

(3) At z=-1.0[cm], the vinicity of the discharge area, with B increased, n_e decreases and then is constant. As B is increased, the difference between n_e at r=0[cm] and that at r=0.3[cm] decreases.

(4) From these results, it is cleared that the radial distribution in the discharge tube varies from the shape which is described as J0 Bessel function to the shape like trapezoid. This shows that the uniform plasma in radial direction, which is proper for CVD, is obtained.

Acknowlegement

This research was supported in part by the Grant-in-Aid for Scientific Research from the Ministry of Education, Science and Culture of Japan. The authors would like to thank Mr. Andoh, bachelor student, for his assistance in this study.

Reference

[1] T. Yamagishi et al:The 55th Autumn Meeting of Jpn. Soc. Appl. Phys., 19p ZV 15(1994)

[2] T. Yamagishi et al:The 12th Symposium on Plasma Processing, I A06(1995)

[3] T. Yamagishi et al:The 42nd Spring Meeting of Jpn. Soc. Appl. Phys., 28p TE 1 (1995)

[4] T. Yamagishi et al:The 56th Autumn Meeting of Jpn. Soc. Appl. Phys., 27p M 9 (1995)

[5] T. Kamiko et al:The 56th Autumn Meeting of Jpn. Soc. Appl. Phys., 27p M 10(1995)

Film Deposition under Control of Sheath Voltage on the Film Surface in MPCVD Apparatus

MPCVDにおける膜前面のシース電圧の制御と成膜

Makoto YAMASHITA, Hirotaka OGIHARA, Isamu KATO
山下　誠、　荻原　博隆、　加藤　勇

School of Science and Engineering, Waseda University
3-4-1, Okubo, Shinjuku-ku, Tokyo, 169
早稲田大学理工学部、　〒169　東京都新宿区大久保3-4-1

Abstract It is necessary to discuss the ion bombardment on the film surface while film deposition when the thin films are fabricated in a plasma CVD method. The ion bombardment energy is caused by not merely DC substrate bias voltage but the sheath voltage on the film surface. Therefore, it is considered that the ion bombard energy can be controlled when the sheath voltage on the film surface is controlled. In this paper, it is clear that the sheath voltage on the film surface can be controlled from 0[V] to -95[V] when DC substrate bias voltage is varied from +40[V] to -80[V]. And then, a-Si:H films are fabricated when the sheath voltage on the film surface is varied from 0[V] to -95[V]. As a result, it is clear that the dangling bond density increases, however, Si concentration and the ratio of the SiH bond density to the SiH_2 bond density increase.

1.Introduction

We have developed the double tubed coaxial line type microwave plasma CVD (MPCVD) apparatus. In this apparatus, the microwave power is confined in the cylindrical cavity. Therefore, a discharge plasma is created only in the cavity region. In the deposition chamber, a spatial afterglow plasma without supply of the microwave power is created by gas flow and diffusion. The discharge region of the apparatus has the double tubed structure that consists of the fused quartz outer discharge tube and the stainless steel inner tube concentrically. The Ar gas is fed to the outer discharge tube and the SiH_4 gas is fed to the inner tube. The argon atoms are ionized in the cavity region by the microwave power. The inner tube guide the SiH_4 gas to the discharge tube end, then SiH_4 is dissociated by the collision with the Ar plasma particles. The substrate table is placed at 10[cm] of the axial distance from the discharge tube end in the spatial afterglow plasma. Under this condition, the distribution of the electron temperature (T_e) and density (n_e) don't change when DC substrate bias voltage (V_{dc}) is varied from +40[V] to -80[V] (in this voltage limits DC discharge doesn't generate). However, the plasma space potential (V_s) change, therefore, the sheath voltage on the film surface (V_{sh}) change. We reported that V_{sh} doesn't become

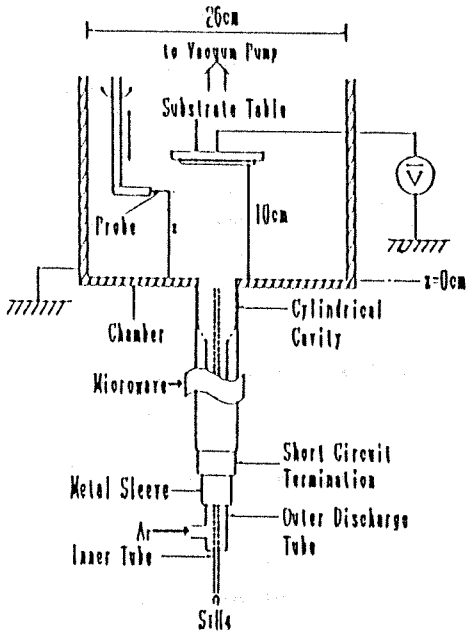

Fig.1 Cnfiguration of the MPCVD apparatus

0[V] with varying V_{dc} when the substrate table area (A_s) is large (about 50[cm^2]), but V_{sh} become 0[V] or positive value with varying V_{dc} when A_s is small[1].

In this paper, it is clear that V_{sh} can be controlled from 0[V] to -95[V] when A_s=40[cm^2] and V_{dc}=+40[V]～-80[V]. And then, a-Si:H films are fabricated when V_{sh} is varied from 0[V] to -95[V] and the film properties are evaluated.

2.Experiment

Figure 1 shows the configuration of the MPCVD apparatus. The axial distance from the discharge tube end is defined as z. The substrate table is placed at z=10[cm]. The substrate table area (A_s) is 40[cm] and V_{dc} is varied from +40[V] to -80[V]. The single probe measurement is performed in the Ar/SiH_4 plasma (Ar gas flow rate: 110[ml/min], SiH_4 gas flow rate: 30[ml/min]). In this plasma a-Si:H films are also fabricated. The cylindrical probe of 0.05[cm] in diameter and 1[cm] in length is used for the probe measurement. The probe measurement is performed at z=9[cm] on the deposition chamber axis. And then, a-Si:H films are fabricated and the film properties are evaluated.

3.Result and Discussion

Figure 2 shows the dependence of T_e and n_e at z=9[cm] on V_{dc}. In fig.2, the values in case of different A_s are showed for reference. The T_e and n_e don't change with varying V_{dc}. Therefore, the reactivity in this plasma is not influenced with varying V_{dc}.

Figure 3 shows the dependence of V_s at z=9[cm] on V_{dc}. The V_s is constant in the range of negative value of V_{dc}, and increases with increasing V_{dc} in the range of positive value of V_{dc}. And then, V_s becomes 40[V] when V_{dc}=+40[V] (on the dotted line in fig.3).

Subtract V_s at z=9[cm] from V_{dc} and we get V_{sh}. Therefore, V_{sh} is calculated by using fig.3. Figure 4 shows the dependence of V_{sh} on V_{dc}. The V_{sh} is 0[V] when V_{dc}=+40[V], and V_{sh} is -95[V] when V_{dc}=-80[V]. This figure indicates that a-Si:H films can be fabricated under controlling V_{sh} from 0[V] to -95[V] by using the substrate table which area is 40[cm^2].

The a-Si:H films are fabricated with varying V_{sh} and these film properties are evaluated. Figure 5 shows the dependence of the deposition rate on V_{sh}. The deposition rate decreases with increasing the ion bombardment energy.

Figure 6 shows the dependence of the Si concentration on V_{sh}. The film density increases

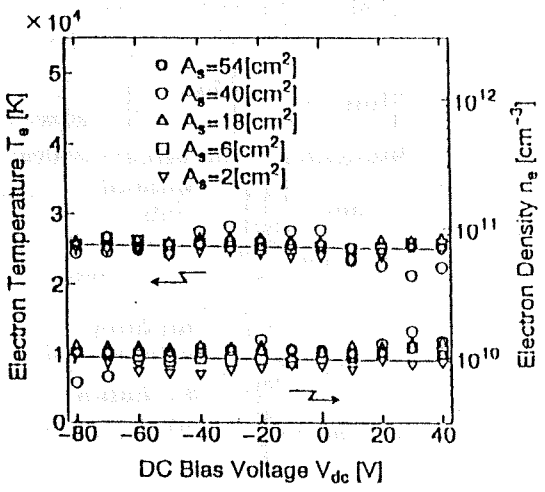

Fig.2 Dependence of T_e and n_e at z=9[cm] onV_{dc}

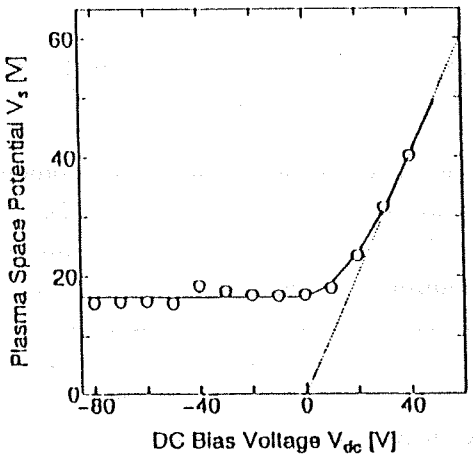

Fig.3 Dependence of V_s at z=9[cm] on V_{dc}

with increasing the ion bombardment energy.

Figure 7 shows the dependence of the ratio of the SiH bond density to the SiH_2 bond density on V_{sh}. The SiH bond density increases with increasing the ion bombardment energy and SiH_2 bond density decreases with increasing the ion bombardment energy.

Figure 7 shows that the hydrogen atoms are disconnected because the film surface is heated by the ion bombardment. Because the film surface heated up, mobility of the radicals on the film surface increase and the radicals fill in the defects caused by the disconnection of the hydrogen atoms. It results high density a-Si:H films as shown in fig.6.

Figure 8 shows the dependence of the amount of Si deposited per unit area and unit time, calculated by (Si concentration (C_{Si}) as shown fig.6 × the deposition rate (D.R.) as shown fig.5), on V_{sh}. The amount of Si deposited per unit area and unit time is constant in the range of V_{sh} > about -40[V] and decreases with increasing the ion bombardment energy in the range of V_{sh} < about -40[V]. This figure indicates the spattering occurs when V_{sh} is about -40[V].

Figure 9 shows the dependence of the Ar atom density on V_{sh}. The Ar atom density is under the limit of detection in the range of V_{sh} > about -40[V]. It is considered that the Ar atom is not implanted in the film. The Ar atom is implanted in the film in the range of V_{sh} < about -40[V][2]. Generally, it is said that the Ar plasma etching occurs when the accelerating voltage is lower than about -50[V] and this figure indicates that Ar ion implantation occurs when the accelerating voltage is lower than about -40[V]. These values show good agreement.

Figure 10 shows the dependence of the dangling bond density on V_{sh}. The dangling bond density increases with increasing the ion bombardment energy. It is considered that the void is formed around Ar atom implanted by the ion bombardment.

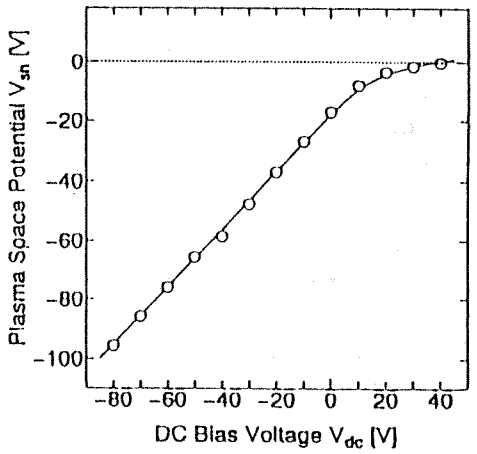

Fig.4 Dependence of V_{sh} on V_{dc}

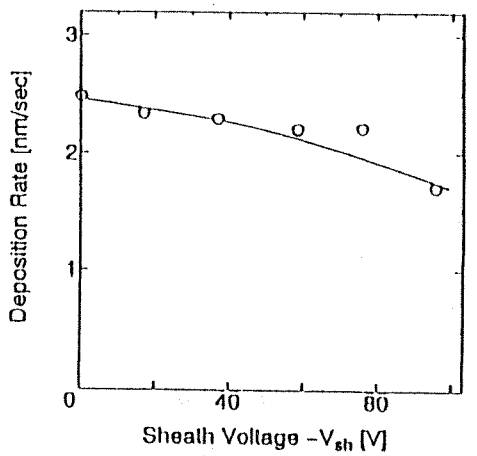

Fig.5 Dependence of the deposition rate on V_{sh}

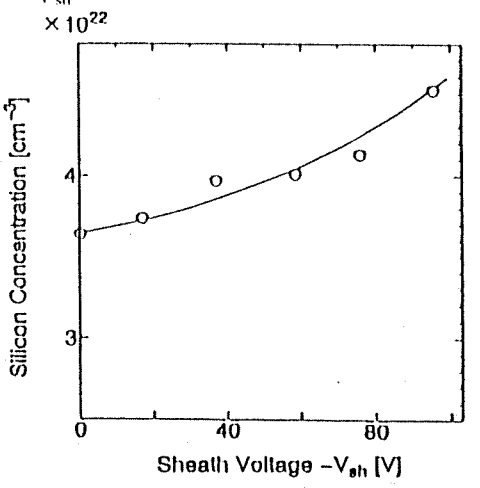

Fig.6 Dependence of the Si concentration on V_{sh}

4.Conclusion

The V_{sh} changes with varying V_{dc}. It has been clear that V_{sh} is controlled from 0[V] to -95[V] by using the substrate table which area is 40[cm^2]. When V_{sh} is 0[V], a-Si:H films can be fabricated under the condition that the ion bombardment energy is zero. The ion bombardment has the effect to make the film properties good because the film surface is heated. However, the ion bombardment has another effect to cut the bond in the film because the Ar atoms are implanted in the film. Thus the effect of the ion bombardment has both merits and demerits.

5.Acknowlegement

This research was supported partially by the Grant-in Aid for Scientific Research for the Ministry of Education, Science and Culture of Japan. The authors thank Mr. Iizuka and Mr. Koshiji, research students, for their experimental assistance.

References

(1)I.Kato, T.Yoneda: T.IEE Japan, 114-A, 5, 375-380 (1994)

(2)I.Kato, T.Yoneda, T.Matsushita: Trans.IEICE, C-II, J77, 9, 384-391 (1994)

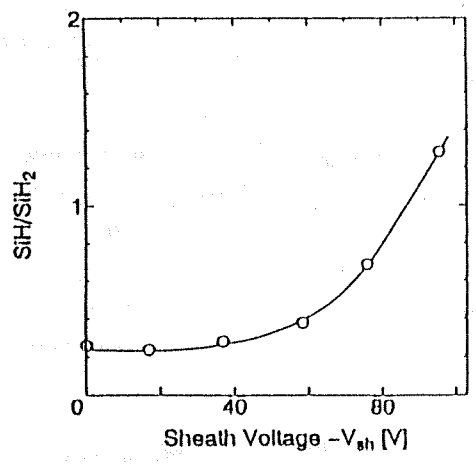

Fig.7 Dependence of the ratio of the SiH bond density to the SiH_2 bond density on V_{sh}

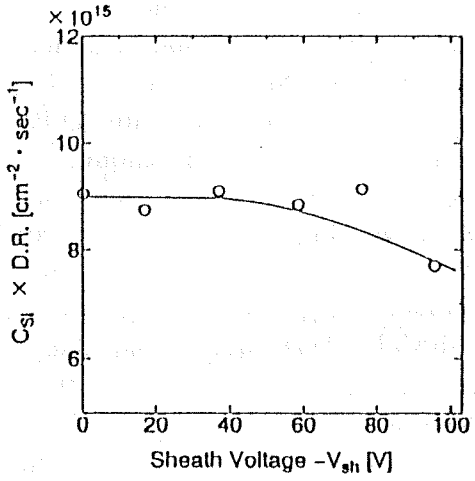

Fig.8 Dependence of the amount of Si deposited per unit area and unit time

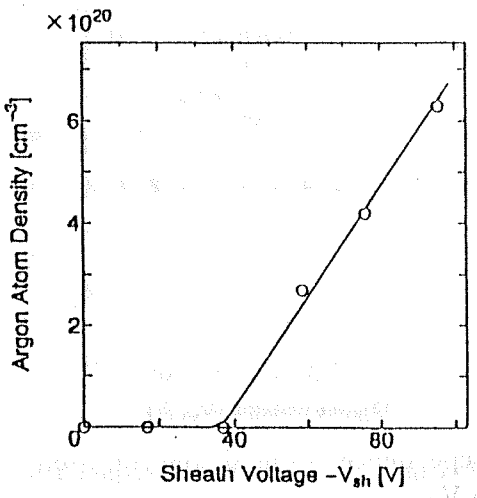

Fig.9 Dependence of the Ar atom density on V_{sh}

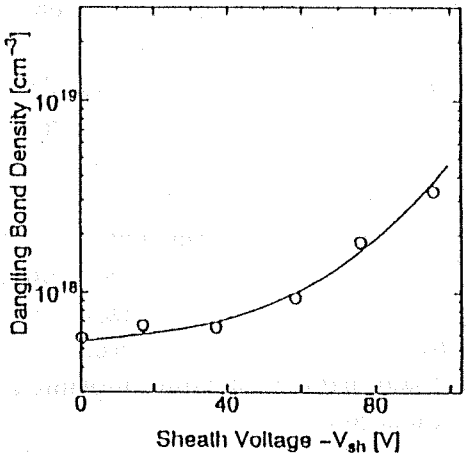

Fig.10 Dependence of the dangling bond density on V_{sh}

論　文

マイクロ波プラズマ中に設置した電極の電位がプラズマパラメータに与える影響

加藤　勇[†]　松下　亨[†]　山下　真[†]

Dependence of Plasma Parameters on Electric Potential of Electrode in Microwave Plasma

Isamu KATO[†], Toru MATSUSHITA[†], and Makoto YAMASHITA[†]

あらまし　筆者らは，これまで2重管式同軸線路形マイクロ波プラズマCVD (MPCVD) の研究を行ってきている．本MPCVD装置の放電管部は溶融石英製の外側放電管とステンレス製の内管の2重管構造となっている．筆者らは，以前に，本MPCVD装置において，空間的アフターグロープラズマ中に設置した基板の電位を変化させることにより，電子密度，電子温度は変化させずにイオン衝撃エネルギーを制御できることを明らかにしている．本研究では，放電プラズマ中に設置されている内管の電位を変化させてもイオン衝撃エネルギーを制御できることを明らかにした．しかしながら，電子密度，電子温度は基板電位を変化させたときとは異なる傾向を示した．そこで，電子密度，電子温度についてマクスウェル・ボルツマン分布に基づく理論計算を行い，異なる傾向を示すのは，プラズマ空間電位が約13 Vから約4 Vと低下するに従い，電子が高エネルギー側から堆積室壁面で順次消滅し，その結果，電子の速度分布が変化することにより説明できることを明らかにした．

キーワード　基板電位，内管電位，イオン衝撃，プラズマパラメータ，マクスウェル・ボルツマン分布

1. はじめに

水素化アモルファスシリコン(a-Si : H)膜は薄膜トランジスタなどの電子材料や太陽電池などの光子材料として用いられている．a-Si : H膜の作製法としては，大面積化が容易である，低温プロセスであるといった特徴をもつプラズマCVD法が広く用いられている．この膜質を制御するためにはプラズマを制御する必要があるにもかかわらず，プラズマの研究はあまり行われていないのが現状である．プラズマCVDにおいて，イオン衝撃に関する問題は切り放すことのできない問題であり，筆者らは，放電プラズマを所定の領域に閉じ込めることにより，イオン衝撃の少ない空間的アフターグロープラズマ中で成膜できる2重管式同軸線路形マイクロ波プラズマCVD (MPCVD) 装置を開発し，いち早くイオン衝撃の問題に取り組んできた[1]～[5]．これらの研究において筆者らは，空間的アフターグロープラズマ中に設置した基板に印加するDCバイアス電圧を変化させることにより，基板に入射するイオンのフラックス密度を変化させずにイオン衝撃エネルギーを制御できることを明らかにしている[1]．

本研究では本MPCVD装置において放電プラズマ中に設置されているステンレス製の内管の電位を変化させてプラズマパラメータの測定を行い，空間的アフターグロープラズマ中に設置されている基板の電位を変化させた場合と同様にイオン衝撃エネルギーを制御できるかどうか検討した．その結果，内管電位を変化させてもイオン衝撃エネルギーを制御できることを明らかにした．しかしながら，プラズマパラメータは基板電位を変化させた場合と内管電位を変化させた場合では一部異なる傾向をもつことがわかった．そこで，この点について理論的に検討を加え，その理由を明らかにした．

2. 実　　験

図1に実験に用いたMPCVD装置の概略図を示す．本装置の放電管部は，溶融石英製の外側放電管 (outer discharge tube) とステンレス製の内管 (inner tube)

† 早稲田大学理工学部電子通信学科，東京都
School of Science and Engineering, Waseda University, Tokyo, 169 Japan

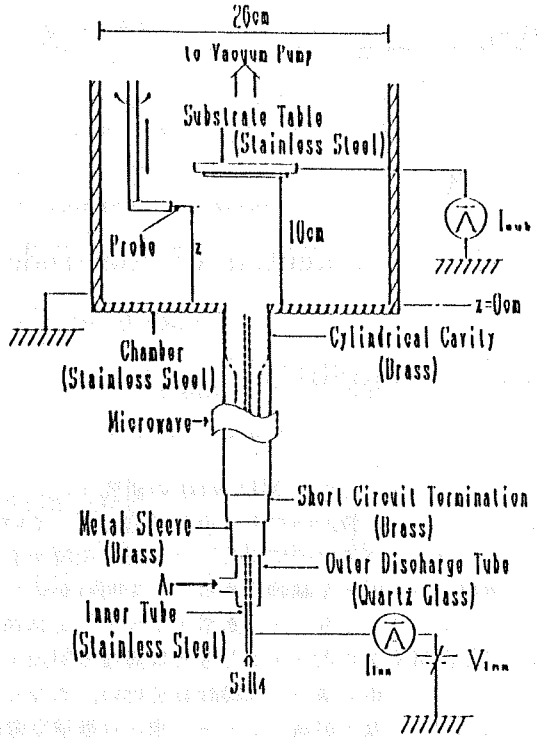

図 1 実験装置概略図
Fig. 1 Schematic diagram of experimental system.

の2重管構造となっている．外側放電管にArガスを流し，内管にSiH_4ガスを流す．マグネトロンで発振した2.45 GHzのマイクロ波(microwave)は，方形導波管内を伝搬し，金属製円筒キャビティ(cylindrical cavity)に導かれる．Arガスはキャビティ領域においてマイクロ波電力により電離される．SiH_4ガスはステンレス製の内管により放電管端まで導かれ，Arプラズマ中に混入され，Arプラズマの粒子と衝突し，解離される．本MPCVD装置ではマイクロ波電力は円筒キャビティ内に閉じ込められており，堆積室内には，マイクロ波電力が注入されていない空間的アフターグロープラズマがフローと拡散により生成されている．本装置の詳細については文献[2], [3], [4]を参照されたい．筆者らはこれまでに内管と堆積室壁をアースして基板電位を変化させて研究を行ってきたが[1]，本研究では基板と堆積室壁をアースして内管電位を変化させている．ここで，内管電位をV_{inn}，基板電位をV_{sub}，内管に流れる電流をI_{inn}，基板に流れる電流をI_{sub}，放電管端からの管軸方向の距離をzと定義する（図1参照）．

実験条件を以下に述べる．マイクロ波電力を150 Wとした．基板をz=10 cmの位置に設置した．V_{inn}が±40 Vを越えると，空間的アフターグロープラズマ内の発光状態が変化することから，内管と堆積室壁の間で直流放電が起こり，プラズマ中に電力が注入されていることがわかる．更に，V_{inn}が−30 Vを越えると内管がArイオンによりスパッタリングされ，ステンレス製の内管壁から飛び出した金属原子が放電管に付着するためマイクロ波放電の状態が変化する．そこで，本研究では直流放電が起きず，かつ内管がスパッタリングされない−30 Vから+40 Vの範囲でV_{inn}を変化させた．このとき，V_{sub}は0 Vとした．プラズマパラメータの測定をシングルプローブ法を用い純Arプラズマ中(Arガス流量：110 ml/min)およびa-Si：H膜作製時と同一条件のAr/SiH_4プラズマ中(Arガス流量：110 ml/min，SiH_4ガス流量：30 ml/min)で行った．プローブには直径0.05 cm，長さ0.3 cmの円筒プローブを用いた．なお，測定は堆積室の中心軸上のz=3, 5, 7, 9 cmの位置で行った．

反応性プラズマであるAr/SiH_4プラズマ中におけるプローブ計測は，プローブ表面に膜が堆積してしまうため，通常の方法ではできない．筆者らはこれまでにAr/SiH_4プラズマ中でも行えるプローブ計測法を確立している[5]．本研究でもこの方法を用いてAr/SiH_4プラズマ中での計測を行った．

なお，本論文では，既に報告している電子密度，電子温度，プラズマ空間電位，I_{sub}のV_{sub}依存性についても再現性をみるために測定しなおした．その結果は，以前報告した結果とよく一致していた．また，I_{inn}のV_{sub}依存性は以前には測定しておらず，今回初めて測定したものである．

3. 結果と考察

図2にI_{inn}のV_{sub}依存性とV_{inn}依存性を示す．なお，電子電流を正にとる．図より，V_{sub}を変化させると，I_{inn}はV_{sub}が負の領域ではほとんど変化しないが，V_{sub}が正の領域では，V_{sub}を増加させるに従い急激に減少することがわかる．V_{sub}が負の領域でI_{inn}が変化しないのは内管表面のシース電圧が変化しないためであると考えられる．V_{sub}が正の領域でI_{inn}が急激に減少するのは，内管表面のシース電圧が急激に増加するためであると考えられる．一方，V_{inn}を変化させた場合は，V_{inn}を増加させるに従い，I_{inn}は急激に増加し，その後飽和する．I_{inn}が急激に増加するのは内管表面のシース電圧が急激に減少するからであり，I_{inn}が飽和するのは，内管表面のシース電圧の変化が小さくなるからであると考えられる．図より，I_{inn}のV_{sub}依存性とV_{inn}依存性はほぼ対称形になっていることが

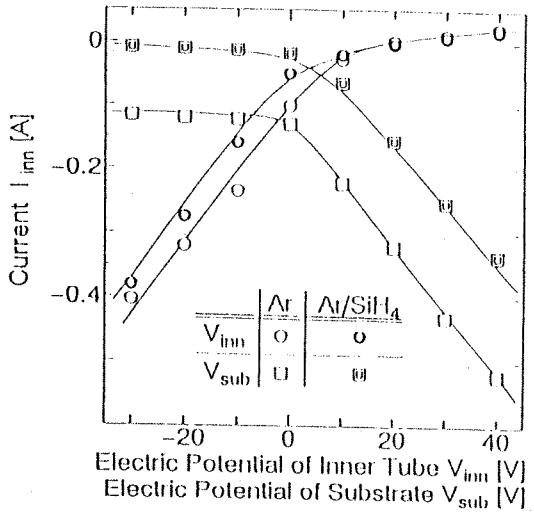

図 2　I_{inn} の V_{inn} 依存性と V_{sub} 依存性
Fig. 2　Dependence of I_{inn} on V_{inn} and V_{sub}.

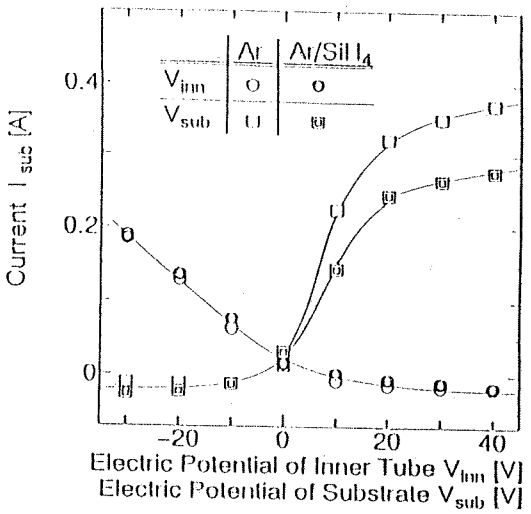

図 3　I_{sub} の V_{inn} 依存性と V_{sub} 依存性
Fig. 3　Dependence of I_{sub} on V_{inn} and V_{sub}.

わかる．

次に，SiH_4 ガスを混入させると両者共に I_{inn} が増加する理由について検討する．まず，図1の装置の概略図から明らかなように，内管の表面積は堆積室の内壁の面積，更に基板テーブル面積より小さい．ガス流は図1上で上向きとなっており，Ar プラズマは上方に流れている．ここで，SiH_4 ガスを混入させると，Ar イオンは SiH_4 の解離に使われ，更にはチャージトランスファにより減少する．すなわち，シラン系のイオンや水素イオンが増加することになる．これらの Ar イオンより軽いイオンは，ガス流によって上方に流されると共に拡散により堆積室の内壁あるいは基板テーブルに到達しやすくなる．従って，内管に流れるイオン電流は減少するので，I_{inn} は増加すると考えられる．しかし，V_{inn} を変化させた場合，V_{inn} が約 15 V より大きい範囲では SiH_4 ガスを混入させても，混入していない場合と一致している．これは，イオン電流が小さくなり，電子電流が主となるため，イオンの種類には依存しなくなるためである．

図3に I_{sub} の V_{sub} 依存性と V_{inn} 依存性を示す．なお，図3においても図2と同様に電子電流を正にとる．図より，V_{sub} を増加させるに従い，I_{sub} は V_{sub} が約 −10 V 以下のとき，緩やかに増加し，約 −10 V から約 20 V のとき，急激に増加し，その後飽和することがわかる．一方，V_{inn} を変化させた場合，V_{inn} を増加させるに従い，I_{sub} は急激に減少し，その後一定となることがわかる．図より I_{sub} の V_{sub} 依存性と V_{inn} 依存性はほぼ対称形となっていることがわかる．

すなわち，図2，図3より内管電位（V_{inn}）を変化させることにより，基板電位（V_{sub}）を変化させたときと同様にイオン衝撃エネルギーを制御できるであろうことが推察できる．

次にプローブ計測の結果を示す．図4は $z=3$ cm におけるプラズマ空間電位（V_s）の V_{sub} 依存性と V_{inn} 依存性である．V_{sub} を変化させた場合は，V_{sub} を増加させるに従い，V_{sub} が負の領域では V_s はわずかに増加し，V_{sub} が正の領域では急激に増加することがわかる．一方，V_{inn} を変化させた場合には，V_s は V_{inn} を増加させるに従い急激に増加することがわかる．なお，他の測定位置においても同様な結果を得ている．

また，図より V_{sub} を負にしたとき，V_s の減少こう配は小さくなり約 13 V までしか減少しないが，V_{inn} を負にした場合には，V_s は減少しつづけ約 4 V まで減少することがわかる．これは，基板が電子密度，電子温度の低い空間的アフターグロープラズマ中に設置されているのに対し，内管は電子密度，電子温度の高い放電プラズマ中に設置されているため，V_{inn} が V_s に強く影響を与えるためである．

基板表面のシース電圧（$V_{sh,sub}$）は，シース端における V_s と V_{sub} の差を取ることにより求められる．シース厚は数ミリであるので基板から数ミリの位置で V_s の測定をする必要がある．しかしながら，本実験において V_s の z 方向へのこう配は，わずかであるのでシース端における V_s は $z=9$ cm における V_s で近似できる [1]．そこで，$z=9$ cm における V_s と V_{sub} の差を取ることにより $V_{sh,sub}$ を求める．図5にその結果を示

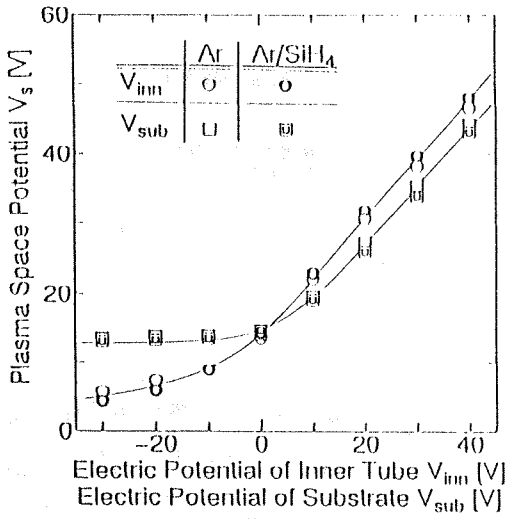

図 4 V_s の V_{inn} 依存性と V_{sub} 依存性
Fig. 4 Dependence of V_s on V_{inn} and V_{sub}.

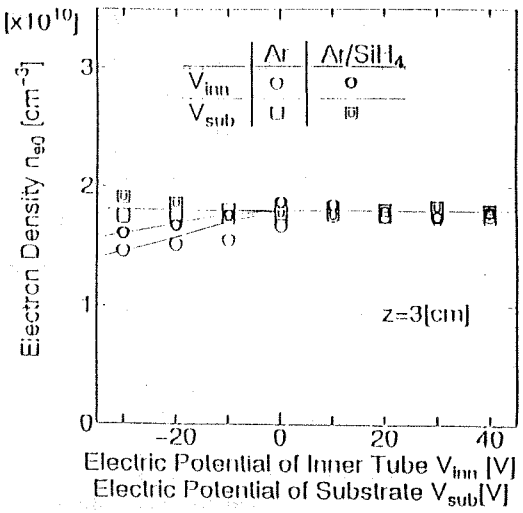

図 6 n_{e0} の V_{inn} 依存性と V_{sub} 依存性
Fig. 6 Dependence of n_{e0} on V_{inn} and V_{sub}.

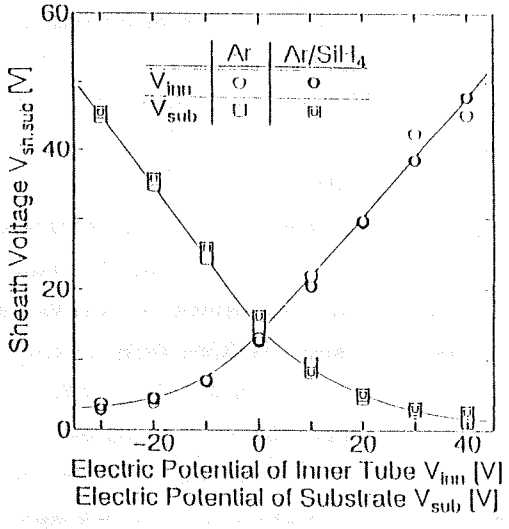

図 5 $V_{sh,sub}$ の V_{inn} 依存性と V_{sub} 依存性
Fig. 5 Dependence of $V_{sh,sub}$ on V_{inn} and V_{sub}.

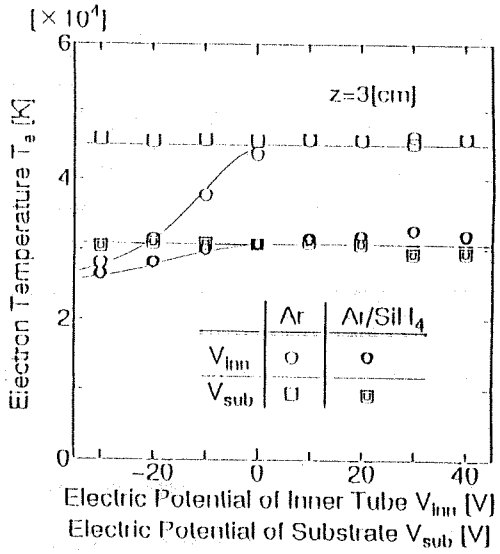

図 7 T_e の V_{inn} 依存性と V_{sub} 依存性
Fig. 7 Dependence of T_e on V_{inn} and V_{sub}.

す．ここで，$V_{sh,sub}$ の V_{inn} 依存性は V_{sub} を 0 V としているので z=9 cm における V_s の V_{inn} 依存性と同じである．図より，V_{sub} を変化させた場合は，V_{sub} を増加させるに従い $V_{sh,sub}$ は減少することがわかる．この結果は V_{sub} を増加させるに従い，イオン衝撃エネルギーは減少することを示している．一方，V_{inn} を変化させた場合には，$V_{sh,sub}$ は V_{inn} を減少させるに従い減少することがわかる．この結果は V_{inn} を減少させるに従い，イオン衝撃エネルギーは減少することを示している．以上の結果より，V_{inn} を変化させても，イオン衝撃エネルギーを制御できることがわかる．

また，イオン衝撃エネルギーは V_{inn} を変化させた場合には V_{inn} を −30 V にしたとき，約 3 eV まで低減でき，V_{sub} を変化させた場合には V_{sub} を +40 V にしたとき，約 3 eV まで低減できることがわかる．しかしながら，V_{sub} と V_{inn} のどちらを変化させてもイオンを跳ね返すような電界は形成されないこともわかる．

図 6 に z=3 cm における電子密度 (n_{e0}) の V_{sub} 依存性と V_{inn} 依存性を示す．図より n_{e0} は V_{sub} を変化させても変化しないことがわかる．一方，V_{inn} を変化させた場合，n_{e0} は V_{inn} が負の領域で V_{inn} を 0 V に近づけるに従いやや増加し，V_{inn} が正の領域では変化しないことがわかる．他の測定位置においても同様な結

果を得ている．

図7に $z=3$ cm における電子温度（T_e）の V_{sub} 依存性と V_{inn} 依存性を示す．図より，T_e は V_{sub} を変化させても変化しないことがわかる．一方，V_{inn} を変化させた場合，T_e は V_{inn} が負の領域で V_{inn} を0Vに近づけるに従い増加し，V_{inn} が正の領域では変化しないことがわかる．この結果は他の測定位置においても同様である．

また，図より，Ar/SiH_4 プラズマの T_e のほうが，純Arプラズマの T_e よりも低くなっていることがわかる．これは Ar/SiH_4 プラズマは分子ガスである SiH_4 ガスをArプラズマに混入して生成されているため，SiH_4 の解離に伴う非弾性衝突が増加しているからである[5]．

以上のように，V_{sub} と V_{inn}，すなわち，放電プラズマ中に設置した電極の電位（V_{inn}）と空間的アフターグロープラズマ中に設置した電極の電位（V_{sub}）は V_s に対しほぼ同様な影響を与えることを明らかにした．しかし，n_{e0} と T_e は V_{sub} を変化させた場合は変化しないのに対し，V_{inn} を変化させた場合には，V_{inn} が負の領域で V_{inn} を負に増加させるに従い減少することを実験的に明らかにした．そこで，この異なる傾向を示す理由について次に検討する．

電子の速度分布は一般にマクスウェル・ボルツマン分布となっている．

$$n_e(v)=4\pi n_{e0}\left(\frac{m_e}{2\pi kT_e}\right)^{3/2}v^2\exp\left(-\frac{m_ev^2}{2kT_e}\right) \quad (1)$$

ここで，k はボルツマン定数，m_e は電子の質量，T_e は電子温度，v は電子の速度，n_{e0} は全電子密度，$n_e(v)$ は速度 v をもつ電子の密度である．ここで

$$\frac{1}{2}m_ev^2=eV \quad (2)$$

であるので，式(1)は

$$n_e(V)=8\pi n_{e0}\left(\frac{m_e}{2\pi kT_e}\right)^{3/2}\frac{eV}{m_e}\exp\left(-\frac{eV}{kT_e}\right) \quad (3)$$

となる．ここで，e は電気素量，V は電圧である．堆積室壁面のシース電圧，すなわち V_s が十分大きければほとんどすべての電子が堆積室壁面で跳ね返されてしまうが，V_s が小さくなるに従い，マクスウェル・ボルツマン分布に従う電子は高エネルギー側の電子から順次，堆積室壁面に到達し，壁面でイオンと再結合することにより消滅することになる．

図8の実線は V_s が十分大きいとき（$V_{inn}>0$）の n_{e0}，T_e の実験値を式（3）に代入し得られた電子の速度分布である．但し，実験値には $z=3$ cm における値を用いた．次に，V_s が小さくなり図中の V_{s1} となったとき，eV_{s1} より小さい運動エネルギーをもつ電子はシース電圧によって跳ね返されるが，これより大きい運動エネルギーをもつ電子はシース電圧に打ち勝って堆積室壁面で消滅すると考えられる．従って，V_s が V_{s1} のときの電子密度 n'_{e0} は図8の斜線部を積分したものであり次式で与えられる．

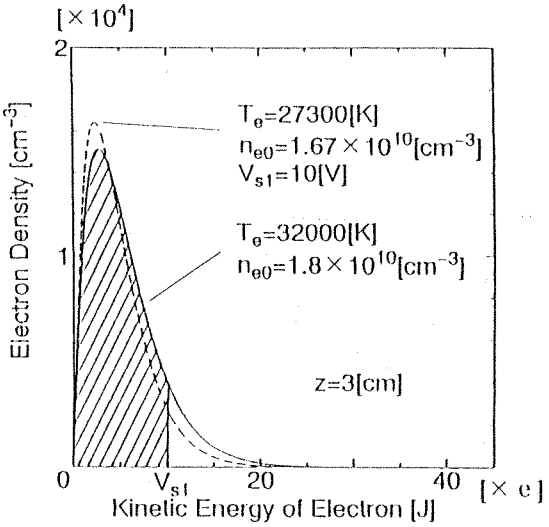

図8　マクスウェル・ボルツマン分布
Fig. 8　Maxwell-Boltzmann's distribution.

$$n'_{e0}=\int_0^{V_{s1}}n_e(V)dV \quad (4)$$

図8の斜線部のような分布になった電子群は，他の粒子と衝突しながら堆積室内を拡散し図8の破線で示すように再びマクスウェル・ボルツマン分布になると考えられる．この再分布したときの電子温度を T'_e とすると，$n_e(V)'$ は次式で与えられる．

$$n_e(V)'=8\pi n'_{e0}\left(\frac{m_e}{2\pi kT'_e}\right)^{3/2}\frac{eV}{m_e}\exp\left(-\frac{eV}{kT'_e}\right) \quad (5)$$

このとき，プラズマ中の全電子のもつエネルギーは保存されることより，

$$\int_0^{V_{s1}}n_e(V)eV\,dV=\int_0^{\infty}n_e(V)'eV\,dV \quad (6)$$

が成り立つ．すなわち，式(5)，(6)を連立することにより1次近似として T'_e を求めることができる．

図9に式（4）より求めた電子密度と実験値を比較した結果を，図10に式（5），（6）を連立させることにより求めた電子温度と実験値を比較した結果をそれぞれ示す．両図において実線が理論計算の結果である．これらの図から，V_s が小さいとき（$V_{inn}<0$）に n_{e0}，T_e が小さくなるという実験結果が前述の理論によって説

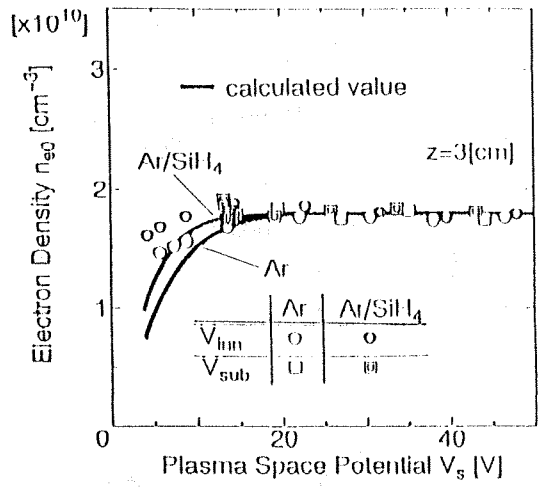

図 9 n_{e0} の計算値と実験値の比較
Fig. 9 Comparison of calculated values with experimental values of n_{e0}.

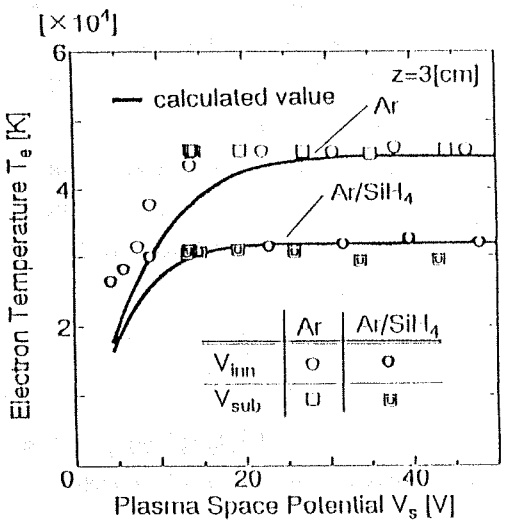

図 10 T_e の計算値と実験値の比較
Fig. 10 Comparison of calculated values with experimental values of T_e.

明できることがわかる.

図9, 図10において計算結果と実験結果は V_s が小さくなると n_{e0} と T_e が減少するという傾向は同じであるが理論計算の結果は減少傾向が大きい. これは先に述べたような反応は堆積室内全空間で起こるのではなく堆積室壁面でのみ起こる反応であるが, 理論計算では全空間で高エネルギー電子が堆積室壁面に到達し消滅するとして計算したため計算結果が実験結果より小さく算出されたためである. これらの結果より V_{sub} を変化させた場合に n_{e0}, T_e が変化しないのは, V_{sub} を負にしても V_s は 13 V 程度までしか減少しないため(図4参照), 堆積室壁面における電子の消滅がほとんどなく電子の速度分布は変わらないからである. 一方, V_{inn} を変化させた場合に n_{e0}, T_e が変化するのは, V_{inn} を負にすると V_s は 4 V 程度まで大きく減少するため(図4参照), 堆積室壁面において高エネルギー側の電子が多量に消滅するので, 電子密度は減少し, 電子温度は低下することを明らかにした.

4. むすび

2重管式同軸線路形マイクロ波プラズマCVD装置において, 基板電位 (V_{sub}) および内管電位 (V_{inn}) を変化させてプラズマパラメータの測定を行った結果, 以下のことが明らかになった.

(1) プラズマ空間電位 (V_s) は, V_{sub} を増加させるに従い, V_{sub} が負のとき, わずかに増加し, V_{sub} が正のとき急激に増加する. V_{inn} を変化させた場合, V_{inn} を増加させるに従い, V_s は急激に増加する. V_{sub} を変化させた場合, V_{sub} を負にしても V_s は約 13 V までしか減少しないのに対し, V_{inn} を変化させた場合, V_{inn} を負にすると V_s は約 4 V まで減少する.

(2) V_{sub} を変化させた場合は, V_{sub} を増加させることによりイオン衝撃エネルギーを低減できる. V_{inn} を変化させた場合には V_{inn} を減少させることによりイオン衝撃エネルギーを低減できる.

(3) V_{sub} を変化させた場合は, 電子密度 (n_{e0}), 電子温度 (T_e) は変化しない. V_{inn} を変化させた場合には, n_{e0}, T_e は V_{inn} が負の領域で, V_{inn} を負に増加させるに従い減少する.

(4) n_{e0}, T_e の上述の(3)における変化は, V_s が小さくなるに従いマクスウェル・ボルツマン分布の高エネルギー電子から順次堆積室壁面で消滅するため電子密度は減少し, 更にプラズマ中の全電子のもつ平均エネルギーが減少するためとして説明できることを明らかにした.

(5) イオン衝撃エネルギーを制御する方法としては基板電位を変化させる方法が一般的であるが, 基板をアースした場合, または基板がアースされてしまう場合にも, マイクロ波プラズマ中の他の電極 (内管) の電位を変化させてイオン衝撃エネルギーを制御できることを明らかにした.

今後, V_{inn} を変化させてa Si : H膜を作製し, V_{sub} を変化させた場合と比較検討する予定である.

文献

[1] 加藤 勇, 来田俊之, 松下 亨, "プラズマCVDによって作

製されたa-Si：H膜に与えるイオン衝撃の影響," 信学論(C), vol. J77-C-II, no. 9, pp. 384-391, Sept. 1994.
[2] I. Kato, S. Wakana, and S. Hara, "Microwave Plasma CVD System to Fabricate a Si Thin Films out of Plasma," Jpn.J. Appl. Phys., vol. 22, no. 1, pp. L40-L42, Jan. 1983.
[3] 加藤　勇, 若菜伸一, "新しいマイクロ波プラズマ化学気相堆積装置," 真空, vol. 26, no. 7, pp. 628-636, July 1983.
[4] 加藤　勇, 矢野元康, "同軸線路形マイクロ波プラズマCVD法によるプラズマ内外でのa-Si：H薄膜の作成," 信学論(C), vol. J69-C, no. 5, pp. 662-668, May 1986.
[5] 加藤　勇, 千原隆志, 阪本　匡, "マイクロ波プラズマCVDにおけるプラズマパラメータの空間分布," 電学論(A), vol. 112, no. 5, pp. 355-362, May 1992.

(平成7年5月2日受付, 8月7日再受付)

加藤　勇 (正員)

昭42早大・理工・電子通信卒. 昭48同大学院博士課程了. 同年工博. 同年早大勤務. 昭53同大助教授. 昭54～56マニトバ大客員教授, カナダ国立研究会議の研究費を受け共同研究ならびに研究指導. 昭58同大教授, 現在に至る. 光子工学, レーザ工学, 電子物性工学, 計測工学, 光子材料, プラズマ・エレクトロニクス, 光・量子エレクトロニクス, 半導体薄膜工学などの研究に従事. 電気工学会, 応用物理学会, テレビジョン学会, 日本真空協会, IEEE各会員.

松下　享 (正員)

平5早大・理工・電子通信卒. 平7同大学院修士課程了. 在学中はマイクロ波プラズマCVDに関する研究に従事. 現在, 日立製作所中央研究所ストレージ研究部勤務. 応用物理学会会員.

山下　真 (学生員)

平6早大・理工・電子通信卒. 現在, 同大学院修士課程在学. マイクロ波プラズマCVDに関する研究に従事. 応用物理学会会員.

Electronics and Communications in Japan, Part 2, Vol. 78, No. 10, 1995
Translated from Denshi Joho Tsushin Gakkai Ronbunshi, Vol. 78-C-II, No. 4, April 1995, pp. 142-148

Control of Radical Species in Microwave Plasma Chemical Vapor Deposition

Isamu Kato, *Member*, Toshiyuki Yoneda,* *Nonmember*, and
Toru Matsushita and Makoto Yamashita, *Associate Members*

School of Science and Engineering, Waseda University, Tokyo, Japan 169

SUMMARY

The spatial distributions of electron temperature and density in pure Ar plasma in a double-tubed coaxial-line type microwave plasma chemical vapor deposition (CVD) system were measured using the probe method. It was found that the electron temperature and electron density dropped sharply in an area 4 cm from the edge of the discharge tube and they decreased slowly in an area farther away from the forementioned area. SiH_4 gas was dissociated in Ar plasma, and the electron temperature and density of the plasma were varied by changing the location of the SiH_4 gas inlet. As a result, it was found that the fragmentation pattern of radical species could be varied by changing the location of the SiH_4 gas inlet.

In addition, films were fabricated under various fragmentation patterns and the qualities of these films were evaluated. It was found that the film quality could be improved by dissociating SiH_4 gas at low electron temperature.

Key words: Microwave plasma CVD; electron temperature; fragmentation pattern; a-Si:H film.

1. Introduction

Hydrogenated amorphous silicon (a-Si:H) films have been used widely for optical and electronic devices and considerable effort has been made to improve the film quality and to find applications of these films for new devices. An a-Si:H film can be deposited on a large-area substrate using the low-temperature plasma chemical vapor deposition (CVD) technique.

To improve the quality of a film fabricated by plasma CVD, it is important to understand reactions in gas and on the film surface. For this purpose, it is necessary to investigate the behavior of radical species and the measurement methods such as LIF [1], IRLAS [2], and so forth. In addition, by comparing the result of evaluating the film formed by only SiH_3 radicals with the result of simulation, the probability of the SiH_3 radical becoming a film and the film surface loss probability have been studied [3].

In this paper, the electron temperature and electron density were changed by changing the location of the SiH_4 gas inlet to Ar plasma. Using Ar plasma with various electron temperatures and electron densities, SiH_4 gas was dissociated to investigate the ratio among the numbers of radical species, that is, fragmentation pattern. As a result, it was found that the fragmentation pattern of radical species could be changed by changing the location of the SiH_4 gas inlet. Films were grown under various

*Presently with Mitsubishi Electric, Inc.

ISSN8756-663X/95/0010-0097

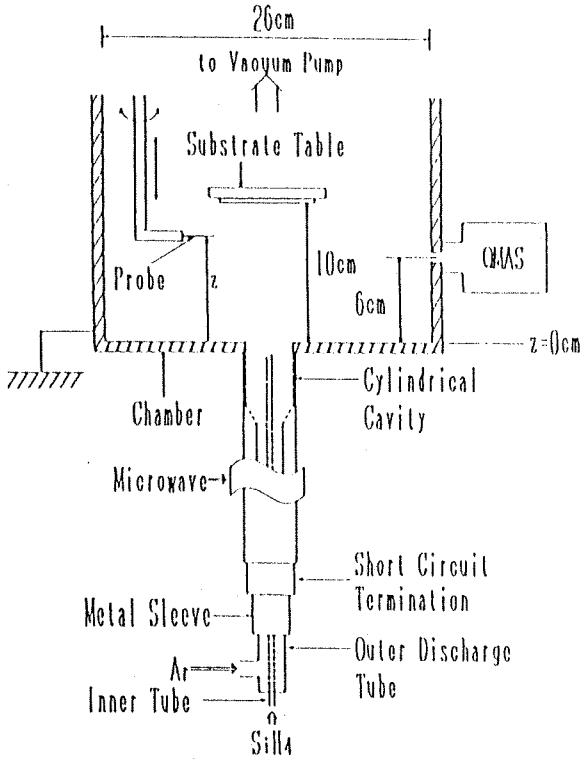

Fig. 1. Schematic diagram of experimental system.

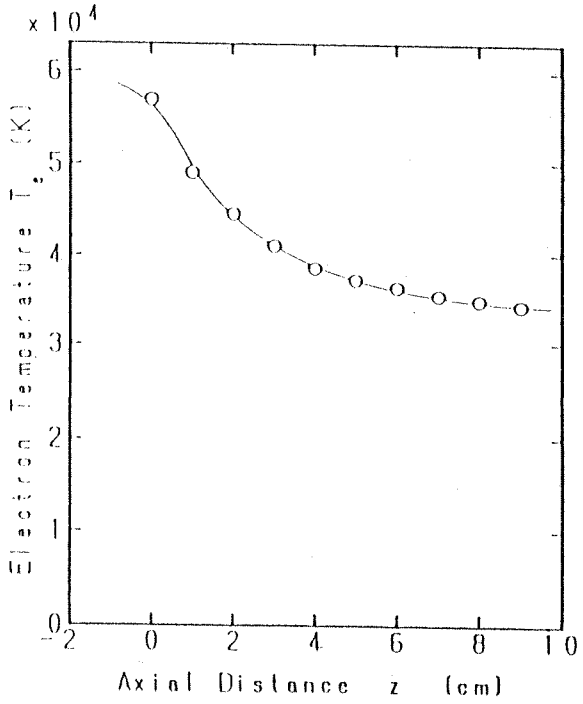

Fig. 2. Dependence of electron temperature on z.

fragmentation patterns and then evaluated. It was found that film quality could be improved.

2. Experiment

The double-tubed coaxial-line-type microwave plasma CVD (MPCVD) system was used in this paper. Figure 1 illustrates the CVD system. Ar gas flows in the outer discharge tube made of fused silica to generate Ar plasma by microwave power. The microwave is coupled with plasma under the fundamental mode of the coaxial line. Since the microwave power is confined in the cylindrical cavity, the discharge plasma is generated only in the cylindrical cavity and flows into the deposition chamber. SiH_4 gas is led through a stainless steel inner tube to the discharge tube end where it is mixed with Ar plasma. Then, SiH_4 gas is dissociated due to collision with Ar plasma particles. Details of this system are reported in [4] and [5].

The distance from the discharge tube end in the direction along the center axis is defined by z.

The substrate table is located at $z = 10$ cm. This location is the spatial afterglow plasma region where no microwave power is provided. Therefore, a film can be grown from radicals without ion bombardment at this location [5]. A cylindrical probe with a diameter of 0.05 cm and length of 0.3 cm is used to measure the electron temperature and density. The probe is installed on a movable shaft and its location can be changed in the deposition chamber. A quadruple mass spectrometer (QMAS) is located at $z = 6$ cm outside the chamber and it is connected to the inside of the chamber via an orifice with a diameter of 200 μm (see Fig. 1).

The discharge condition is as follows. Microwave power of 150 W was used for probe measurement where the Ar gas flow was 110 ml/min and the gas pressure in the chamber was about 3.5 mtorr. The probe measurement was carried out along the center axis of the chamber at $z = 0 \sim 9$ cm. The same condition was used for the QMAS analysis and film deposition. During film deposition, the SiH_4 gas flow as 50 ml/min and the gas pressure was about 5 mtorr. The location of the SiH_4 gas inlet was varied from $z = -2$ cm to $z = 3$ cm to vary the electron temperature and density.

The film thickness was measured by using a needle-type film-thickness measurement apparatus. The

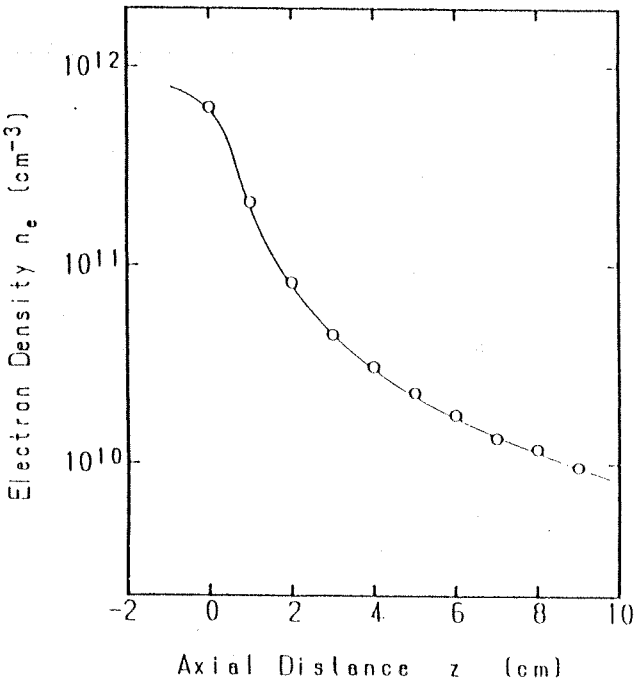

Fig. 3. Dependence of electron density on z.

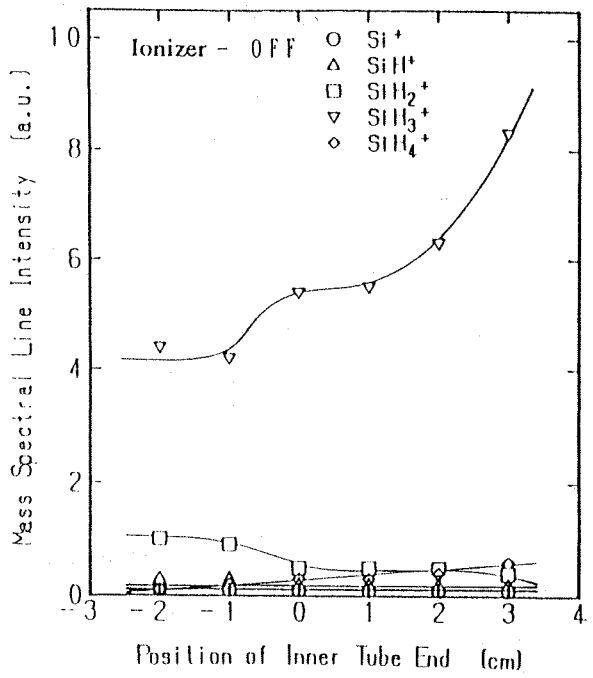

Fig. 4. Dependence of mass spectral line intensity on the position of the inner tube end (ionizer off).

atomic density of Si in the film was measured by Rutherford backscattering spectra. The integrated intensities of stretching modes of SiH and SiH_2 bonds were obtained by using the infrared absorption spectra and film thickness. By multiplying these intensities by 1.4×10^{20} cm^{-2}, the hydrogen atomic densities in both bonds were calculated [6]. The optical energy gap was obtained by using the ultraviolet and visible absorption spectrum and film thickness. The dangling bond density was obtained by using the result of electron spin resonance measurement and film thickness.

3. Experimental Results

Figure 2 shows the dependence of electron temperature on z. The electron temperature decreases rapidly as z increases to 3 cm, and when z exceeds 3 cm, the electron temperature decreases slowly.

Figure 3 shows the dependence of electron density on z. The electron density decreases rapidly as z increases to 3 cm. When z exceeds 3 cm, the electron density decreases exponentially [7]. No experiment was carried out for the area of negative value of z, namely in the discharge tube, because the probe could not reach the

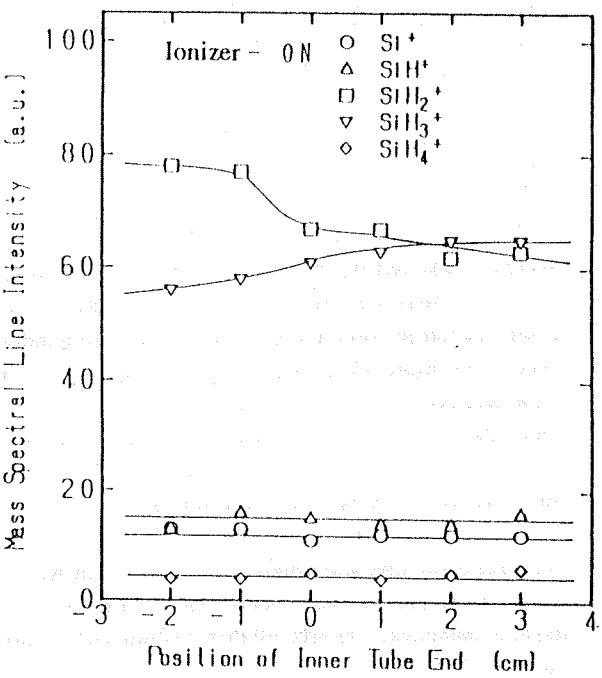

Fig. 5. Dependence of mass spectral line intensity on the position of the inner tube end (ionizer on).

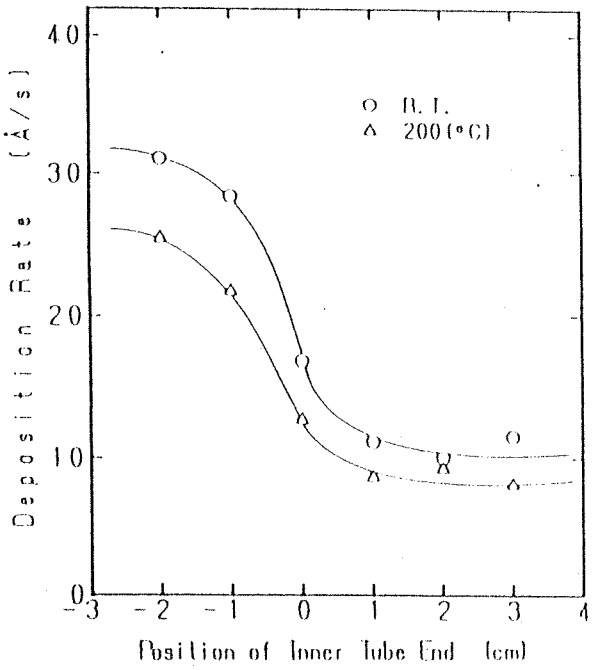

Fig. 6. Dependence of deposition rate on the position of the inner tube end.

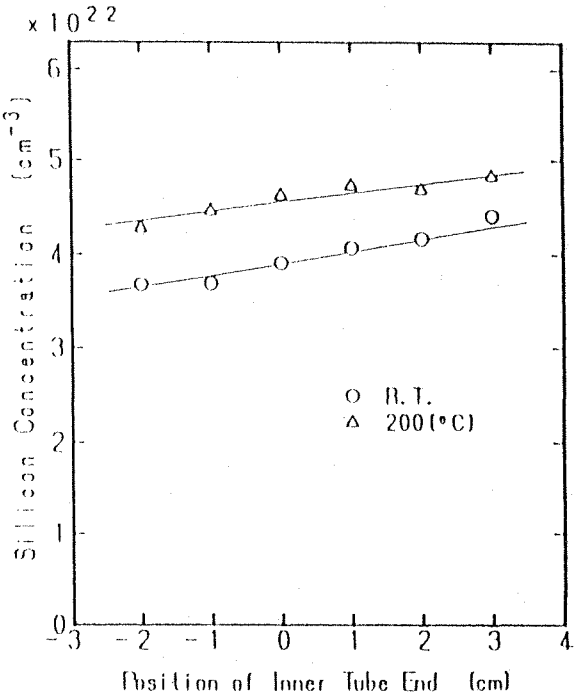

Fig. 7. Dependence of silicon concentration on the position of the inner tube end.

area of a negative value of z. However, since the incident microwave power is uniform in the area of negative value of z, both electron temperature and density are believed to saturate when $z < -2$ cm.

As described above, SiH_4 gas is led to the discharge tube end via the inner tube and is dissociated by Ar plasma particles. Therefore, by changing the position of the inner tube end (the location of the SiH_4 gas inlet), SiH_4 gas confronts Ar plasma with various electron temperatures and densities. In this way, the fragmentation pattern of radical species can be varied.

Figures 4 and 5 show the dependence of the mass-spectral line intensity obtained by QMAS on the position of the inner tube end. Figure 4 shows the result on the ionized radicals when the ionizer is off. Figure 5 shows the result when the ionizer is on. In both results, SiH_2^+ decreases and SiH_3^+ increases as the position of the inner tube end moves from a negative to a positive value of z. This indicates that the fragmentation pattern can be varied by varying the position of the inner tube end in the MPCVD system.

The increase of SiH_2^+ and the decrease of SiH_3^+ occur because when the electron temperature and density decrease, the degree of dissociation causing ionization which generates SiH_2^+ is suppressed and the degree of dissociation causing ionization which generates SiH_3^+ increases. The change of ionized radicals is not always in proportion to the change of neutral radicals. However, it is considered that the former is in proportion to the latter under a weakly ionized plasma where the degree of ionization is less than several percent. Therefore, when the number of SiH_2 radicals decreases, the number of SiH_3 radicals increases.

It has been reported that the film quality is improved selectively introducing radicals with a high surface mobility such as SiH_3 radicals [8]. Therefore, by moving the position of the inner tube end from negative to positive values of z, the film quality can be optimized; a-Si:H films were fabricated under various fragmentation patterns by changing the position of the inner tube end and the qualities of these films were evaluated.

Figure 6 shows the dependence of the deposition rate on the position of the inner tube end. The deposition rate decreases rapidly as the position of the inner tube end is moved from $z = -1$ to $+1$ cm regardless of the substrate temperature. When z exceeds +1 cm, the deposition rate becomes constant, also regardless of the substrate temperature. This symptom is due to the large

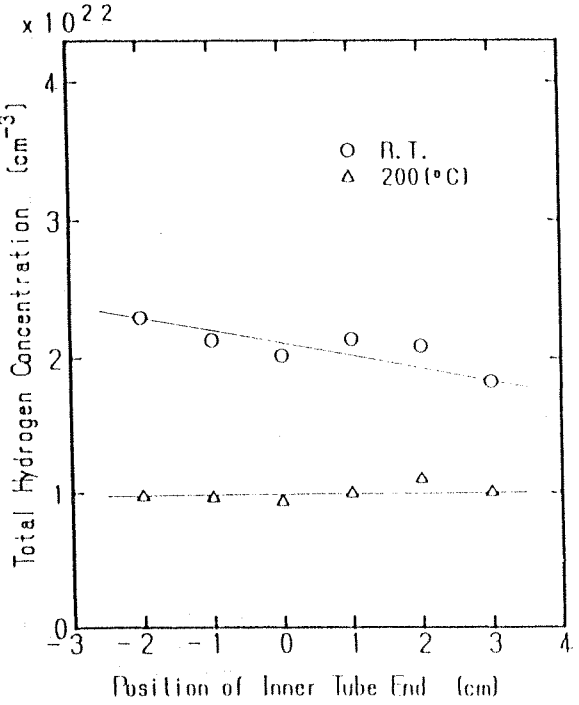

Fig. 8. Dependence of total hydrogen concentration on the position of the inner tube end.

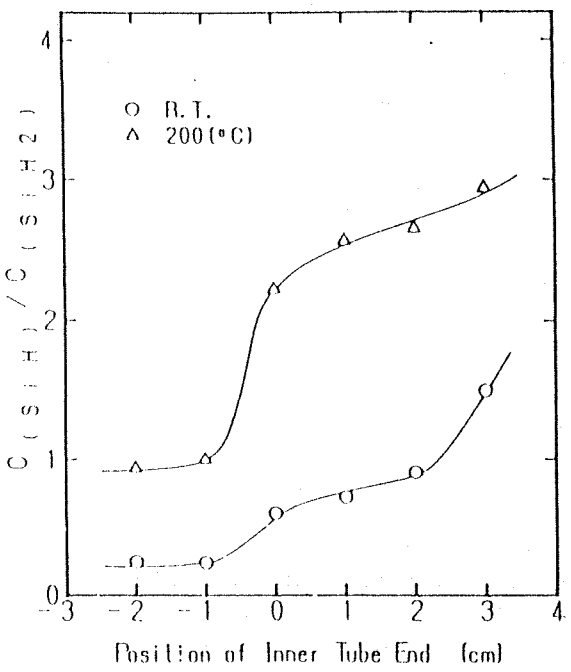

Fig. 9. Dependence of (SiH bond density)/(SiH_2 bond density) ratio on the position of the inner tube end.

changes in the degree of dissociation of SiH_4 and fragmentation pattern. The deposition rate is constant when the position is between $z = -1$ and $z = -2$ cm because electron temperature and density do not change in this region. When the substrate temperature is 200°C, the deposition rate is lower than when it is room temperature as reported [9], because the silicon concentration in a film increases as substrate temperature increases.

Figure 7 shows the dependence of silicon concentration on the position of the inner tube end. Regardless of substrate temperature, silicon concentration increases as the position changes from a negative to a positive value of z, indicating that the film becomes more dense. The densification of the film is caused by the number of SiH_3 radicals which have a high mobility. When the substrate is heated at 200°C, the concentration of Si is higher than when the substrate temperature is room temperature, as reported [10].

Using the results shown in Figs. 6 and 7, the amount of Si contributing to the formation of the film per unit time per unit area, which is given by silicon concentration times deposition rate, was calculated. The amount of Si in a film per unit time per unit area depends on the position of the inner tube end which is similar to the dependence of the deposition rate on the position of the inner tube end as shown in Fig. 6. Therefore, it is clear that the decrease of the deposition rate is due not only to the densification of the film.

As the position of the inner tube end is moved from a negative to a positive value of z, the deposition rate decreases because the range of the position of the tube end (-2 cm $< z <$ 3 cm) includes the transition area from the discharge plasma region where microwave power is supplied to the spatial after-glow plasma region where no microwave power is supplied. That is, in the transition area, the dissociation of SiH_4 degrades and the number of SiH_2 radicals with high adherence decreases because of the suppression of the dissociation of SiH_4 [8], causing the increase of the number of SiH_3 radicals with a low adherence [8]. The dependence of the amount of Si in a film per unit time per unit area on the position of the inner tube end is independent of the substrate temperature. Therefore, the decrease of the deposition rate by increasing the substrate temperature is caused by the densification of the film.

Figure 8 shows the dependence of total hydrogen concentration on the position of the inner tube end. As

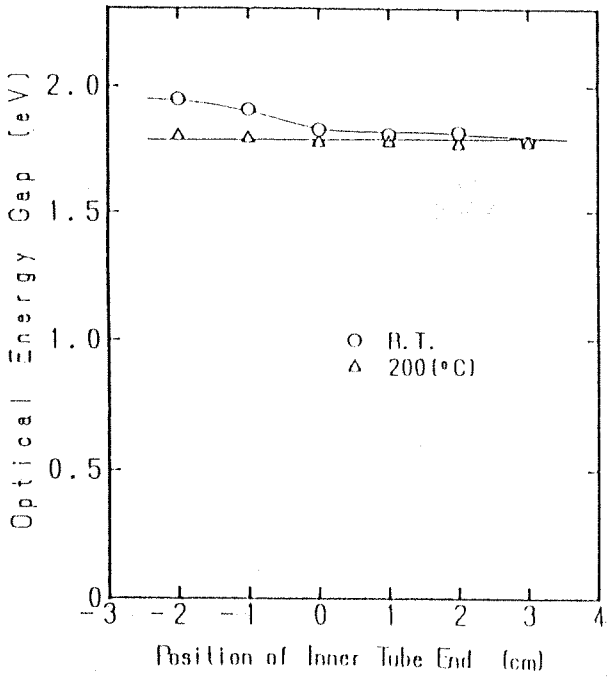

Fig. 10. Dependence of optical energy gap on the position of the inner tube end.

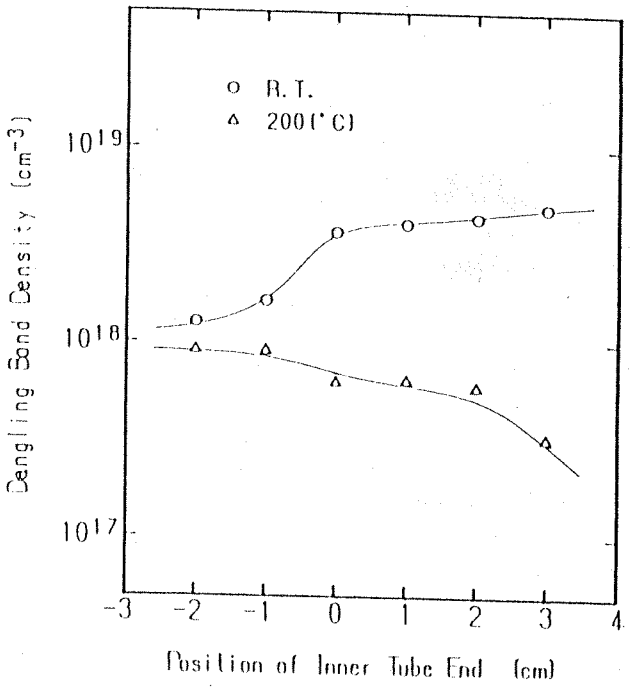

Fig. 11. Dependence of dangling bond density on the position of the inner tube end.

the position of the inner tube end moves from a negative to a positive value, the hydrogen concentration decreases. When the substrate temperature is 200°C, the hydrogen concentration is almost constant at about 1×10^{22} cm^{-3}, regardless of the position of the inner tube end.

As the position of the inner tube end moves from a negative to a positive value, the SiH bond density increases and the SiH_2 bond density decreases. Figure 9 shows the dependence of (SiH bond density)/(SiH_2 bond density) ratio on the position of the inner tube end. Regardless of the substrate temperature, the a-Si:H films contain more SiH bonds as the position of the inner tube end moves from a negative to a positive value. When the substrate temperature is 200°C, the films contain more SiH bonds than when the substrate temperature is room temperature, as reported.

Figure 10 shows the dependence of the optical energy gap on the position of the inner tube end. When the substrate temperature is room temperature, the optical energy gap decreases as the position of the inner tube end moves from a negative to a positive value. When the substrate temperature is 200°C, the optical energy gap is about 1.78 eV, regardless of the position of the inner tube end. This tendency is similar to the dependence of total hydrogen concentration on the position of the inner tube end.

Figure 11 shows the dependence of the dangling bond density on the position of the inner tube end. When the substrate temperature is room temperature, the dangling bond density increases slightly as the position of the inner tube end moves from negative to positive value. That is, when the substrate is not heated, the dangling bond density can be minimized if the number of SiH_2 radicals is increased by installing the position of the inner tube end at negative value. When the mobilities of radicals are increased by heating the substrate temperature at 200°C, the dangling bond density decreases and the quality of the a-Si:H film improves as the position of the inner tube end moves from negative to positive value.

The above results show that as the position of the inner tube end moves from a negative to a positive value, the film quality improves although the deposition rate decreases because of the increase in the number of SiH_3 radicals with high mobility.

4. Conclusions

The spatial distributions of electron temperature and density in pure Ar plasma in the deposition chamber of a double-tubed coaxial-line-type microwave plasma CVD system was investigated. In addition, by introducing SiH_4 gas into Ar plasma at various inlet locations, namely the position of the inner tube end, SiH_4 gas was dissociated by Ar plasma with different electron temperatures and densities to measure the fragmentation pattern by mass spectroscopy. As a result, the following facts were found.

(1) As z increased to about 3 cm, the electron temperature decreased rapidly. When z exceeded 3 cm, the decrease of electron temperature became slower with an increase of z.

(2) As z increased to about 3 cm, the electron density decreased rapidly. When z exceeded 3 cm, the decrease of electron density became exponential with an increase of z.

(3) As the position of the inner tube end moved from a negative to a positive value, the concentration of SiH_2, decreased and that of SiH_3, increased.

In addition, films were fabricated by changing the position of the inner tube end and the qualities of these films were evaluated. As the position of the inner tube end was moved from a negative to a positive value of z, the deposition rate and film quality changed as follows.

(1) The deposition rate decreased rapidly as the position of the inner tube end was moved to $z = 1$ cm. When the position exceeded 1 cm, it saturated. This was because the degree of dissociation of SiH_4 decreased and the number of SiH_3 radicals with low-adhesion increased.

(2) The Si concentration, total hydrogen concentration, hydrogen bond state, and optical energy gap represented the film quality improved.

(3) As the position of the inner tube end was moved from negative to positive value, the dangling bond density increased when the substrate temperature was room temperature, but it decreased when the substrate temperature was 200°C.

The above results indicate that the film quality improved by dissociating SiH_4 in plasma at lower electron density because the number of SiH_3 radicals with a high mobility increased.

In the future, the fragmentation pattern of neutral radicals should be investigated quantitatively to discuss the detailed deposition mechanism.

REFERENCES

1. Y. Matsumi, T. Hayashi, H. Yoshikawa, and S. Komiya. Laser diagnostics of a silane plasma-SiH radicals in an a-Si:H chemical vapor deposition system. J. Vac. Sci. Tech., A4, 1786-1790 (May 1986).
2. N. Itabashi, N. Nishiwaki, M. Magane, T. Goto, A. Matsuda, C. Yamada, and E. Hirota. SiH_3 radical density in pulsed silane plasma. Jpn. J. Appl. Phys., 29, 3, pp. 585-590 (March 1990).
3. A. Matsuda, K. Nomoto, Y. Takeuchi, A. Suzuki, A. Yuuki, and J. Perrin. Temperature dependence of the sticking and loss probabilities of silyl radicals on hydrogenated amorphous silicon. Surface Science, 227, pp. 50-56 (1990).
4. I. Kato, S. Hara, and S. Wakana. Microwave plasma CVD system to fabricate a-Si thin films out of plasma. Jpn. J. Appl. Phys., 22, 1, pp. L-40-42 (Jan. 1983).
5. Kato and Yano. Fabrication of a-Si:H thin films in and out of plasma by coaxial-line-type microwave plasma CVDs. I.E.I.C.E. (C), J69-C, 5, pp. 662-668 (1986).
6. Kato, Ueda, and Hatanaka. Fabrication of a-Si:H films by coaxial-line-type microwave hydrogen plasma CVD. I.E.I.C.E. (C), J70-C, 1, pp. 78-88 (1987).
7. Kato, Usui, and Sakamoto. Spatial distribution of plasma parameters in microwave plasma chemical vapor deposition. Trans. I.E.E., Japan, A, 112-A, 5, pp. 355-362 (1992).
8. Matsuda. Growth procedure and new method of film quality control. Solid-State Physics, Japan, 27, pp. 777-784 (1992).
9. Kato, Ueda, and Hatanaka. Effect of substrate temperature on a-Si:H thin films fabricated by double-tubed coaxial-line-type microwave plasma CVD. Trans. I.E.E., Japan, A, 106-A, 8, pp. 391-397 (1986).
10. T. Hama, H. Okamoto, Y. Hamakawa, and T. Matsubara. Hydrogen content dependence of the optical energy gap in a-Si:H. J. Noncryst. Solid, 59 & 60, pp. 333-336 (1983).

AUTHORS (from left to right)




Isamu Kato received his B.S. and Ph.D. degrees from Waseda University in 1967 and 1973, respectively. He became an Associate Professor later at the same university. He was invited to the University of Manitoba, Canada, as guest Professor from 1979 to 1981. He became a Professor at Waseda University in 1983. He has been engaged in research on photonics, lasers, electronic materials, electronic measurement, plasma electronics, optical and quantum electronics, and semiconductor thin films. He is a member of the Japanese Electrical Society; Japanese Society of Applied Physics; TV Society; Japanese Vacuum Society; and IEEE.

Toshiyuki Yoneda received his B.S. and M.S. degrees from Waseda University in 1992 and 1994, respectively. Presently, he is at the Mitsubishi Electronic Technological Center. As a student, he was involved in research on microwave plasma CVD. He is a member of the Japanese Society of Applied Physics.

Toru Matsushita received his B.S. degree in 1993 from Waseda University where, at present, he is enrolled in the Master's Program. He has been involved in research on microwave plasma CVD. He is a member of the Japanese Society of Applied Physics.

Makoto Yamashita received his B.S. degree in 1994 from Waseda University where, at present, he is enrolled in the Master's program. He has been involved in research on microwave plasma CVD. He is a member of the Japanese Society of Applied Physics.

論　文

マイクロ波プラズマCVDにおけるラジカル種の制御

正員　加藤　勇[†]　　非会員　米田　俊之[†,*]
准員　松下　亨[†]　　准員　山下　真[†]

Control of Radical Species in Microwave Plasma CVD

Isamu KATO[†], *Member*, Toshiyuki YONEDA[†,*], *Nonmember*, Toru MATSUSHITA[†] *and* Makoto YAMASHITA[†], *Associate Members*

あらまし　純Arプラズマ中でプローブ法を用いて，2重管式同軸線路形マイクロ波プラズマCVD装置の堆積室内における電子温度，電子密度の空間分布測定を行った．その結果，電子温度，電子密度は，放電管端から4cm程度までは急激に減少し，その後，減少こう配は緩やかになることを明らかにした．SiH_4ガスの混入位置を変化させることにより，電子温度，電子密度の異なるArプラズマ中でSiH_4ガスを解離させた．その結果，SiH_4ガスの混入位置を変化させることにより，ラジカルのフラグメンテーションパターンを変化させることができることを明らかにした．更に，フラグメンテーションパターンを変化させて成膜し，その膜質評価を行い，低い電子温度のプラズマでSiH_4を解離させることにより，膜質を改善できることを明らかにした．

キーワード　マイクロ波プラズマCVD，電子温度，電子密度，フラグメンテーションパターン，a-Si:H膜

1. まえがき

今日，水素化アモルファスシリコン(a-Si:H)膜は，光・電子素子の材料として用いられており，膜質の向上，新しいデバイスへの応用を目指し研究開発が盛んに進められている．a-Si:H膜の作製法としては，大面積化が容易である，低温プロセスであるといった特長をもつプラズマCVD法が広く用いられている．

プラズマCVD法において，膜質の向上をはかるためには，気相中および膜表面における反応を解明する必要がある．そのためには，ラジカル種の測定が必要であり，LIF[1]，IRLAS[2]等，ラジカル種測定法の開発が進められてきている．また，SiH_3ラジカルだけを選択的に基板表面に導いて成膜した結果とシミュレーションの結果とを比較することにより，SiH_3ラジカルの膜となる確率（付着確率）や膜表面損失確率等に関する検討が進められてきている[3]．

本論文では，SiH_4ガスのプラズマ中への混入位置を変化させることにより，電子温度，電子密度の異なるArプラズマ中でSiH_4ガスを解離させることにより，各ラジカル種の割合，すなわちフラグメンテーションパターン，を変化させることを試みた．その結果，SiH_4ガスの混入位置を変化させることにより，ラジカルのフラグメンテーションパターンを変化させることができることを明らかにした．そこで，フラグメンテーションパターンを変化させて成膜し，その膜質評価を行い，膜質が改善できることを明らかにした．

2. 実　　験

実験には筆者らが研究開発を進めてきている2重管式同軸線路形マイクロ波プラズマCVD (MPCVD) 装置を用いた．図1に本MPCVD装置の概要図を示す．溶融石英製の外側放電管 (outer discharge tube) にArガスを放電ガスとして流し，マイクロ波によりArプラズマを生成する．このとき，マイクロ波は同軸線路の基本モードでプラズマと結合する．マイクロ波電力は円筒キャビティ (cylindrical cavity) 内に閉じ込められているので，電力の注入されている放電プラズマは円筒キャビティ内でのみ生成され，堆積室 (chamber) 内に拡散，流入する．SiH_4ガスは，放電管端までステンレス製の内管 (inner tube) を用いて導かれ，放電管端でArプラズマ中に混入され，Arプラズマ粒子

† 早稲田大学理工学部電子通信学科，東京都
School of Science and Engineering, Waseda University, Tokyo, 169 Japan
* 現在，三菱重機株式会社

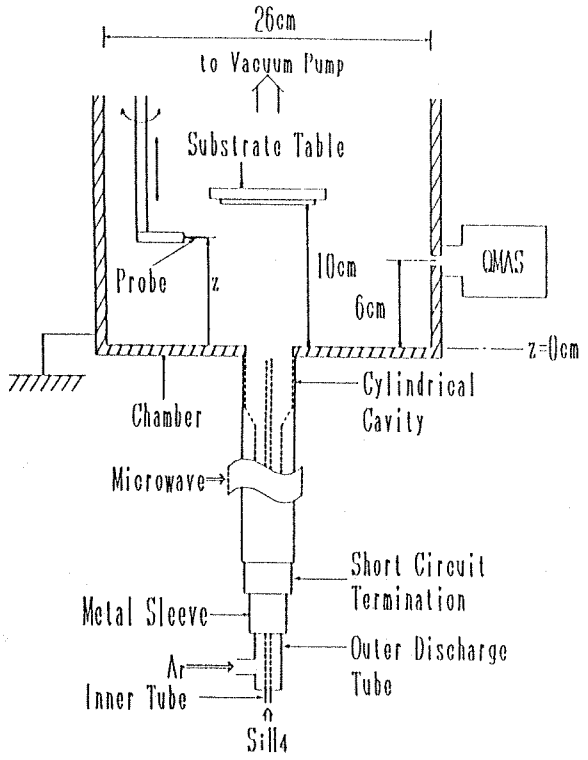

図 1　実験装置概略図
Fig. 1　Schematic diagram of experimental system.

との衝突により解離される．本装置の詳細については文献 (4), (5) を参照されたい．

ここで，堆積室内における位置を示す座標として，放電管端から中心軸方向への距離を z と定義する．

基板テーブル (substrate table) は $z=10$ cm の位置に設置した．この位置は，マイクロ波電力の供給がない空間的アフターグロープラズマ領域であり，イオン衝撃なしに，ラジカルをソフトランディングさせて成膜できる位置である[5]．電子温度，電子密度の測定には，直径 0.05 cm，長さ 0.3 cm の円筒プローブ (probe) を用いた．プローブは駆動シャフトに取付けられており，堆積室内を可動である．4 重極質量分析装置 (QMAS) は $z=6$ cm の位置の堆積室の側壁に直径 200 μm のオリフィスを介して設置した (図 1 参照)．

次に放電条件を示す．プローブ測定においては，マイクロ波電力を 150 W とし，Ar ガス流量を 110 ml/min とした．このときの堆積室内のガス圧は約 3.5 mTorr となった．プローブ測定は $z=0$ cm～9 cm で，堆積室の中心軸上で行った．4 重極質量分析および成膜においても，マイクロ波電力，Ar ガス流量をプローブ測定のときと同じ条件にしている．また，成膜時の SiH_4 ガス流量は 50 ml/min とした．このとき，堆積室内のガス圧は約 5 mTorr となった．SiH_4 ガスを Ar プラズマ中に混入させる位置である内管端の位置を $z=-2$ cm～3 cm まで変化させた．これは，後述のように Ar プラズマの電子温度，電子密度が大きく変化する範囲である．

膜厚の測定には，触針式膜厚計を用いた．ラザフォード・バックスキャッタリング測定より得たスペクトルから，膜中の Si 原子密度を求めた．赤外吸収スペクトルと膜厚より，SiH 結合と SiH_2 結合のストレッチングモードの積分強度を求め，これに，係数 1.4×10^{20} cm^{-2} をかけることにより，両結合の形で含まれる水素原子密度を算出した[6]．紫外可視吸収スペクトルと膜厚より，光学エネルギーギャップを求めた．電子スピン共鳴測定の結果と膜厚より，ダングリングボンド密度を求めた．

3. 実験結果

図 2 に電子温度の z 依存性を示す．図より，電子温度は $z=3$ cm 程度までは急激に減少し，その後は減少こう配が小さくなることがわかる．

図 3 に電子密度の z 依存性を示す．図より，電子密度は $z=3$ cm 程度までは急激に減少し，その後は指数関数的に減少することがわかる[7]．なお，z が負の領域 (すなわち放電管内) にはプローブが入らないため測定していないが，この領域ではマイクロ波電力が均一に入射するので，電子温度，電子密度ともに $z=-2$ cm 程度までで急速に飽和して一定となると考えられる．

先に述べたように本 MPCVD 装置では，SiH_4 ガスを放電管端まで内管を用いて導き，そこで Ar プラズマ中に混入させ，Ar プラズマ粒子との衝突により解離させている．以上のことから，内管端の位置を変化させることにより，電子温度，電子密度の異なる Ar プラズマ中で SiH_4 ガスを解離させることができ，ラジカルのフラグメンテーションパターンを変化させることができると考えられる．

図 4, 5 に 4 重極質量分析により求めたマススペクトル線強度の内管端位置依存性を示す．図 4 がイオナイザを OFF にしたときの結果であり，シラン系のイオンラジカルの変化を示す．図 5 はイオナイザを ON にしたときの結果である．いずれの結果においても，内管端の位置を z 軸上で負から正にするに従い，SiH_2^+ が減少し，SiH_3^+ が増加していることがわかる．このことから，本 MPCVD 装置において内管端の位置を変化

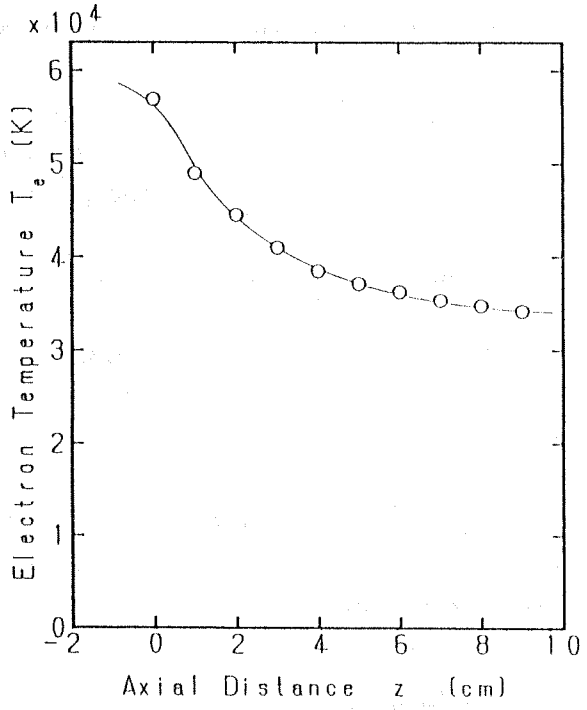

図 2 電子温度の z 依存性
Fig. 2 Dependence of electron temperature on z.

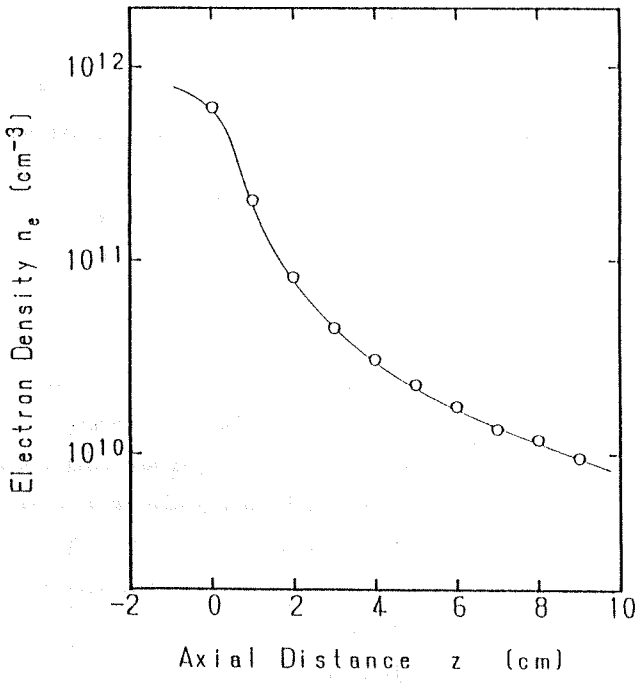

図 3 電子密度の z 依存性
Fig. 3 Dependence of electron density on z.

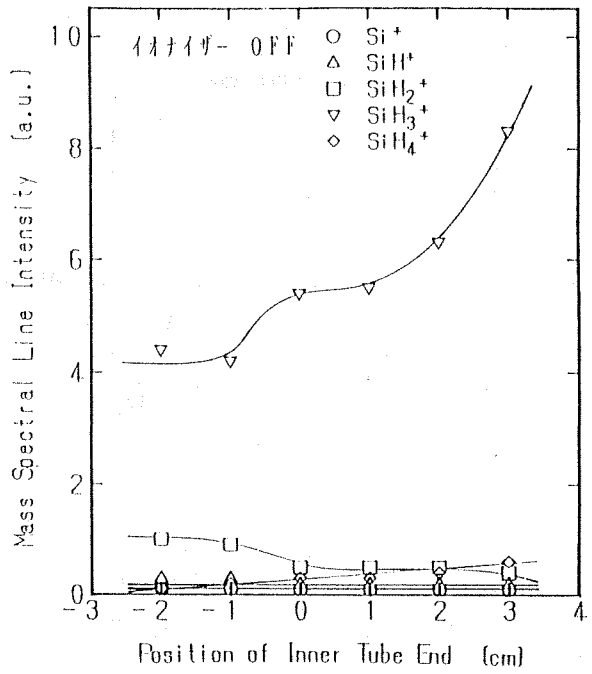

図 4 マススペクトル線強度の内管端位置依存性（イオナイザ OFF）
Fig. 4 Dependence of mass spectral line intensity on the position of the inner tube end (ionizer off).

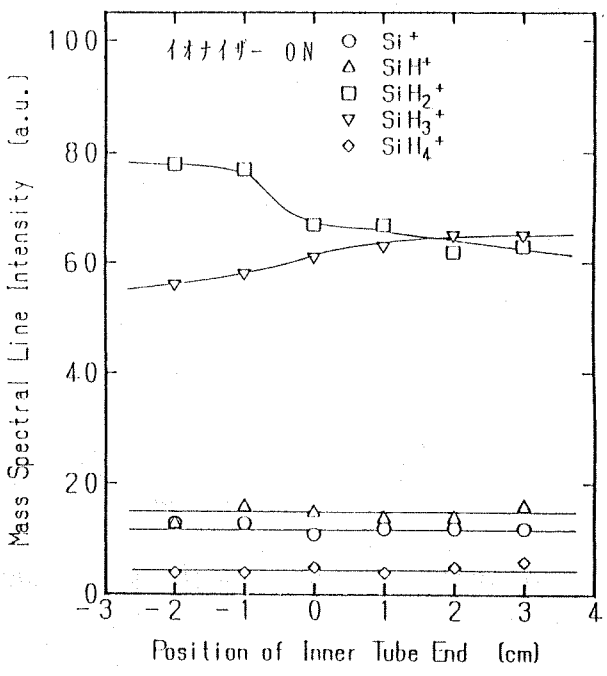

図 5 マススペクトル線強度の内管端位置依存性（イオナイザ ON）
Fig. 5 Dependence of mass spectral line intensity on the position of the inner tube end (ionizer on).

させることにより，ラジカルのフラグメンテーションパターンを変化させることができることが明らかである．このように，SiH_2^+ が減少し，SiH_3^+ が増加するのは電子温度，電子密度が低下するので，SiH_2^+ を作る電離を伴う解離の度合いが抑制され，SiH_3^+ を作る電離を伴う解離の度合いが増加したためである．イオンラジカルの変化と中性ラジカルの変化は必ずしも比例す

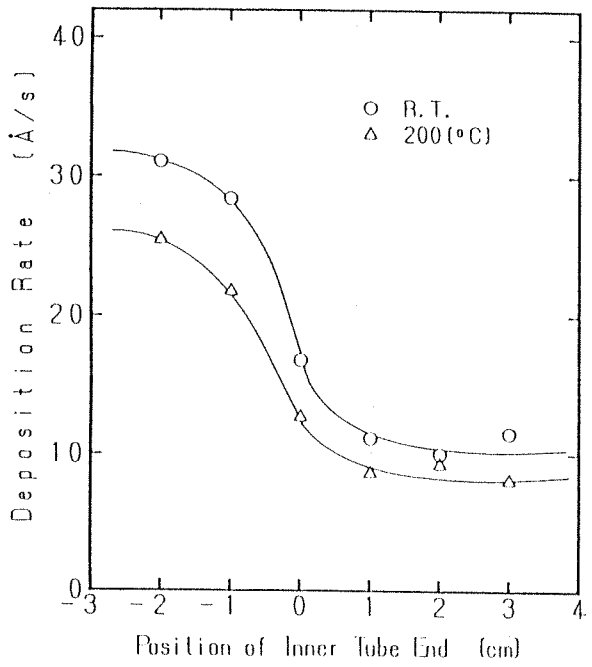

図 6 堆積速度の内管端位置依存性
Fig. 6 Dependence of deposition rate on the position of the inner tube end.

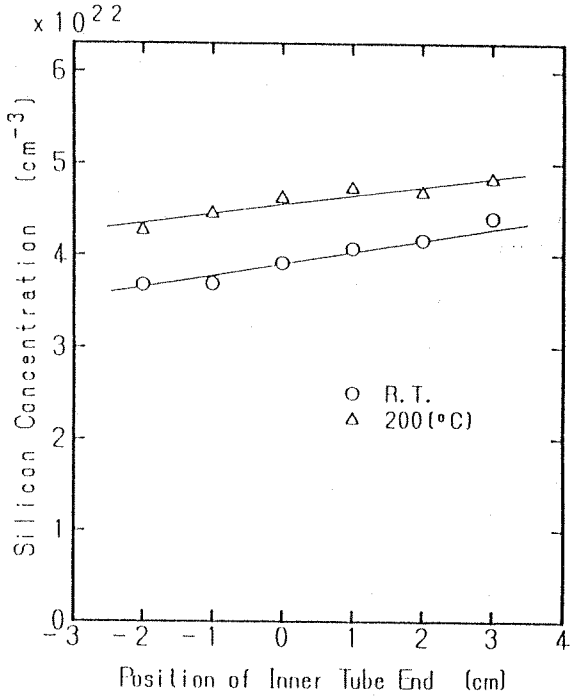

図 7 単位体積当たりのシリコン含有量の内管端位置依存性
Fig. 7 Dependence of silicon concentration on the position of the inner tube end.

るとは限らないが，本研究で用いている電離度数%以下の弱電離プラズマにおいてはほぼ比例すると考えるのが妥当である．従って，SiH_2 ラジカルは減少し，SiH_3 ラジカルは増加していると考えられる．これまでに，SiH_3 ラジカルのような膜表面でのモビリティの大きいラジカルを選択的に膜表面に導くことにより，膜質が改善されたという結果が報告されている[8]．以上のことから，内管端の位置を負から正にして成膜することにより，膜質の改善が期待できる．そこで，内管端の位置を変化させることにより，ラジカルのフラグメンテーションパターンを変化させてa Si:H膜を作製し，その膜質評価を次に行う．

図6に，堆積速度の内管端位置依存性を示す．図より，堆積速度は基板温度にかかわらず，内管端の位置が $z=-1$ cm 程度から $+1$ cm 程度の間に急激に減少し，その後は飽和傾向を示すことがわかる．これは，前述のように SiH_4 の解離度およびフラグメンテーションパターンが大きく変化するためである．また，$z=-1$ cm 程度から -2 cm では堆積速度が大きく変化していないのは，前述のように電子温度，電子密度が大きく変化しないためと考えられる．なお，基板を200°Cに加熱して成膜すると基板温度を室温として成膜したときに比べ，従来の報告どおり[9]，堆積速度は遅くなることがわかる．これは，後述のように膜中の単位体積当たりのシリコン含有量が増加するためである．

図7に，単位体積当たりのシリコン含有量の内管端位置依存性を示す．図より基板温度にかかわらず，内管端の位置を負から正にするに従い，シリコン含有量は増加し，膜がち密化していることがわかる．これは，膜表面でのモビリティの大きい SiH_3 ラジカルが増加したため，より安定な準位に入りながら膜堆積が進むためであると考えられる．なお，基板温度を200°Cに加熱して成膜すると基板温度を室温にして成膜したときに比べ，従来の報告どおり[10]，更にシリコン含有量が高くなることがわかる．

図6，7より，(単位体積当たりのシリコン含有量)×(堆積速度)で与えられる単位時間，単位面積当たりに膜となるシリコンの量を算出した．その結果，単位時間，単位面積当たりに膜となるシリコンの量は内管端の位置の変化に対し，図6に示した堆積速度と同様な傾向を示した．この結果から，内管端の位置を負から正に変化させることにより堆積速度が減少するのは，膜がち密化するためだけではないことがわかる．

内管端の位置を負から正に変化させることにより堆積速度が減少するのは，本実験における内管端位置の変化範囲($z=-2$ cm から $z=3$ cm)が電力供給のある

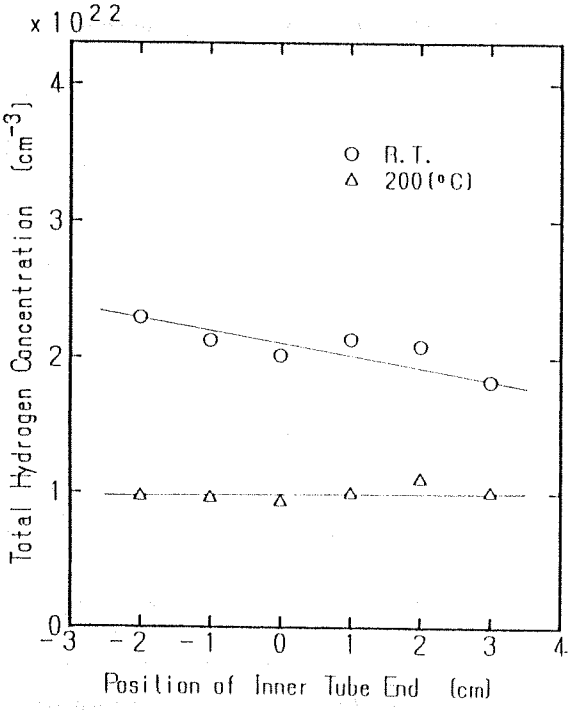

図 8 単位体積当たりの全水素含有量の内管端位置依存性
Fig. 8 Dependence of total hydrogen concentration on the position of the inner tube end.

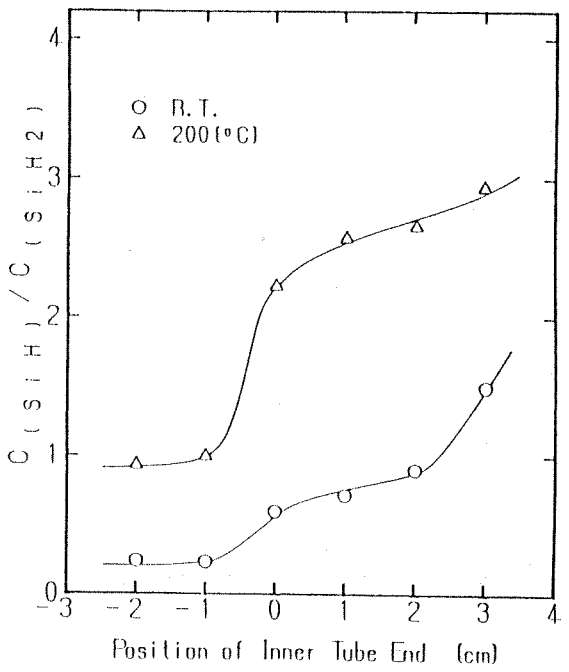

図 9 (SiH 結合密度)/ (SiH_2 結合密度) 比の内管端位置依存性
Fig. 9 Dependence of (SiH bond density)/(SiH_2 bond density) ratio on the position of the inner tube end.

放電プラズマ領域から電力供給のない空間的アフターグロープラズマ領域への遷移領域を含むためである．すなわち，この間に SiH_4 の解離度が低下すること，および解離の度合いが抑制され付着確率の高い SiH_2 ラジカル[8]が減少し，付着確率の低い SiH_3 ラジカル[8]が増加することによると考えられる．また，基板温度を変化させても単位時間，単位面積当たりに膜となるシリコンの量の内管端位置依存性は変化せずほぼ一定である．このことから，基板を加熱することにより堆積速度が減少するのは，膜がち密化されるためであることがわかる．

図 8 に，単位体積当たりの全水素含有量の内管端位置依存性を示す．図より，基板温度が室温の場合は内管端の位置を負から正にするに従い，全水素含有量は減少することがわかる．基板温度を 200°C にすると，水素含有量は内管端の位置にかかわらず，約 1×10^{22} cm^{-3} でほぼ一定となった．

内管端位置を負から正にするに従い，膜中の SiH 結合密度は増加し，SiH_2 結合密度は減少した．図 9 に，(SiH 結合密度)/ (SiH_2 結合密度) 比の内管端位置依存性を示す．図より基板温度にかかわらず内管端の位置を負から正にするに従い，SiH 結合優勢な a-Si : H 膜が作製されることがわかる．なお，基板温度を 200°C

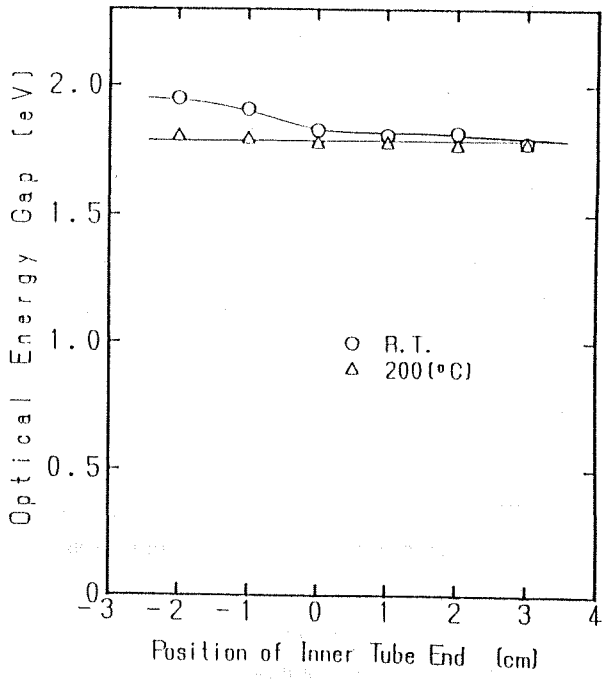

図 10 光学エネルギーギャップの内管端位置依存性
Fig. 10 Dependence of optical energy gap on the position of the inner tube end.

に加熱して成膜すると基板温度を室温にして成膜したときに比べ，更に SiH 結合優勢な膜が作製できるという従来どおりの結果が得られている．

図 10 に，光学エネルギーギャップの内管端位置依存

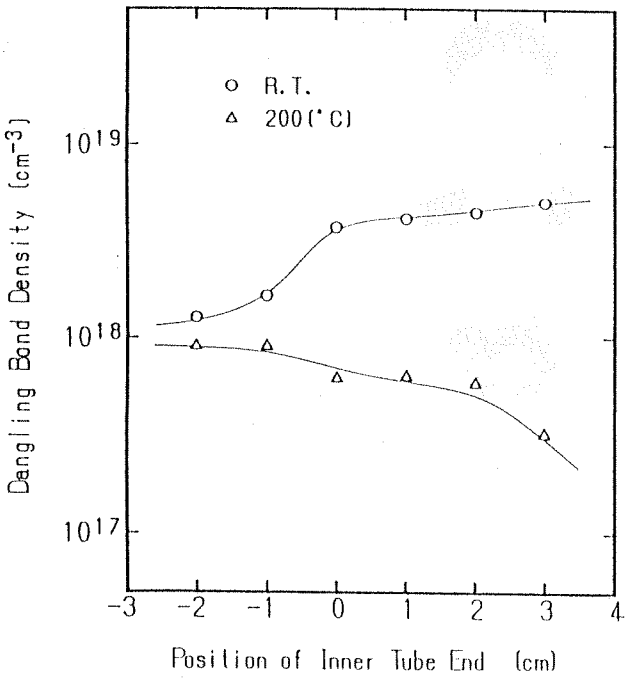

図 11 ダングリングボンド密度の内管端位置依存性
Fig. 11 Dependence of dangling bond density on the position of the inner tube end.

性を示す．図より，基板温度が室温の場合は内管端の位置を負から正にするに従い，光学エネルギーギャップは減少することがわかる．基板温度を200°Cにすると，光学エネルギーギャップは，内管端の位置にかかわらず，約1.78 eVでほぼ一定となった．この傾向は，全水素含有量の内管端位置依存性と一致している．

図11に，ダングリングボンド密度の内管端位置依存性を示す．図より，基板温度が室温の場合は内管端の位置を負から正にするに従い，ダングリングボンド密度はやや増加することがわかる．すなわち，基板を加熱しない，または加熱できない場合には，内管端位置を負にしてSiH_2ラジカルの割合を大きくしたほうがダングリングボンド密度を低減できることを示している．基板を200°Cに加熱し膜表面でのラジカルのモビリティを大きくすると，ダングリングボンド密度は内管端の位置を負から正にするに従い減少し，より良質なa-Si:H膜を作製できることがわかる．

以上の結果から，内管端の位置を負から正にして成膜するに従い，堆積速度は低下するものの，膜質を改善できることが明らかとなった．これは，膜表面でのモビリティの大きいSiH_3ラジカルが増加したためである．

4. むすび

2重管式同軸線路形マイクロ波プラズマCVD装置の堆積室内において，純Arプラズマ中で電子温度，電子密度の空間分布測定を行った．更に，SiH_4ガスのArプラズマ中への混入位置（内管端の位置）を変化させることにより，電子温度，電子密度の異なるArプラズマ中でSiH_4ガスを解離させ，そのフラグメンテーションパターンを質量分析法により測定した．その結果，以下のことが明らかになった．

（1） 電子温度は$z=3$ cm程度までは急激に減少し，その後，減少こう配が小さくなる．

（2） 電子密度は$z=3$ cm程度までは急激に減少し，その後，指数関数的に減少する．

（3） 内管端の位置を負から正にするに従い，SiH_2^*は減少し，SiH_3^*は増加する．

更に，内管端の位置を変化させて成膜し，その膜質評価を行った．その結果，内管端の位置をz軸上で負から正にするに従い，堆積速度および膜質は以下のように変化することが明らかになった．

（1） 堆積速度は内管端の位置が$z=1$ cm程度までは急激に減少し，その後飽和傾向を示す．これは，SiH_4の解離度の低下および付着確率の低いSiH_3ラジカルの増加によると考えられる．

（2） シリコン含有量，全水素含有量，水素の結合状態および光学エネルギーギャップの変化は，膜質の改善を示す．

（3） ダングリングボンド密度は，室温で成膜した場合にはやや増加するものの，基板温度を200°Cとして成膜すると減少する．

以上の結果から，低い電子温度のプラズマでSiH_4を解離させることにより，膜表面でのモビリティの大きいSiH_3ラジカルを増加させることができるので，膜質の改善がはかれることがわかる．

今後，中性ラジカルのフラグメンテーションパターンを定量的に明らかにし，堆積機構のより詳細な検討を行う予定である．

文　献

（1） Matsumi Y., Hayashi T., Yoshikawa H. and Komiya S.: "Laser diagnostics of a silane plasma-SiH radicals in an a-Si:H chemical vapor deposition system", J. Vac. Sci. Tech., A4, 1786-1790 (May 1986).

（2） Itabashi N., Nishiwaki N., Magane M., Goto T., Matsuda A., Yamada C. and Hirota E.: "SiH_3 Radical Density in Pulsed Silane Plasma", Jpn. J. Appl. Phys.,

29, 3, pp.585-590 (March 1990).
(3) Matsuda A., Nomoto K., Takeuchi Y., Suzuki A., Yuuki A. and Perrin J.: "TEMPERATURE DEPENDENCE OF THE STICKING AND LOSS PROBABILITIES OF SILYL RADICALS ON HYDROGENATED AMORPHOUS SILICON", Surface Science, 227, pp.50-56 (1990).
(4) Kato I., Hara S. and Wakana S.: "Microwave Plasma CVD System to Fabricate a-Si Thin Films out of Plasma", Jpn. J. Appl. Phys., 22, 1, pp.L40-42 (Jan. 1983).
(5) 加藤 勇, 矢野元康: "同軸線路形マイクロ波プラズマCVD法によるプラズマ内外でのa-Si:H薄膜の作成", 信学論(C), J69-C, 5, pp.662-668 (1986).
(6) 加藤 勇, 土田哲也, 畑中和久: "二重管式同軸線路形マイクロ波水素プラズマCVDによるa-Si:H膜の作成", 信学論(C), J70-C, 1, pp.78-88 (1987).
(7) 加藤 勇, 白居隆志, 阪本 匡: "マイクロ波プラズマCVDにおけるプラズマパラメータの空間分布", 電学論A, 112-A, 5, pp.355-362(1992-05).
(8) 松田彰久: "成長過程と新しい膜質制御法", 固体物理, 27, pp.777-784 (1992).
(9) 加藤 勇, 土田哲也, 畑中和久: "二重管式同軸線路形マイクロ波プラズマCVD法によるa-Si:H薄膜の基板温度特性", 電学論A, 106-A, 8, pp.35-41 (1986-08).
(10) Hama T., Okamoto H., Hamakawa Y. and Matsubara T.: "HYDROGEN CONTENT DEPENDENCE OF THE OPTICAL ENERGY GAP IN a-Si:H", J. Non-Cryst. Solid, 59&60, pp.333-336 (1983).

(平成6年8月19日受付, 11月16日再受付)

加藤 勇

昭42早大・理工・電子通信卒. 昭48同大学院博士課程了. 同年工博. 同年早大勤務. 昭53同大助教授. 昭54～56マニトバ大客員教授, カナダ国立研究会議の研究費を受け共同研究ならびに研究指導. 昭58同大教授, 現在に至る. 光子工学, レーザ工学, 電子物性工学, 計測工学, 光子材料, プラズマエレクトロニクス, 光・量子エレクトロニクス, 半導体薄膜工学などの研究に従事. 電気工学会, 応用物理学会, テレビジョン学会, 日本真空協会, IEEE各会員.

米田 俊之

平4早大・理工・電子通信卒. 平6同大学院修士課程了. 現在, 三菱電機生産技術センター勤務. 在学中はマイクロ波プラズマCVDに関する研究に従事. 応用物理学会会員.

松下 亨

平5早大・理工・電子通信卒. 現在, 同大学院修士課程在学. マイクロ波プラズマCVDに関する研究に従事. 応用物理学会会員.

山下 真

平6早大・理工・電子通信卒. 現在, 同大学院修士課程在学. マイクロ波プラズマCVDに関する研究に従事. 応用物理学会会員.

Electronics and Communications in Japan, Part 2, Vol. 78, No. 2, 1995
Translated from Denshi Joho Tsushin Gakkai Ronbunshi, Vol. 77-C-II, No. 9, September 1994, pp. 384-391

Influence of Ion Bombardment on a-Si : H Films Fabricated by Plasma Chemical Vapor Deposition

Isamu Kato, *Member*, and Toshiyuki Yoneda* and Toru Matsushita, *Nonmembers*

School of Science and Engineering, Waseda University, Tokyo, Japan 169

SUMMARY

Plasma parameters of Ar/SiH_4 plasma were measured as a function of dc bias in a double-tubed coaxial line-type microwave plasma chemical vapor deposition (CVD) apparatus. The results indicate that it is possible to control the ion bombardment energy without affecting either the gas phase reaction or ion flux density incident to the substrate. Hydrogenated amorphous silicon films were deposited as a function of the ion bombardment energy and characteristics of the deposited films were investigated. The results indicate that the ion bombardment improves film density, bonding characteristics of hydrogen, and optical band gap but increases the concentration of dangling bonds due to Ar ion implantation. The ion bombardment not only causes the heating of the films but also induces sputtering and ion implantation.

Key words: Plasma CVD; a-Si : H; dc bias voltage; sheath voltage; ion bombardment.

1. Introduction

Hydrogenated amorphous silicon (a-Si : H) has been used extensively as optoelectronic materials for solar cells and copiers and as semiconducting materials for thin-film transistors. To improve the performance and to develop new applications, amorphous silicon has been a focus of intensive studies. The deposition of a-Si : H has been investigated extensively using high-frequency discharge and electrocyclotron resonance (ECR) discharge plasma chemical vapor deposition (CVD) methods.

It has been reported [1, 2] that ion bombardment improves the film characteristics. The authors have also reported [3, 4] that ion bombardment causes the increase in the film density, the decrease of SiH_2 bonds and the increase of SiH bonds due to film heating.

Because films fabricated by the commonly used high-frequency plasma CVD method are deposited in a discharge plasma to which electric energy is supplied, the films are exposed to ion bombardment. The ion bombardment has been controlled by discharge voltage that causes the variation in self-bias of the substrates. The self-bias is controlled by changing electron temperature and electron density, and thus the process also influences gas phase reactions. Therefore, it is not possible to investigate the sole influence of ion bombardment on film characteristics.

We have developed a double-tubed coaxial-line-type microwave plasma CVD (MPCVD) apparatus that allows the film deposition in a spatial afterglow plasma region with very little ion bombardment by confining the discharge plasma to a restricted area [3-9]. DC bias (V_{dc}) is

*Presently with Mitsubishi Manufacturing Technology Center.

ISSN8756-663X/95/0002-0070

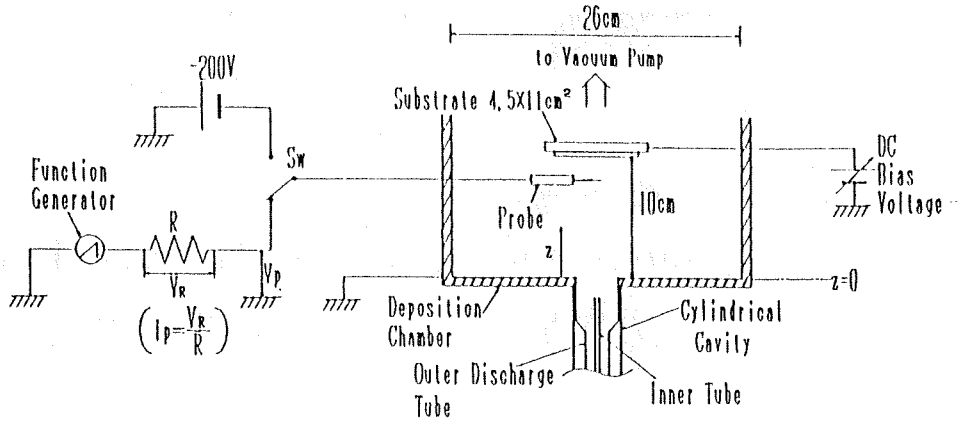

Fig. 1. Schematic diagram of experimental system.

applied to substrates in the deposition chamber and its influence on the plasma parameters has been investigated using a probe. The results indicate that it is possible to control ion bombardment energy (E_i) by V_{dc} without affecting the gas phase reaction and ion flux density. The influence of ion bombardment on the film characteristics is delineated by evaluating films deposited with various V_{dc}.

2. Experimental

Figure 1 shows a schematic of the double-tubed coaxial-line microwave plasma CVD apparatus. The discharge tube is made of two coaxial tubes. Ar gas flows through an annulus between the outer discharge tube made of fused quartz and the inner tube made of stainless steel. SiH_4 gas flows through the inner discharge tube. Microwave (2.45 GHz) generated by a magnetron is transmitted through a rectangular microwave guide to a cylindrical metallic cavity where a discharge occurs in Ar gas. At the end of the discharge tube, SiH_4 gas is mixed with Ar plasma and dissociated. Si radicals created are transported to a low-pressure (~mtorr) deposition chamber and deposited on a substrate as an a-Si : H film.

Because microwaves are confined in the cylindrical metallic cavity of the MPCVD apparatus [5], the spatial afterglow plasma region is created without the presence of microwave in the deposition chamber [6]. By placing the substrate in the spatial afterglow plasma, it is possible to deposit the thin films without ion bombardment [6-8]. The deposition chamber as well as the inner metallic tube are grounded. The substrate is located 10 cm from the end of the discharge tube and is biased by a dc voltage source. The MPCVD apparatus has been described in detail elsewhere [5, 6]. A cylindrical probe, 0.025 cm in radius and 1 cm in length, is employed for measuring plasma parameters. The probe is movable in the deposition chamber. A parameter z denotes the distance of the probe from the end of the discharge tube as indicated in Fig. 1.

The flow rates of Ar and SiH_4 gases were fixed at 110 ml/min and 30 ml/min, respectively. The resulting gas pressure in the deposition chamber was about 4 mtorr. The microwave power was fixed at 150 W. The bias voltage V_{dc} was varied from +40 V to -80 V. In this range, the plasma parameters were unaffected by the dc bias. From the change in glow condition around the substrate, dc discharge was noted between the substrate and the grounded deposition chamber and inner tube for V_{dc} higher than 40 V and less than -80 V. The dc discharge caused a drastic change in the plasma parameters, which were detected by the metallic probe at the center of the deposition chamber. The measurements were taken at z values of 3, 5, 7, and 9 cm. The single probe method for the reactive Ar/SiH_4 plasma was described in detail in [9].

Film thicknesses were determined by a stylus thickness meter. The concentrations of Si and Ar were determined from Rutherford backscattering spectra. Integral strengths of stretching modes of SiH and SiH_2 bonds as well as of wagging mode of $(SiH_2)_n$ chains were determined from IR absorption spectra. The concentration of hydrogen was determined by multiplying integral strengths of SiH and SiH_2 bonds with a factor of 1.4×10^{-20} cm^{-2} [10]. The film densities were determined

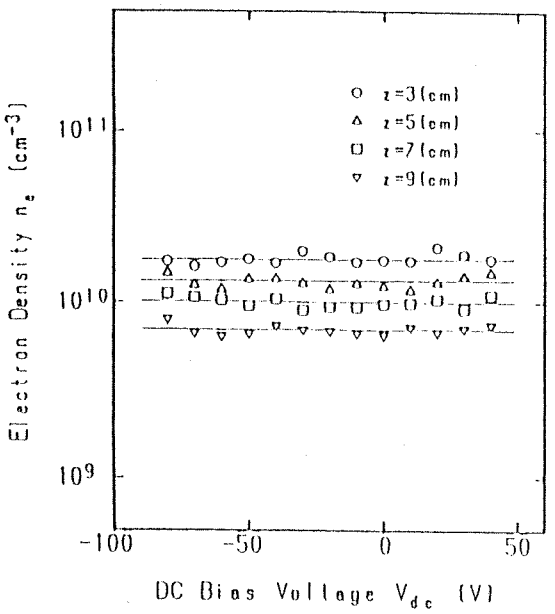

Fig. 2. Dependence of n_e on V_{dc}.

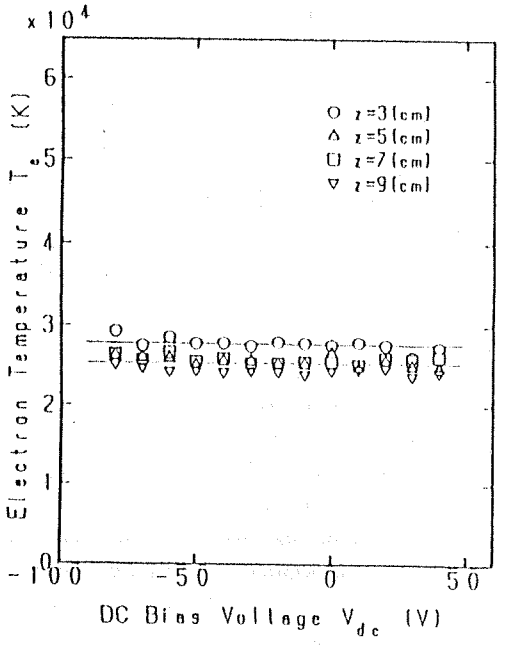

Fig. 3. Dependence of T_e on V_{dc}.

from concentrations of Si, Ar, and total H, the optical band gaps from UV absorption spectra and film thickness, and the densities of dangling bonds from the result of electron spin resonance measurements and film thickness.

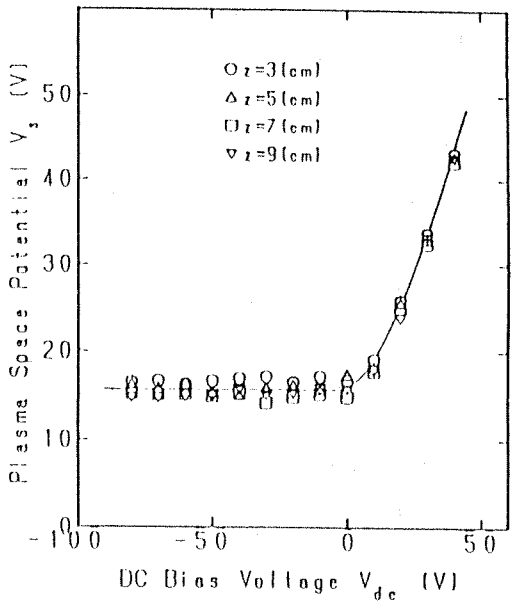

Fig. 4. Dependence of V_s on V_{dc}.

3. Experimental Results

3.1. Influence of V_{dc} on the plasma parameters

Figure 2 shows the dependence of the electron densities (n_e) on V_{dc} at various z positions; n_e is constant regardless of V_{dc} at a given z position but decreases with increasing z.

Figure 3 shows the dependence of the electron temperature (T_e) on V_{dc}; T_e is constant regardless of V_{dc} but decreases slightly with increasing z to 5 cm but remains constant above 5 cm.

The independence of T_e and n_e on V_{dc} in Figs. 2 and 3 indicates the absence of dc discharge, which in turn indicates no effect of V_{dc} on the gas phase reaction.

It has been reported [1] that the influence of positive bias voltage on the film characteristics can be attributed to the presence of positive electric field at the surface of the substrate, which causes the acceleration of electrons. But we have observed the dependence of plasma space potential (V_s) on V_{dc} when the substrate was positively biased. This indicates that it is not necessarily correct to assume the acceleration of electrons [12]. In this study V_s was measured for a substrate table with a surface area of 54 cm^2 and the results were analyzed to quantify the electric field at the surface of the substrate.

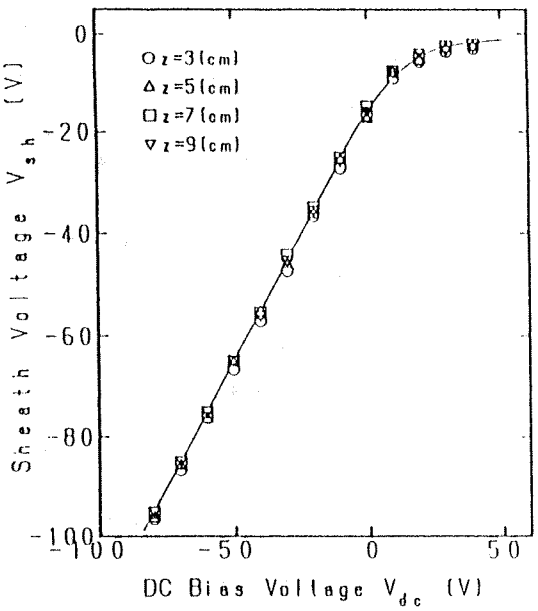

Fig. 5. Dependence of V_{sh} on V_{dc}.

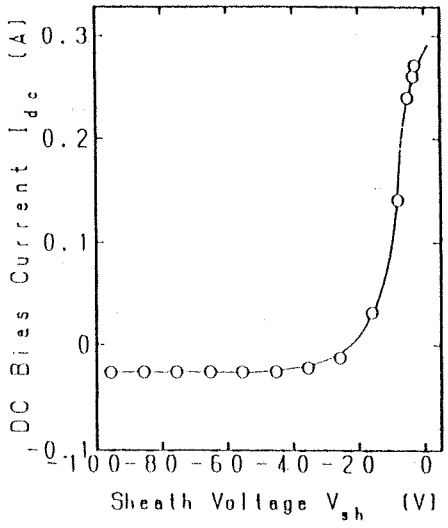

Fig. 6. Dependence of I_{dc} on V_{sh}.

Figure 4 shows the dependence of V_s on V_{dc}. The figure indicates that V_s remains constant for negative bias but increases with increasing positive bias. It also indicates that V_s does not depend on z in the range between 3 and 9 cm.

The sheath voltage (V_{sh}) is defined by V_{dc}-V_s. The sheath voltages were calculated from the data presented in Fig. 4 and are shown in Fig. 5. Ions are either accelerated or decelerated by the sheath voltage. Since V_{sh} is negative regardless of V_{dc} as indicated in Fig. 5, it is evident that ions are neither decelerated nor recoiled at the surface of the substrate even by the application of positive bias.

Because electrons are recoiled by the electric field in the sheath, the ion density becomes higher than n_e at the surface of the substrate even when a positive bias voltage is applied. This indicates the formation of an ion sheath. Since it is not possible for the ions to follow the microwave field and there exists no electric field gradient in the deposition chamber as indicated earlier, it is expected that the kinetic energy of the ions is quite small and about the order of room temperature prior to the injection into the sheath. Therefore, the kinetic energy of the ions at the moment of incidence to the substrate can be determined solely by the sheath voltage. The mean-free path of the ions is about 2 cm for the gas pressure of 4 mtorr in the deposition chamber.

Since the thickness of the ion sheath is about 2 mm [12], the ions pass through the sheath without colliding with other particles. Thus the kinetic energy of the ions at the moment of incidence to the substrate, i.e., the energy of ion bombardment (E_i), is given by the product of the unit electric charge and the absolute value of the sheath voltage when all ions are assumed to be singly charged. By varying V_{dc} from -80 V to +40 V, it is possible to change E_i from about 95 eV to about 3 eV.

Figure 6 shows the dependence of electric current through the substrate (I_{dc}) on V_{sh}; I_{dc} is the sum of electron and ion currents. Since V_s is always larger than V_{dc} whose values are between -80 V and +40 V in this study, there always exists an electric field that accelerates ions at the surface of the substrate; but there does not exist any electric field that recoils ions even when a positive bias voltage is applied. The figure indicates that I_{dc} remains constant for V_{sh} less than about -45 V. The constant value of I_{dc} is the saturated ion current (I_{is}). This indicates that the ion current is constant regardless of V_{sh} and equals I_{is}. For V_{sh} higher than -45 V, I_{dc} increases with increasing V_{sh}. The increase is not due to ion current but due to electron current. Electrons have some kind of energy distribution, generally Maxwell distribution. With increasing V_{sh}, a part of the electrons with high energy overcome the electric field and begin passing through the substrate, thereby causing the increase of I_{dc}. Assuming that all ions are singly charged in the plasma, the ion flux density incident to the substrate (Γ_i) is given by the following equation:

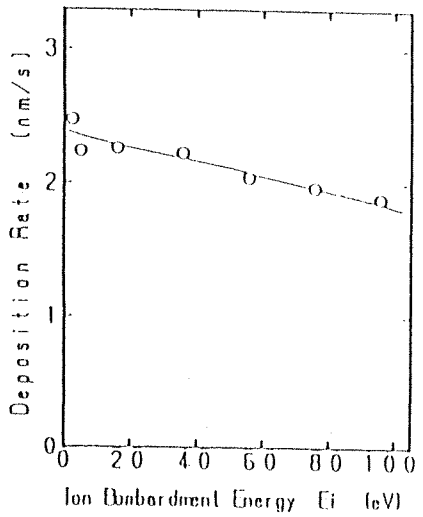

Fig. 7. Dependence of deposition rate on E_i.

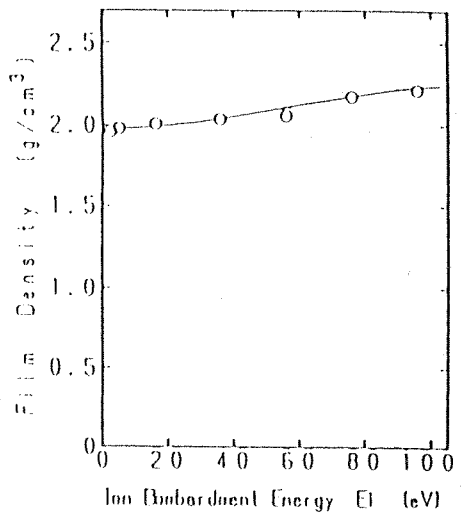

Fig. 8. Dependence of film density on E_i.

$$\Gamma_i = \frac{I_{is}}{e \cdot S}$$

where e and S are the unit electric charge and the surface area of the substrate table, respectively. In the experimental range of this study, Γ_i is constant regardless of V_{dc}.

Since T_e and n_e are not affected by V_{dc} as shown in Figs. 2 and 3, the gas phase reaction is not affected by V_{dc} either. Since the gas phase reaction is not affected, the ionic species incident to the substrate remains unaffected.

In the experimental range of this study where the ion sheath is formed at the surface of the substrate, the ionic current remains constant and therefore Γ_i also remains constant as can be seen in Fig. 6. Therefore, it is possible to control E_i without affecting the gas phase reaction and Γ_i by using the MPCVD apparatus.

3.2. Influence of ion bombardment on film characteristics

To delineate the influence of ion bombardment on film characteristics, thin films of a-Si : H were deposited as a function of E_i by varying V_{dc} and their film characteristics were evaluated.

Figure 7 shows the dependence of the deposition rate on E_i. The deposition rate decreases almost linearly with increasing E_i. As will be discussed later, the decrease is due to the densification of the films, sputtering of the films and decreasing residence time of the molecules caused by the increasing kinetic energy of the ions.

Figure 8 shows the dependence of film density on E_i. The film density increases with increasing E_i. Since we observed previously that the film density increased by the heating of the substrate [7], the increase of film density is inferred to the heating of the film surface by ion bombardment. The film deposited at E_i of about 95 eV has about 15 percent higher density than that deposited at E_i of about 3 eV.

By comparing the density of the film deposited at E_i of about 95 eV with the previously reported results on film density as a function of substrate temperature [7], the surface temperature of the film is estimated to be about 250°C for E_i of about 95 eV. As discussed earlier, the densification of the film is a cause of the decrease in deposition rate. The deposition rate decreased about 40 percent with increasing E_i from 3 eV to 95 eV. On the other hand, the film density increased about 15 percent. Hence, about 40 percent ($\sim 15/40 \times 100$) of the decrease in the deposition rate can be attributed to the densification of the films.

Figure 9 shows the dependence of the optical band gap on E_i. The optical band gap decreases with increasing E_i.

Figure 10 shows the dependence of hydrogen concentration in the film on E_i. The hydrogen concentration

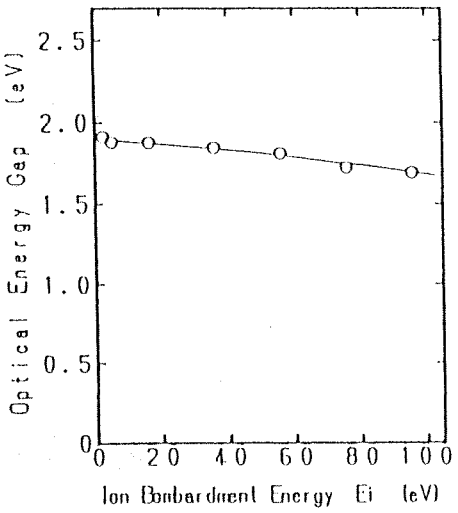

Fig. 9. Dependence of optical energy gap on E_i.

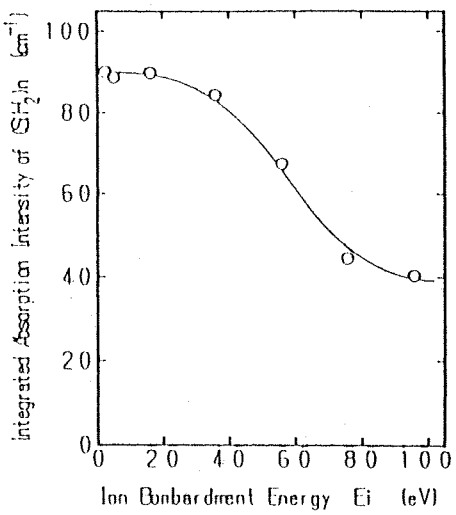

Fig. 11. Dependence of integrated absorption intensity of $(SiH_2)_n$ on E_i.

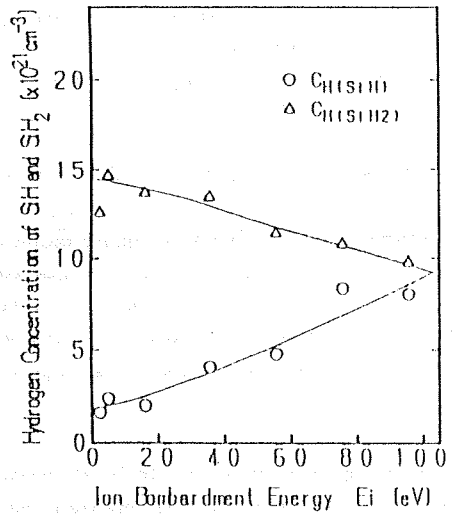

Fig. 10. Dependence of hydrogen concentration of SiH and SiH_2 on E_i.

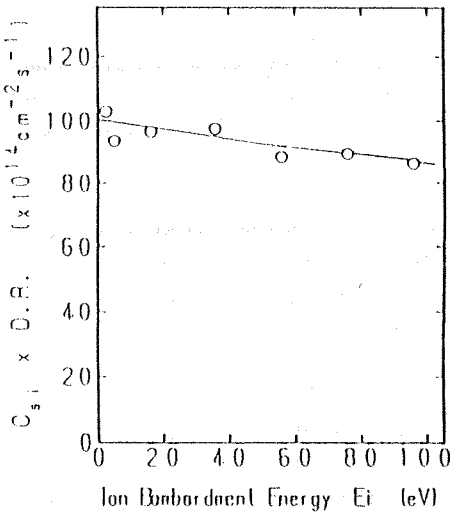

Fig. 12. Dependence of $C_{si} \times$ D.R. on E_i.

of SiH bonds increased with increasing E_i, while the hydrogen concentration of SiH_2 decreased. At E_i of about 60 eV the concentration of SiH bonds (= $C_{H(SiH)}$) in the film surpassed that of SiH_2 bonds $C_{H(SiH2)}/2$). Therefore, the films deposited at E_i higher than 60 eV contain SiH bonds predominantly.

Figure 11 shows the dependence of integrated absorption intensity of $(SiH_2)_n$ chains on E_i. The concentration of $(SiH_2)_n$ chains decreased with increasing E_i.

The amount of Si deposited for a unit time per unit area can be calculated from the product of the deposition rate and Si concentration (C_{si}). The results are shown in Fig. 12 as a function of E_i. The amount of Si deposited for a unit time per unit area decreased with increasing E_i. The decrease might be the result of sputtering of the films by ion bombardment and the decreasing residence time of molecules due to increasing kinetic energy. The contribution of these effects on the deposition rate is estimated similarly to that of the film densification, and a value of about 60 percent is obtained as expected.

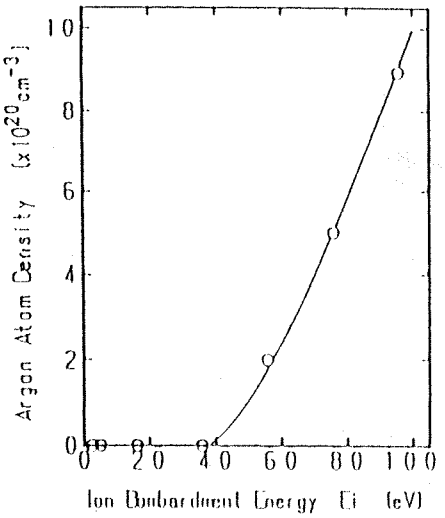

Fig. 13. Dependence of Ar concentration on E_i.

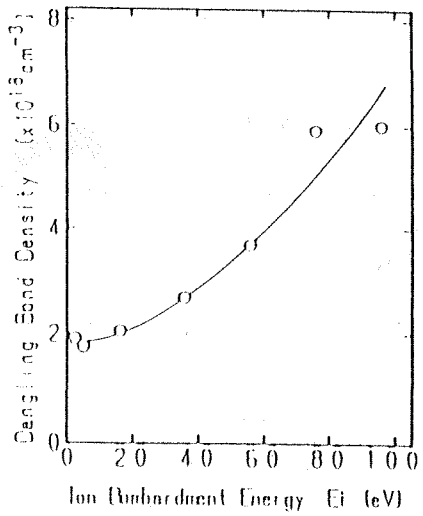

Fig. 14. Dependence of dangling bond density on E_i.

Figure 13 shows the dependence of Ar concentration on E_i. The Ar concentration of the films deposited at E_i less than about 40 eV is less than the detection limit of the instrument, but the Ar concentration of the films deposited at E_i higher than about 40 eV increases with increasing E_i. At E_i higher than about 40 eV, the kinetic energy of Ar ions is high enough to cause the deeper penetration of the ions into the film and, therefore, the probability of Ar retention increases. Specifically, the ion bombardment causes the implantation of Ar ions in the films.

Figure 14 shows the dependence of dangling bond density on E_i. The dangling bond density increases with increasing E_i. The increase is caused by the implantation of Ar ions that damaged the films [8].

The results in Figs. 8 to 11 indicate that the ion bombardment improves the film quality due to heating during deposition. However, as indicated in Figs. 13 and 14, the ion bombardment causes the implantation of Ar ions which in turn causes the increase of Ar concentration and of dangling bond density in the films. Although the ion bombardment has pros and cons, it is desirable to avoid ion bombardment during the deposition of high-quality a-Si : H films due to the increase of dangling bonds.

4. Conclusions

The plasma parameters were measured for dc bias voltage (V_{dc}) between −80 V and +40 V in the double-tubed coaxial-line microwave plasma CVD apparatus. The results are as follows:

(1) Neither electron temperature nor electron density is affected by V_{dc}.

(2) The plasma space potential is not affected by negative V_{dc}, but the plasma space potential increases with increasing V_{dc} when V_{dc} is positive. The application of positive V_{dc} does not create an electron sheath but rather an ion sheath.

(3) It is possible to control ion bombardment energy (E_i) by V_{dc} without affecting either the gas phase reaction or the ion flux density incident to the substrate.

a-Si : H films were deposited for various values of E_i. The results are as follows:

(1) The ion bombardment causes the heating of the film surface as well as ion implantation and sputtering.

(2) The film heating improves the film density, the bonding characteristic of hydrogen, and the optical band gap.

(3) The ion implantation increases the Ar concentration and dangling bond density in the films.

(4) The amount of Si deposited for a unit time per unit area decreases due to sputtering and decreasing residence time of molecules on the film surface caused by increasing kinetic energy.

A further study will be conducted to delineate the mechanism of film growth during ion bombardment.

REFERENCES

1. K. Akiyama, E. Tanaka, A. Takimoto, and M. Watanabe. Effect of ions on properties of a-Si : H films prepared by ECR plasma CVD method. Jpn. J. Appl. Phys., **27**, 12, pp. 2192-2198 (Dec. 1988).
2. G. P. Ryun, M. Aozawa, and K. Ando. Preparation of a-Si : H Film by the Triode Glow Discharge System. Memoirs of the Faculty of Engineering, Osaka City Univ., **24**, pp. 67-80 (1983).
3. I. Kato and S. Wakana. A new microwave plasma chemical vapor deposition system. Vacuum, **26**, 7, pp. 628-636 (July 1983).
4. K. Kato and I. Kato. Deposition of hydrogenated amorphous silicon films using a microwave plasma chemical vapor deposition method with dc bias. Jpn. J. Appl. Phys., **30**, 6, pp. 1245-1247 (June 1991).
5. I. Kato, S. Wakana, and S. Hara. Microwave plasma CVD system to fabricate α-Si thin films out of plasma. Jpn. J. Appl. Phys., **22**, 1, pp. L40-L42 (1983).
6. I. Kato and M. Yano. Fabrication of a-Si : H films in and out of plasma by coaxial-line type microwave plasma CVD. Trans. Inst. Electron. & Commun. Eng., Jpn, Part C, **J69-C**, 5, pp. 662-668 (1986).
7. I. Kato, T. Ueda, and K. Hatanaka. Effect of substrate temperature on a-Si : H thin films fabricated by a double-tubed coaxial line-type microwave plasma CVD. Trans. I.E.E., Japan, **106-A**, 8, pp. 391-397 (Aug. 1986).
8. I. Kato, K. Hatanaka, and T. Tatsumi. Deposition mechanism of a-Si : H films fabricated by coaxial-line-type microwave plasma chemical vapor deposition. Bull. Sci. Eng. Res. Lab., Waseda Univ., **123**, pp. 1-12 (May 1989).
9. I. Kato, T. Usui, and T. Sakamoto. Spatial distribution of plasma parameters in a microwave plasma chemical vapor deposition. Trans. I.E.E., Japan, **112-A**, 5, pp. 355-362 (May 1992).
10. C. J. Fang, K. J. Gruntz, L. Ley, and M. Cardona. The hydrogen content of a-Ge : H and a-Si : H as determined by IR spectroscopy, gas evolution, and nuclear reaction techniques. J. Noncryst. Solids, **35 & 36**, pp. 255-260 (Jan. 1980).
11. J. Tauc, R. Grigorovici, and A. Vancu. Optical properties and electronic structure of amorphous germanium. Phys. Status Sol., **15**, pp. 627-637 (1966).
12. I. Kato and T. Yoneda. Influence of dc bias and area of substrate table on plasma parameters in a microwave plasma. Trans. I.E.E., Japan, **14-A**, 5, pp. 375-380 (May 1994).

AUTHORS

Isamu Kato received his B.E. and Dr. of Eng. degree in 1967 and 1973, respectively, from Waseda University and subsequently joined the faculty of Waseda University. From 1979 to 1981, he was a Visiting Professor at Manitoba University in Canada where he received grants from the Canadian National Research Council and engaged in a joint research effort. Presently, he is a Professor at Waseda University and is directing research in photonics, laser engineering, electronic materials, plasma electronics, optical and quantum electronics, and semiconductor thin-film engineering. He is a member of the Electrical Engineering Society, Applied Physics Society, Television Society, Japan Vacuum Society, and IEEE.

AUTHORS (from left to right, continued)

Toshiyuki Yoneda received his B.E. and M.E. degrees in 1992 and 1994, respectively, from Waseda University. While he was at Waseda University, he engaged in research on microwave plasma chemical vapor deposition. Presently, he is at Mitsubishi Manufacturing Technology Center. He is a member of the Applied Physics Society.

Toru Matsushita received his B.E. degree in 1993 from the Department of Electronic and Communications, Waseda University, where at present he is in the graduate program, engaged in research on microwave plasma chemical vapor deposition. He is a member of the Applied Physics Society.